POLITECNICO DI MILANO
SCHOOL OF INDUSTRIAL AND INFORMATION ENGINEERING
MASTER OF SCIENCE COURSE IN AERONAUTICAL ENGINEERING

Conceptual Design of Hybrid-Electric Aircraft

SUPERVISOR: Prof. Lorenzo Trainelli

CO-SUPERVISORS:

- **Prof. Carlo E.D. Riboldi**
- **Prof. Alberto Rolando**

NICCOLÒ ROSSI
ID - 852348

ACADEMIC YEAR 2016/2017

Contents

List of Figures

List of Tables

Sommario

Un aumento nell'interesse su applicazioni elettriche alla propulsione sia per veicoli di terra che per aeroplani è stato osservato nel corso degli ultimi anni, grazie a batterie e motori elettrici più affidabili e performanti. La propulsione elettrica per applicazioni aeronautiche rappresenta tuttora una porzione ridotta nell'aviazione corrente, a causa delle penalità in termini di peso delle batterie e a causa della scarsità di tecniche di progettazione adeguate. Il presente lavoro si focalizza sullo stabilire una procedura generale per la progettazione concettuale di un velivolo completamente elettrico o ibrido-serie e di simularne il profilo di missione per valutare i consumi energetici, per assicurare la massima accuratezza. Un programma Matlab™chiamato *Hyperion* è stato sviluppato e validato utilizzando velivoli esistenti come riferimento, considerando un caso limite di un velivolo convenzionale simulato. La procedura considerata si basa sull'assunzione di un velivolo ad elica propulso da motori elettrici alimentati da batterie, eventualmente caricate da un generatore nel caso di velivolo ibrido. Il dimensionamento preliminare è condotto considerando potenze richieste ed energie stimate, mentre l'effettiva performance è simulata step-by-step con una procedura iterativa, basata sul livello finale di carica delle batterie e, se presente, del carburante nei serbatoi. Studi di letteratura e analisi tecnologiche sono stati effettuati per stabilire una base di lavoro solida, che è poi utilizzata in un ampio set di studi parametrici per valutare la sensitività di parametri chiave come raggio, performance di batteria, velocità e quota di crociera, su parametri del velivolo quali massa al decollo, di batterie e carburante, superficie alare, potenze richieste e grado di ibridizzazione in energia.

Parole chiave: Aereo Elettrico, Velivolo Ibrido-Elettrico, Mahepa, Simulazione di Volo, Progetto di Velivolo Ibrido-Elettrico, Sensitività su Progetto di Velivolo, Programma Hyperion.

Abstract

An increased focus on electric applications to propulsion for both ground vehicles and airplanes has been observed in recent years, thanks to more reliable and more performing batteries and electric motors. Electric propulsion for aircraft applications is still representing a very small portion of current standard aviation due to large mass penalties of batteries and due to rather unexplored design procedures. The present work focuses on establishing a general procedure to design an all-electric and serial hybrid-electric aircraft from a conceptual point of view and to simulate their flight profile to assess energy consumption to ensure the highest accuracy possible. A Matlab™code named *Hyperion* was developed and validated using existing aircraft as a reference, considering the limit case of a simulated conventional aircraft. The considered procedure is based on the assumption of a propeller-driven aircraft powered by electric motors fed by batteries, which are, in case of a hybrid airplane, charged by a generator. Preliminary aircraft sizing is conducted by means of required power and estimated required energy, and actual performance is simulated step by step with an iterative procedure based on final state of charge and fuel tank, if present, levels. Literature studies and technology survey are carried out to establish a robust working base, that is considered in a wide set of parametric studies to assess sensitivity of key parameters such as battery performance, cruise speed and altitude, aircraft range among others, on parameters as takeoff, battery and fuel mass, wing surface, motor power and energy degree of hybridization.

Key words: Electric Aircraft, Hybrid-Electric Aircraft, Mahepa, Aircraft Flight Simulation, Hybrid-Electric Aircraft Design, Aircraft Design Parametric Analysis, Hyperion Program.

Chapter 1

Introduction

The field of aviation is historically rich of innovation and always had a pioneering role in modern society: as airplanes started to connect distant places in a safer, faster and more reliable way, more and more people started to travel; the challenges that aeronautical companies had to face changed in time, and shaped the path followed by aviation itself. One of the biggest challenges of the 21^{st} century is to face climate change, a challenge that can be faced only through the reduction of the environmental impact of our machines, airplanes included. The reduction of the environmental impact of airplanes has been a secondary effect, being the main one to reduce the amount of fuel used during a standard mission in order to reduce both weight of the aircraft and expenses for a company.

Current European plans [1] for future aviation involve the reduction of both noise and pollutant emissions from airplanes to grant a sustainable growth of this field, increasing safety, innovation and air transport effectiveness, allowing to more and more people to travel quickly within the European boundaries. The solutions to this challenging task are to be found both in the way that airplanes are used and designed: this latter field includes both the improvement of existing technologies, mainly for airliners and large aircraft, and the creation of new technologies, which is the focus of this work.

One of the answers to the needs of the future European aviation is the *MAHEPA* project, namely *Modular Approach to Hybrid-Electric Propulsion Architecture*[41], which is a 4-years project devoted to establish a milestone in European aviation in terms of an *Electric Revolution*: the task is to develop and test the best technologies for present and future hybrid-electric and all-electric aviation, by means of finding the most promising solutions in terms of energy storage and power generation, developing new ways of flying the new aircraft and also how to design it. This latter topic, the design of hybrid-electric and all-electric airplanes is the target of this work: we will focus on establishing a design procedure that will allow to size an all-electric or hybrid-electric aircraft by considering all the potential differences with the traditional techniques used with fuel-based airplanes and involving high-performance computational techniques in order to have the most accurate solution possible.

The present work starts with a survey on available technologies and relative trends, discussed in Chapter 2, that are focused on:

- Batteries: as primary energy storage devices and power source for electric aircraft;

- Electric motors: as an important difference with standard propulsive systems, and the key component to grant high overall flexibility;
- Generators: a review on thermal engines and possible fuel-saving improvement;
- Electric aircraft: existing electric and/or hybrid-electric airplanes, ongoing projects and conceptual studies.

A brief analysis on design methods proposed by the literature is discussed in Chapter 3 to provide a general basis of sizing procedures for electric airplanes; a general hybrid-electric sizing procedure is yet unavailable, thus a view on possible architectures is presented, and may be summarized as:

- Series hybrid: where electric motors drive propellers and thermal engines provide energy to batteries;
- Parallel hybrid: where both electric motors and thermal engines are mechanically connected to propellers;
- Series/parallel hybrid: as for parallel case, but thermal engines are also connected to a generator to provide energy to batteries;
- Partial hybrid: combinations that may vary case by case.

Chapter 4 deals with the description of the selected sizing procedure: starting with basic hypotheses, a general procedure for all-electric or turboelectric/serial hybrid aircraft design is presented, involving a preliminary phase conducted through statistical regression data and then an iterative simulation of the overall mission profile to have a realistic estimation of needed power and energy.

Procedure is implemented in a Matlab™program named *Hyperion* and results are provided in Chapter 5; relevant physical quantities are visualized and their time evolution is discussed. A validation process is conducted and airplane design examples are presented and discussed, by analyzing four main aircraft classes:

- General aviation aircraft;
- Micro feeders, with 8-9 passengers;
- Commuters, with a maximum of 19 passengers;
- Regional aircraft, up to 80 passengers.

A parametric analysis is conducted in Chapter 6, where a description of the procedure is presented and the sensitivity on some relevant parameters is investigated using test aircraft obtained before. The aim is to study the impact of parameters as battery data or generator power-to-weight ratio on key aircraft ones such as takeoff weight or battery and fuel mass.

Work ends in Chapter 7, where a summary about what has been observed by literature and what has been obtained in previous chapters is presented, considering a critical discussion of overall results as a starting point for future work in this exciting and promising aviation field.

Chapter 2

Technology Survey

As European policies strive towards greener aviation, the key element still lies in available technology which is rapidly evolving as the market opens. In this section available technologies in terms of batteries, electric motors and generators will be investigated, with a particular focus on forecasts for the next two-three decades, some of the current projects and trends predicted by companies. Aircraft examples will be presented as well as concepts and projects under development by the industry.

2.1 Batteries and Energy Storage systems

Energy storage is the first aspect to consider while analyzing the differences with conventional airplanes: as standard aviation fuel is characterized by very high energy density[1], around $12000 - 13000$ Wh kg^{-1}, batteries are generally much less dense in terms of energy and also introduce the concept of specific power. Conventional thermal engines need a certain fuel flow rate to the combustion chamber, regardless of the kind of engine and thermal cycle: what is needed to produce mechanical power is derived from combustion; the flow rate is provided by a pumping system, which design is conducted with high flexibility, since the size is not forced by tanks size. The same pumping system could be used on tanks characterized by different internal volume, as the main constraint is given by the flow rate that has to be provided to the engines; this is not true for batteries: in this case we both have requirements in terms of energy, as for fuel, and also on power, since storage and delivery are not decoupled as for conventional systems.

Batteries and other systems hence must be able to meet both power density and energy density requirements, as well as they must be able to show high convenience from an economical and ecological point of view [2]; in this subsection the first two aspects will be investigated by comparing different technologies, since cost and environmental impact are still subjected to a too high uncertainty to be treated in a general way. Technologies are compared using the Ragone diagram [3], where the relationship between specific power and energy (at cell level in case of batteries) is shown in a log-

[1] Low Heat Value (LHV) of aviation kerosene is around $43-44$ MJ kg^{-1}; in this work the unit for energy will be Wh, since it is the widest used in the battery field: the reader simply has to keep in mind that 1 J is actually 1 Ws, thus 1 Wh $=$ 3.6 kJ.

log plot to visualize an optimal working region where both parameters are sufficiently high. A general way to model energy storage devices (ESD) is presented in [4], where a generic ESD is modeled as a RL circuit, with a voltage source as a function of battery charge, an ideal resistor and an ideal inductor; this model is well beyond the scope of this work, but it allows to model the battery from a mathematical point of view through an empirical estimation of circuit coefficients, and to eventually visualize the W_{sp} - E_{sp} relationship for a given technology.

2.1.1 Li-ion and Li-poly batteries

Lithium-ion and Lithium-polymers batteries are the most common batteries due to very high performance compared to other technologies available on the market: as in figure 2.1 we can observe that Li-ion batteries grant the highest flexibility to be either used as capacitors, with a high power - low energy setting, and as batteries, with high energy and high to medium power; Li-poly technology shares the same kind of performance in this latter case.

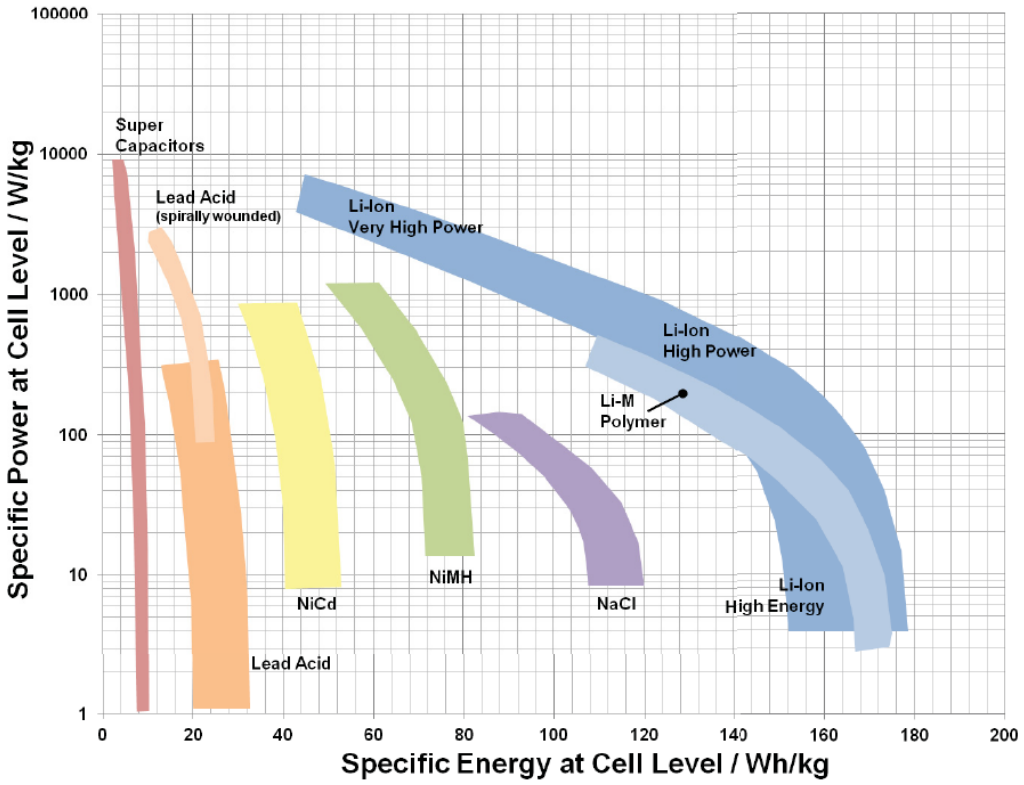

Figure 2.1: Ragone diagram displaying available technologies in 2008, from [2].

Lithium battery performance is determined by materials used as electrodes [2] [5]: state-of-art batteries are equipped with Lithium metal oxides (the most commonly used are based on Cobalt and Manganese) as positive electrodes and graphite as a negative electrode, with theoretical specific energies limited at a maximum value of 300 Wh kg^{-1} and specific powers below 100 W kg^{-1}, which are insufficient even for general aviation

airplanes [2]. We can consider available battery data for Tesla Model S supercar to analyze Li-ion ESD performance: considering the P85 model, the battery has a maximum continuous power output of 311 kW and a total stored energy of 85 kWh, with a total mass of 540 kg [42]; specific parameters are thus around 575 W kg^{-1} and 157 Wh kg^{-1}.

Continental [6] shows that the state-of-art Li-ion batteries based on $LiFePO_4$ cathode, with a theoretical specific energy of around 350 Wh kg^{-1} at 3.2 V are still providing rather insufficient performance for long range vehicle applications, while future batteries, based on $LiMnPO_4$, $LiCoPO_4$ and $LiNiPO_4$ cathodes could reach theoretical values of 450 Wh kg^{-1} at 4.1 V, 520 Wh kg^{-1} at 4.8 V and 600 Wh kg^{-1} at 5.1 V respectively. They also distinguish between two categories of vehicles: Hybrid-Electric (HEV) and Electric (EV) vehicles, underlining that in case of HEVs future trends are towards high power - low energy battery solutions, while for EVs medium power - high energy ones; this principle can be extended to aircraft as well. Future trends for Li-ion based batteries in figure 2.2 show that the main goal for HEV cells is to increase specific power performance, ensuring lighter ESD at the same power output, increasing specific energy in such a way that total energy content will be conserved; EV cells will have to double their specific energy performance, with little improvements in terms of power, in accordance with figure 2.1, with an overall practical specific energy below 300 Wh kg^{-1} as predicted also by [2].

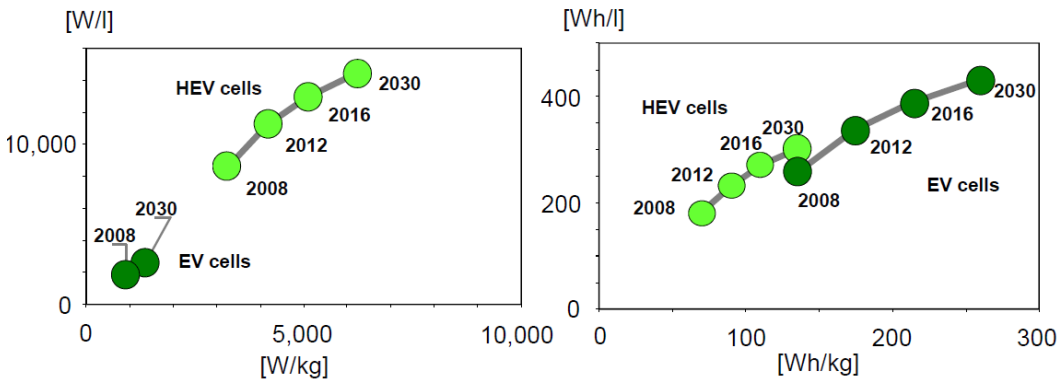

Figure 2.2: Available and predicted specific power (left) and energy (right) trends for Li-ion based cells for HEVs and EVs, from [6].

Studies conducted by Safran company [7] show that for commuter applications the battery-level specific energy should amount at least 500 Wh kg^{-1}, while studies on larger aircraft conducted by Boeing show the need of at least $600 - 750$ Wh kg^{-1}, as reported by NASA [8]; as from above data, Li-ion and Li-poly batteries can provide good performance on today's hybrid or electric vehicles and promising products in the next 15-20 years, but still not adequate for a wide range of aircraft applications.

[2] Let's consider the case of a Cessna-172 aircraft: with an installed power of 120 kW, a 100 W kg^{-1} battery would weigh 1200 kg to provide needed power for the engine, a value that is even higher than the maximum takeoff weight of the airplane, around 1115 kg.

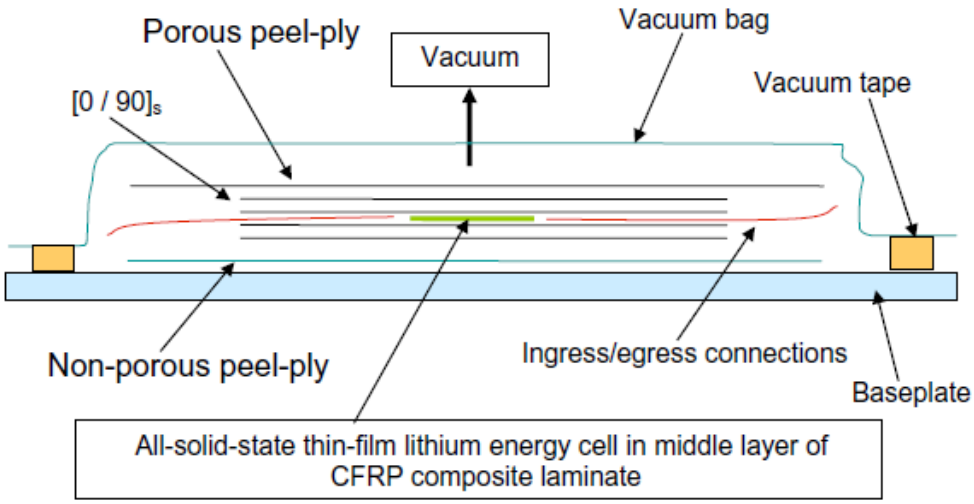

Figure 2.3: Schematic of the practical realization of a smart structure with thin-film Lithium cells in CFRP laminate with traditional vacuum bag technique, from [11].

2.1.2 Structural batteries

A very promising energy storage solution is given by structural batteries [8], as they aim to reduce the amount of pure *parasitic* battery by creating a load-bearing fiber-reinforced composite structure capable of storing energy between fibers and matrix. Fibers will serve as anode, while matrix as cathode [9], combining the ability of carbon fibers to work as current collectors and to provide mechanical load-carrying functionality with solid polymer electrolytes as matrix [10], creating a multifunctional material able to dramatically reduce total ESD solution mass being simultaneously able to bear mechanical loads and to transport Li-ions.

The most common approach so far has been to embed thin-film batteries within a conventional composite laminate, as discussed by T. Pereira et al. [11]: a smart structure can be created by embedding all-solid-state thin-film Li-ion energy cells into carbon fiber reinforced plastic (CFRP) as shown in figure 2.3. Work conducted in [11] proves that this approach is valid, since cells are able to sustain autoclave temperature and pressure, thus maintaining standard CFRP manufacturing, and are also able to operate with little deviations from prior base performance also under mechanical loading, while avoiding significant degradation in mechanical performance. While this solution could benefit from future improvements in Li-ion cells as discussed above, Pereira et al. show that the most suitable applications in aerospace field are related to small systems, as micro-electromechanical systems (MEMS) for satellites, health monitoring systems (HMS) in airplanes, micro aerial vehicles (MAVs) and unmanned aerial vehicles (UAVs).

The approach proposed by Asp et al. in [9] and [10] is to maximize the benefits arising from this technology by creating a new kind of material that may be used for larger applications, such as cars and aircraft, with carbon fiber electrodes (CFE) and solid polymer electrolyte (SPE) matrix. Asp et al. report that CFE tensile stiffness is virtually unaffected by effects of electrical charging and discharging [12] [13], while a

reduction of ultimate tensile strength about 10% of the base value was obtained [14]; internal stress state variations in fibers due to electrochemical cycling have been observed to be critical, especially in radial direction, and must be included in battery design. Challenges in SPE design are related to the ability to achieve high stiffness and Li-ion conductivity to grant wanted overall performance both in terms of mechanical and energy storage capabilities. Two main architectures are presented: a laminated composite battery [15] and a 3D battery design [16]. The first solution is sharing the well established manufacturing techniques of standard laminates, with a major issue related to the need to provide a proper coating of the fiber: to produce a laminated composite battery an insulator separating fibers from the matrix is required to grant electrical insulation of electrode layers using a fiber glass separator which thickness would be around 4 times larger than for standard batteries. 3D batteries, shown in 2.4 have been studied by Asp et al. [16] by means of a SPE spray coating on the carbon fiber, allowing good fiber insulation as proved also by [8]. Both solutions, even if promising, are still characterized by uncertainties in terms of mathematical models, design methods, manufacturing processes and economic advantage, thus are still not feasible in practical large-scale applications.

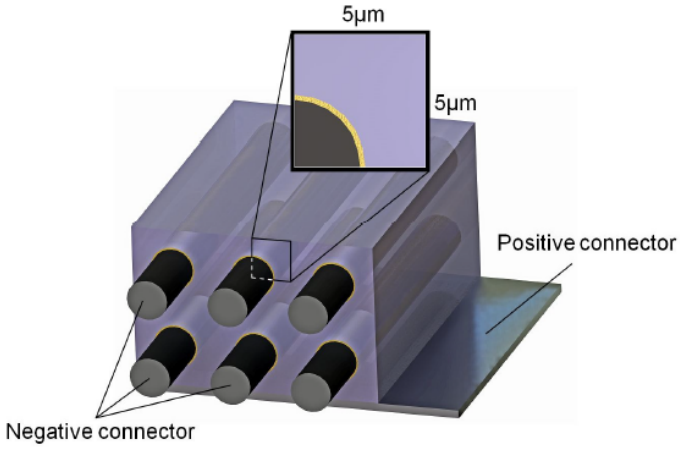

Figure 2.4: Schematic of 3D CFE+SPE battery, from [10].

2.1.3 Li-air batteries

Another promising technology [2] [6] lies in Lithium-air batteries, with a theoretical specific energy around 11500 Wh kg^{-1}, very close to gasoline performance, but characterized by a very short life time. Actual theoretical performance strongly depends on the type of employed reaction [17], divided in aqueous and non-aqueous systems: the first may reach 3460 Wh kg^{-1} for discharge state [3], while the latter 1910 Wh kg^{-1}, again for discharge state. The specific power of these batteries is in the range of mW kg^{-1} [18], well below the range of $500-2000$ W kg^{-1} of Li-ion batteries: Li-air ESDs are thus still not capable of being charged and discharged at competitive rates and plus are also characterized by Lithium losses during cycling; for these reasons are excluded from further analysis.

[3] A value of 11680 Wh kg^{-1} may be reached in charge state, when oxygen is excluded.

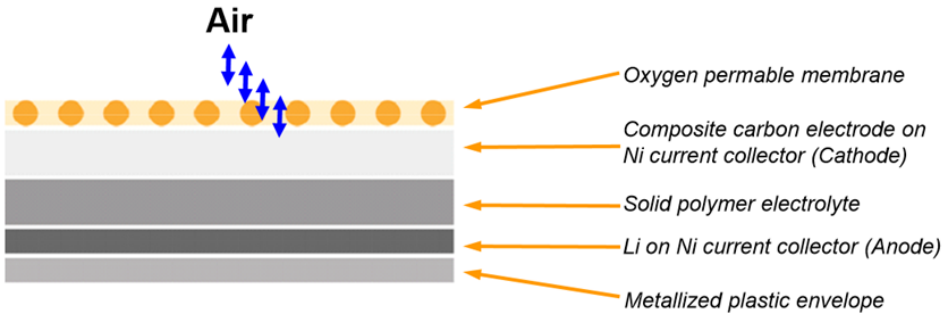

Figure 2.5: Schematic of a Lithium-air battery, from [6].

2.1.4 Li-S batteries

Lithium-Sulfur batteries are proving to be the most promising [19] energy storage devices in the future few years, thanks to their high specific energy compared to standard Li-ion devices that can reach a theoretical value of 2567 Wh kg^{-1} at 2.2 V [18], and are already available on the market from American companies as OxisEnergy [43] and SionPower [44], with battery packs with specific energies around 250 Wh kg^{-1} and with planned improvement to the double within 5 years.

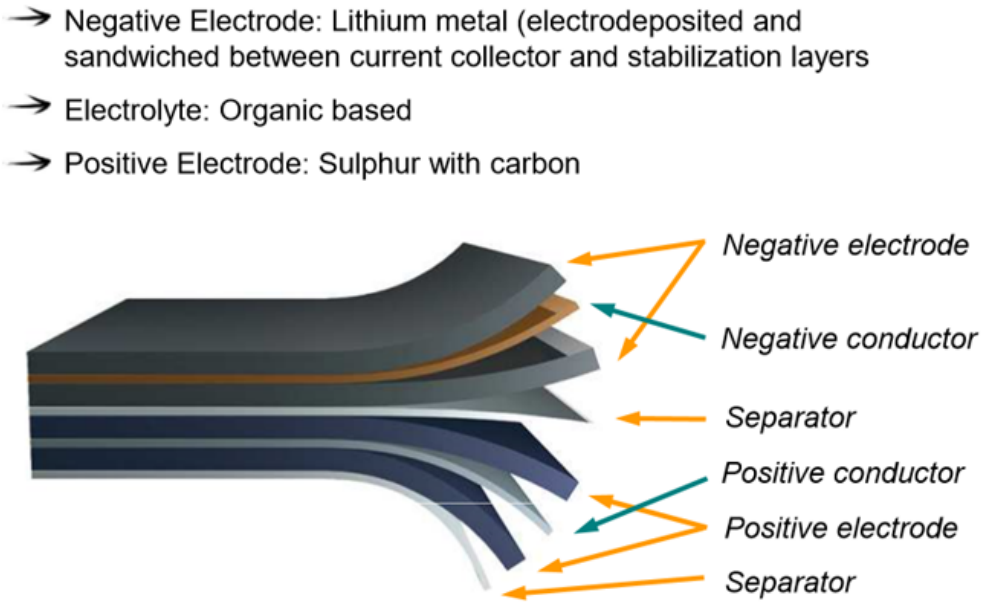

Figure 2.6: Schematics of Lithium-Sulfur battery layout, from [6].

These batteries are characterized by an anode consisting of Lithium and a cathode of Sulfur as shown in figure 2.6, resulting in a very high energy density; during discharging phase, Lithium reacts with Sulfur to form Li_2S and during charging phase the compound formed is solubilized again [19]. The employed materials are shown in figure 2.7, where we can see in blue the current state-of-art electrodes [4] and possible improvements

[4]Metallic Lithium shows the highest performance but is excluded due to safety risks related to short-

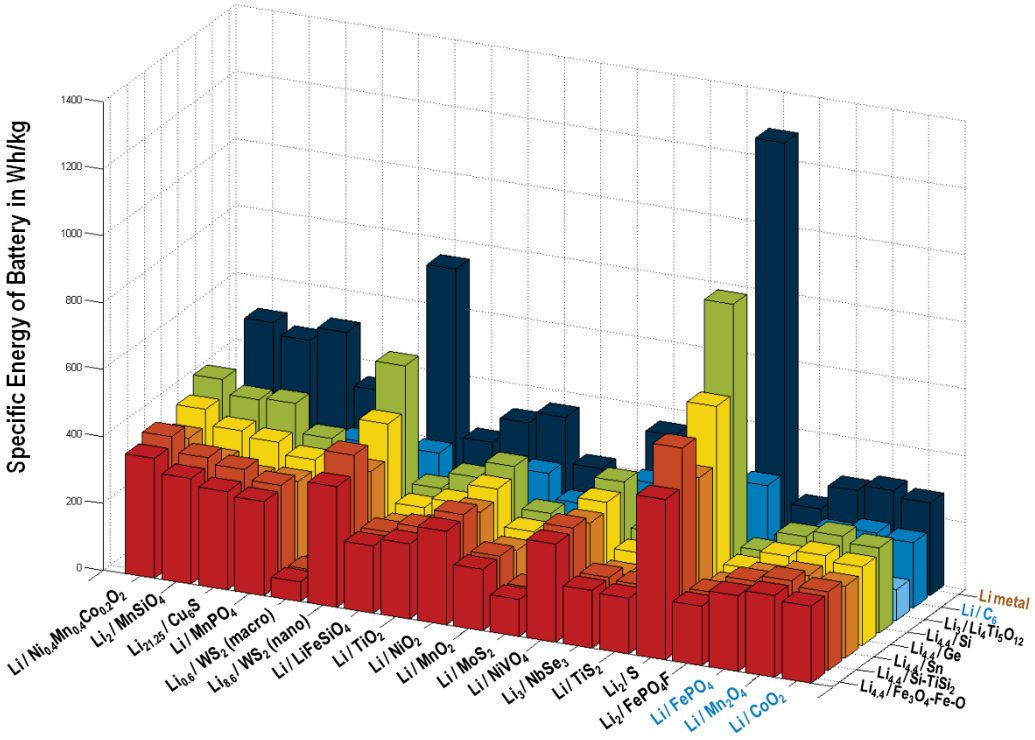

Figure 2.7: Specific energy of different batteries resulting from combinations of different positive and negative electrodes, from [2].

arising from this technology.

Current issues related to Li-S batteries lie in rather limited life cycles with respect to Li-ion technology: while the latter reach values of about 2500 cycles, Li-S ESD currently on the market are limited to $500-1000$ cycles, but with lower cost per unit energy of 250€/kWh versus 475€/kWh [19]; manufacturers plan to reach values between $1500-2500$ cycles in the next few years [43].

Practical Li-S batteries specific energy trends are thus moving from current 250 Wh kg^{-1} to 500 Wh kg^{-1} within 2021, as planned by manufacturers, to values around 650 Wh kg^{-1} by 2030 and 1000 Wh kg^{-1} around 2040 [2] [8]. In the following discussions and simulations battery performance values will be considered to be close to forecasts about Li-ion and Li-S ESDs as presented in this section.

2.2 Electric Motors and Systems

Regardless of the final architecture of the power-train for the aircraft, another key component in our discussion is given by electric drives: in recent years the electrification of automobiles pushed the industry towards more powerful or more compact high-reliability motors to be compliant with market growth. Aeronautical propulsive applications of electric motors are found in Siemens work [20], where key aspects regarding drive systems are underlined: electric machines must be efficient ($\eta > 95\%$),

circuits and thermal issues.

extremely lightweight ($W_{sp} > 6$ kW kg^{-1}), safe and redundant; moreover, this technology is shown to be scalable and thus it can be extended from existing small aircraft application to larger regional airplanes. Aircraft motors must be designed with particular focus to achieve the lightest possible solution through some key steps [20]:

- High performance magnetic materials: high electric frequencies to grant a high torque density;
- High performance cooling: increase motor efficiency reducing losses due to high temperatures in copper wires, using optimal coolers at high coolant temperature (90-100 °C);
- Optimization of passive structural components through better computational and manufacturing techniques such as 3D printing;
- Optimization of motor design rotational speed: aircraft application benefits from direct motor-propeller connection, avoiding a gearbox.

All these aspects led Siemens to produce the SP260D induction motor shown in figure 2.24, characterized by a maximum continuous power output of 260 kW at 2500 RPM and a total mass of only 50 kg, being the strongest motor ever built [5] with a power density of at least 5 kW kg^{-1}. This motor has been installed and tested on the Extra 330 LE aircraft [45], proving its high performance with a world record climb performance of 4 minutes and 22 seconds climb to 3000 m [46].

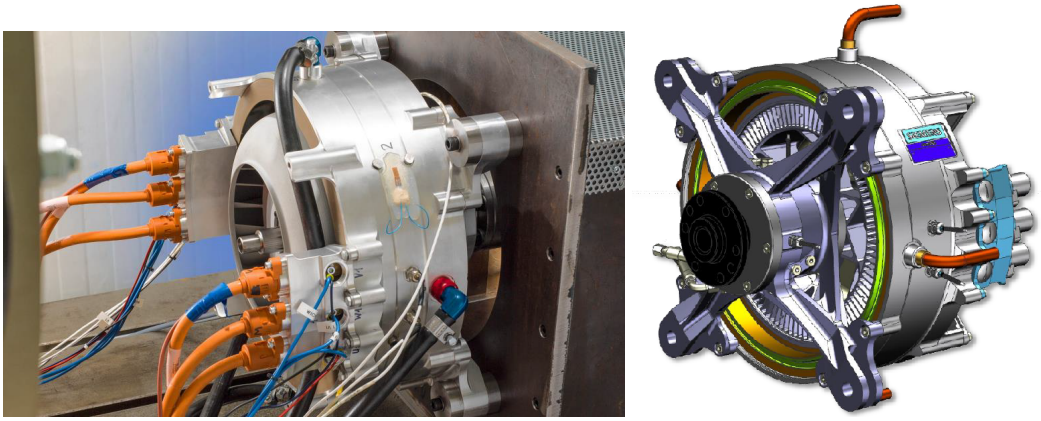

Figure 2.8: SP260D motor during testing phase (left) and motor optimization concept (right), from [20].

Future automotive and aeronautical applications could involve so called High Temperature Superconducting (HTS) motors [21], characterized by particular zero-resistance HTS wires at liquid Nitrogen temperature of 77 K [6], allowing very high performance motors with liquid Nitrogen coolant. The superconducting motor concept could work

[5] Up to January 2015.

[6] The name "High Temperature" is due to the fact that actual superconductors operate at extremely low temperatures of 4 K, preventing practical applications; in this case operative temperatures, even if very low, are much higher than for standard superconducting wires.

at higher current values, thus resulting in a higher torque per unit mass and thus the possibility to downsize the motor and to avoid the need of a transmission, and at a low voltage, without the need of transformers and with fewer cells in series, increasing reliability [21]. The major difference in system's architecture lies in the need of an on-board active refrigerating unit using a cryogenic coolant such as liquid Nitrogen to keep motor wires below their critical temperature for the whole mission duration.

The HTS motor, as shown in figure 2.9, is composed of a series-wound DC motor with a superconducting wire coil, providing constant magnetic field, immersed in cryogenic coolant; the motor is thermally insulated through a copper insulation vessel. Motor voltage is in the order of 150 V, about 10-20 times lower than expected values for AC induction motors as tested by Shinzato et al. [21], with a HTS motor of 110 kg with a 30 kW power output on an electric car. Although obtained performance is insufficient if compared to the SP260D, HTS motors are still in an early stage and research [22] show that it will be possible to reach an overall specific power of 20 kW kg^{-1} including refrigerating unit and coolant masses, with an efficiency around 99.7 %.

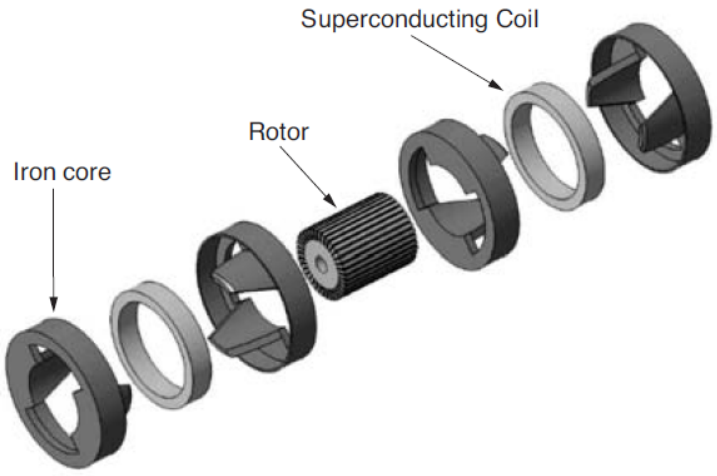

Figure 2.9: Schematic of a high-temperature superconducting motor, from [21].

HTS motors are thus expected to provide a higher power with a higher efficiency with respect to AC induction motors: they will be the most suitable candidates both for commuter applications and for possible Hybrid-Electric airliners as studied by Isikveren et al. [23] [24] with the application of HTS drives to a concept of *Electro-Fan*, where electric motors would replace thermal turbojet part of standard turbofan engines and drive the fan directly. A concept developed by Isikveren et al. under the name *SAFE* (Silent Advanced Fan utilizing Electrical power) as shown in figure 2.10, where composite CFRP fan blades are driven by a Fan Drive Gear System (FDGS) connected to a HTS motor; a Variable Nozzle Device (VND) is considered to obtain extra thrust at take-off, while thrust reverse can be achieved by inverting rotational direction of the electric motor. This *Electro-Fan* concept, as its name suggests, is capable of reducing emitted

noise, since no turbomachines are employed and no high-speed jet is expelled from the exhaust nozzle [7].

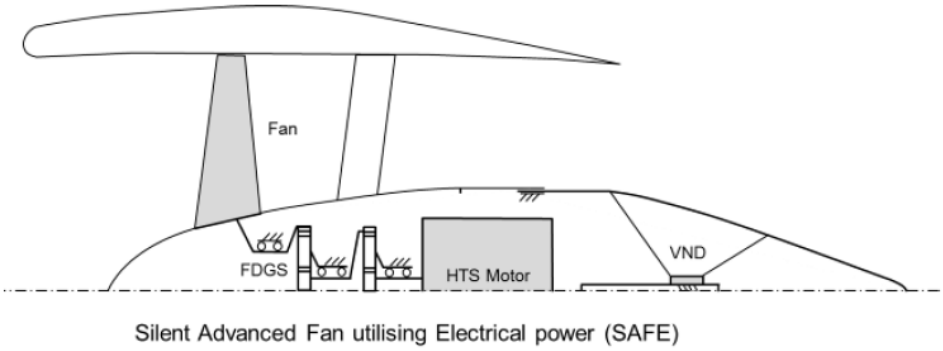

Figure 2.10: Schematic of Silent Advanced Fan utilizing Electrical power (SAFE), from [23].

In aircraft applications we have to consider that both motors and systems require a high power output, thus needing a large cable mass. Isikveren et al. [23] show that to improve performance DC systems should be preferred, since they reduce:

- electromagnetic interference with on board systems;
- cable cross section, reducing mass and losses;
- need of inverters;

electric airplanes would benefit from DC operation of batteries reducing AC systems as much as possible, operating with voltage values between 1-3 kVDC.

2.3 Power Generators

Generators and power systems are considered to be composed of an energy carrier and an energy converter and thus are required to be able to either charge batteries during the mission or to provide extra energy to electric motors, at relatively high rates; [2] shows that power systems can be compared using Ragone plots, by means of relative analysis with respect to state-of-art turbo-engine (*SoA-TE*) power systems. In figure 2.11 we can observe that power and energy needs for a typical medium-range aircraft are still not achievable with today's technologies: battery-based systems (*Batt*) are only able to supply the needed power but with less than 10% of energy, fuel cells (*FC*) are on the contrary able to supply needed energy at a too low specific power, while only serial turbo-electric systems (*Serial-TE*) are close to meet the requirements.

[7] We remind that acoustic power of a jet is proportional to V^8, where V is jet speed; thus noise is greatly reduced if no high-speed hot exhaust gases are emitted from the engine.

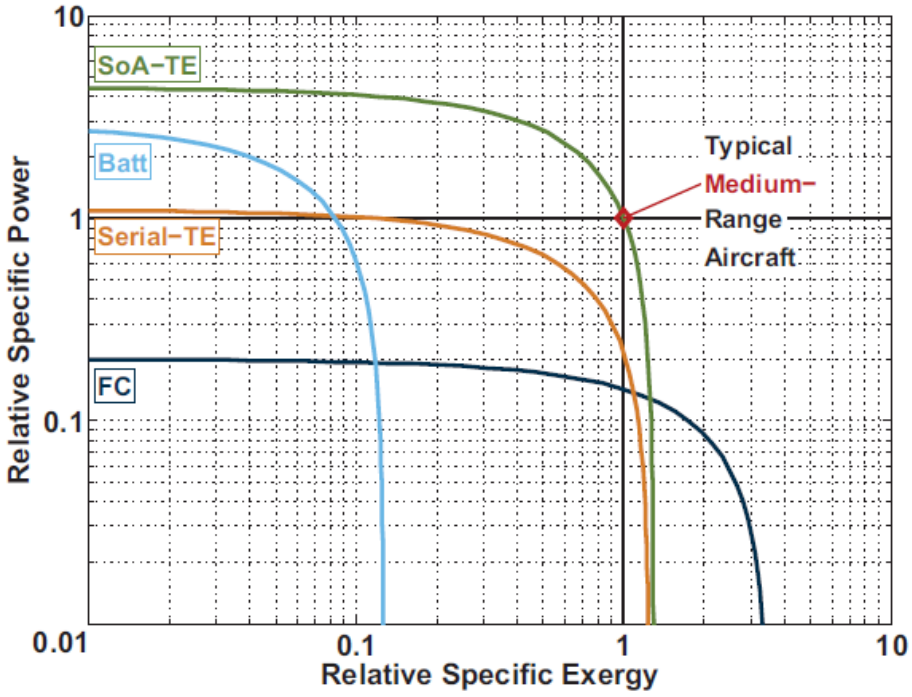

Figure 2.11: Relative Ragone diagram for power systems, from [2].

Although fuel cells are virtually zero-emission power systems, they are most suitable only for low power applications for general aviation aircraft, to avoid large penalties in terms of installed mass [25]; their application could be more convenient in auxiliary power systems rather than as primary power source. Questions are raised also about cryogenic hydrogen availability, price and overall systems safety. Larger airplanes would require combustion engines to provide enough power to sustain flight at a competitive pace; two main power sources can be analyzed: reciprocating engines (labeled as ICE) and gas-turbine (GT) turboshaft engines.

2.3.1 Reciprocating engines

Reciprocating engines are the most suitable candidates at low power requirements due to their low fuel consumption if compared to gas-turbine counterparts, but are characterized by a lower power-to-weight ratio: a comparison between the two requires an in-depth analysis for each case if aircraft under study could be powered either by ICE or GT engines. Aircraft engines are characterized by turbocharge systems, providing high performance at all operative altitudes, and suitable lightweight reduction gear. These power generators are then divided in three main categories, depending on the thermodynamic cycle:

- Gasoline-based: using Otto cycle, the four-stroke engine provides high performance at most altitudes;
- Diesel-based: they work through Diesel cycle and are becoming more popular in last decade due to improved power-to-weight ratio and low fuel price;

- Wankel: rotary engines that grant a very high power-to weight ratio, but are characterized by higher fuel consumption and require a heavier reduction gear.

2.3.2 Turboshaft engines

Turboshaft engines represent the most suitable candidate to meet high power requirements at high efficiency levels, capable of providing very high power densities with respect to reciprocating engines, with the possibility of an overall generator performance optimization thanks to uncoupling between power generation and propulsive devices [25].

A possible optimization is currently studied for helicopter applications, involving heat regeneration to increase engine performance and decrease fuel consumption, as shown by Fakre et al. [26]. A Heat Exchanger (HE) is added to the the turboshaft in such a way that the hot side of the HE is placed downstream of the Free Power Turbine (FPT) and the cold side upstream the combustion chamber: in this way hot exhaust gases from the turbine are used to increase temperature of compressor delivered air, reducing the amount of fuel that is actually needed to reach combustion chamber temperature. Fakre et al. studied the sensitivity of HE effectiveness, defined as its ability to transfer heat from turbine to compressors, on fuel consumption and on overall emissions. As in figure 2.12, we can observe that the higher the HE effectiveness, the lower the needed fuel per unit energy for a given power output, while this in turn increases NO_X emissions due to excessive combustion temperature, leading to Nitrogen dissociation. It has been considered that an effectiveness of no more than 40% should be considered to keep emissions under an acceptable threshold: at this levels a 22% fuel burn for a standard helicopter mission has been obtained.

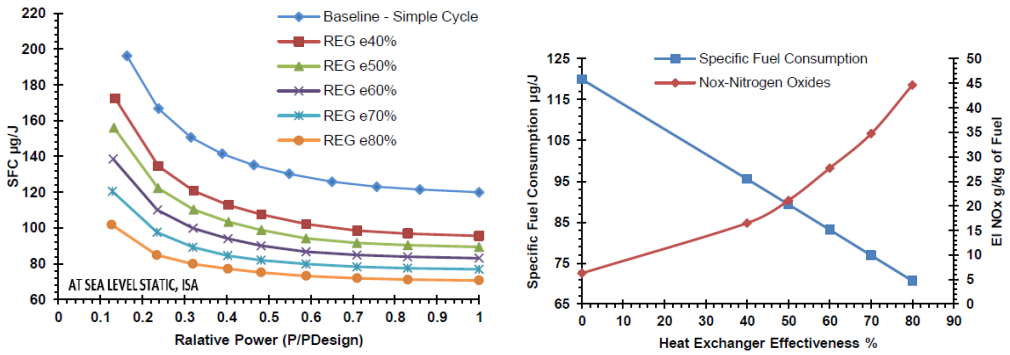

Figure 2.12: Sensitivity of HE effectiveness on fuel consumption - power relationship (left) and on NO_X oxides (right), from [26].

These results are rather promising concerning fuel consumption and subsequent CO_2 reduction, while further performance improvements are hindered by NO_X emissions increase. Several solutions are proposed by Fakre et al. as flame cooling, staged combustion, diluted combustion or lean premixed combustion; all these possibilities are more easily achievable if the engine is decoupled from the main power user as in our case, where the propeller may be driven by an electric motor, unlike the helicopter case, where the turboshaft directly drives the rotor.

2.4 Review of Aircraft

After a technology survey about available batteries, motors and generators, a set of aircraft using these technologies is now presented; airplanes are divided in three categories: existing flying aircraft, projects that are under development and some other peculiar conceptual designs.

2.4.1 Existing airplanes

Five aircraft will be considered here: four general aviation airplanes, Pipistrel Alpha Electro and HY-4, Airbus E-Fan, Solar Impulse 2, and the aerobatic Extra 330LE.

Pipistrel Alpha Electro

Pipistrel Alpha Electro is an all-electric high-wing light-sport aircraft developed by Slovenian company Pipistrel from the prototype WATTsUP; it is currently available on market and is specifically designed to satisfy needs of flight schools, needing an average endurance of one hour. 17 kWh Li-poly batteries are employed and are rechargable in less than one hour [48].

Figure 2.13: Pipistrel Alpha Electro, from [47].

Aircraft	Pipistrel Alpha Electro
Type	All-Electric aircraft
Crew	2 passengers
Energy storage	Li-poly battery pack
Propulsion	60 kW electric motor
Top speed	105 kn
Endurance	90 min
Range	150 km

Table 2.1: Pipistrel Alpha Electro specifications, from [48].

Airbus E-Fan

Airbus E-fan is an all-electric twin-seat mid-wing experimental that first flew in July 2014; the airplane has an unique feature of a ducted 8-blades propeller and an autonomous landing gear electric system capable of providing extra power through wheels during takeoff [50]. The aircraft was intended for pilot training and mass production was planned to start in 2017 but program was canceled in April 2017.

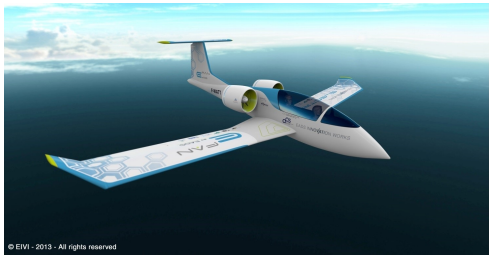

Figure 2.14: Airbus E-Fan, from [49].

Aircraft	Airbus E-fan
Type	All-Electric aircraft
Crew	2 passengers
Energy storage	Li-poly battery pack
Propulsion	60 kW electric motor
Top speed	105 kn
Endurance	60 min
Range	N.Av.

Table 2.2: Airbus E-Fan specifications, from [50].

Solar Impulse 2

Solar Impulse 2 is a solar-powered all-electric high-wing aircraft capable of flying virtually *forever*, being entirely powered by solar energy; although a world record aircraft [51], this technology is still prohibitive due to too low photovoltaic cells' specific power, resulting in a very large aircraft size.

Figure 2.15: Solar Impulse 2, from [52].

Aircraft	Solar Impulse 2
Type	All-Electric aircraft
Crew	1 passenger
Energy storage	Photovoltaic cells
Propulsion	4x10HP electric motors
Top speed	116.6 kn
Endurance	*unlimited*
Range	*unlimited*

Table 2.3: Solar Impulse 2 specifications, from [52].

Pipistrel HY-4

Pipistrel HY-4 is a hybrid-electric twin-fuselage aerotaxi developed by Slovenian company Pipistrel that is powered by a 80 kW electric engine fed by fuel cells [53]. The aircraft is intended to serve as aerotaxi to cover all possible routes in Germany to offer a faster and more flexible transportation solution with zero emissions.

Figure 2.16: Pipistrel HY-4, from [53].

Aircraft	Pipistrel HY-4
Type	Hybrid-Electric aircraft
Crew	4 passengers
Energy storage	Li-poly + Fuel Cells
Propulsion	80 kW electric motor
Top speed	108 kn
Endurance	N.Av.
Range	800-1500 km

Table 2.4: Pipistrel HY-4, from [53].

Extra 330LE

Extra 330LE is an aerobatic aircraft developed by Extra Aircraft from the conventional Extra 330L family, in cooperation with Siemens, MT-Propeller and Pipistrel [45] that first flew in July 2016; it is equipped with the Siemens SP260D electric motor, fed by 14 Li-ion batteries with a total capacity of 18.6 kWh.

Figure 2.17: Extra 330LE, from [45].

Aircraft	Extra 330LE
Type	All-Electric aircraft
Crew	1 passenger
Energy storage	Li-ion
Propulsion	260 kW electric motor
Top speed	182 kn
Endurance	20 min
Range	N.Av.

Table 2.5: Extra 330LE data, from [45].

2.4.2 Ongoing projects

Three ongoing projects are presented: the Hybrid-Electric version of Pipistrel Panthera, NASA's distributed propulsion demonstrator X-57 Maxwell and Airbus E-Fan X, a large regional Hybrid-Electric demonstrator.

Pipistrel Panthera Hybrid

Pipistrel Panthera Hybrid is a Hybrid-Electric aircraft under development by Pipistrel as a hybrid version of the already existing Panthera. The goal of the project is to design an airplane that can be equipped with three different types of propulsion: a conventional version, already on the market, the hybrid-electric version, now under development, and a future all-electric one. Panthera Hybrid will be powered by a 150 kW electric motor fed by Li-poly batteries charged by Rotax-915 internal combustion engine [54].

Figure 2.18: Pipistrel Panthera conventional version, from [55].

Aircraft	Pipistrel Panthera Hybrid
Type	Hybrid-Electric aircraft
Crew	4 passengers
Energy storage	Li-poly
Propulsion	150 kW electric motor
Top speed	212 kn
Endurance	N.Av.
Range	1000 nm

Table 2.6: Pipistrel Panthera expected specifications, from [56].

NASA X-57 Maxwell

The X-57 Maxwell aircraft is a prototype developed by NASA from a Tecnam P2006T with a very high wing loading to reduce drag, using distributed propulsion to increase overall lift due to high-energy flow coming from 6 propellers for each half-wing, with a larger one at the tip to control flow separation to reduce induced drag. Each propeller can be controlled independently to optimize high-lift performance during takeoff and landing, while during cruise only tip motors are used [57].

Figure 2.19: NASA X-57 Maxwell concept, from [57].

Aircraft	NASA X-57 Maxwell
Type	All-Electric aircraft
Crew	4 passengers
Energy storage	Li-ion
Propulsion	14 electric motors
Top speed	150 kn
Endurance	60 min
Range	160 km

Table 2.7: NASA X-57 Maxwell available specifications, from [57].

Airbus E-Fan X

Airbus E-fan X is a Hybrid-Electric concept that is under development by a team composed by Airbus, Rolls-Royce and Siemens, started in November 2017 [58], to demonstrate that a high-speed regional aircraft could be powered by ducted propellers driven by electric motors. Airbus states that a testing campaign will start in 2020 on a BAe 146 aircraft with a 2 MW electric motor replacing one of the 4 turbofan engines.

Figure 2.20: Airbus E-Fan X concept (left) and schematic (right), from [58].

2.4.3 Conceptual projects

Four conceptual projects are here presented and are intended to be considered as feasibility studies on three main aviation fields. The first three projects have been carried out by teams of students from Politecnico di Milano: Flynk, an all-electric aerotaxi developed in compliance with AIAA 2015 graduate aircraft design competition, Hybris, a hybrid-electric trainer participating to the First Annual General Aviation Design Competition – "E-conditions Fixed-Wing Aircraft Design Challenge", and Flybrid, a regional hybrid-electric aircraft developed for Airbus Fly Your Ideas 2013 challenge. The last project is a study carried out by Boeing under the name SUGAR to investigate the feasibility of a hybrid-electric version of the 787 Dreamliner.

Flynk

Flynk is an all-electric aerotaxi designed by a group of graduate students in Politecnico di Milano, winner of the AIAA 2015 graduate aircraft design competition [59]. With an entry into service date in 2020, it is equipped with Li-S batteries and it is capable of

transferring 9 passengers up to 43 nm in the city of New York, with the ability to take off from very short runways of 150 m, thanks to large high-lift devices and movable tip motors, up to 30° [27].

Figure 2.21: Flynk aircraft, from [27].

Aircraft	Flynk
Type	All-Electric aircraft
Crew	9 passengers
Energy storage	Li-S
Propulsion	4x110 kW electric motors
Top speed	200 kn
Endurance	N.Av.
Range	80 km

Table 2.8: Flynk specifications, from [27].

Hybris

Hybris is a general aviation aircraft concept, developed in compliance with Royal Aeronautical Society (RAeS) 2016 contest "E-conditions Fixed-Wing Aircraft Design Challenge", to design an innovative aircraft to fly on UK scenario. The proposed aircraft, that eventually won the competition, is a hybrid electric aircraft using Li-ion plus structural batteries to reduce the total ESD mass to meet the contest requirements [28].

Figure 2.22: Hybris aircraft, from [60].

Aircraft	Hybris
Type	Hybrid-Electric aircraft
Crew	3 passengers
Energy storage	Li-ion + Structural
Propulsion	100 kW electric motor
Top speed	150 kn
Endurance	N.Av.
Range	500 nm

Table 2.9: Hybris specifications, from [28].

Flybrid

Flybrid is a hybrid-electric regional airliner developed in compliance with Airbus "Fly Your Ideas 2013" challenge, with a entry into service date expected in 2030s, eventually reaching the top 5 finalist rank; the proposed aircraft uses a parallel hybrid solution without in-flight battery recharge, with the key feature of a fast battery pack substitution in airports to reduce turnaround time [29].

Figure 2.23: Flybrid aircraft, from [61].

Aircraft	Flybrid
Type	Hybrid-Electric aircraft
Crew	90 passengers
Energy storage	Li-air
Propulsion	2.4 MW EM + 2xICE
Top speed	N.Av.
Endurance	N.Av.
Range	700 km

Table 2.10: Flybrid specifications, from [29].

SUGAR

Subsonic Ultra Green Airplane Research (SUGAR) is a family of airplanes as a result of a feasibility study by Boeing on possible improved versions of the 787 Dreamliner aircraft using hybrid-electric technologies. Starting from the baseline aircraft, labeled as *SUGAR Free*, Boeing studied two versions, *SUGAR High* and *SUGAR Volt*, respectively with 58% and 88% block fuel reduction; both are equipped with a braced high-wing, and powered by a combination of fuel cells, batteries and hybrid generators [30].

Figure 2.24: SUGAR High (left) and SUGAR Volt (right) concepts, from [30].

Chapter 3

Electric and Hybrid-Electric Aircraft Sizing Approaches

After a technology survey where all important aspects of electric aviation are discussed, different approaches to aircraft sizing and design will be presented, with particular focus on differences with traditional design.

3.1 Battery Mass Sizing

Batteries are the most critical component to size, since they will have to provide both power and energy, thus they will have to be able to discharge enough electric current to safely feed motors at maximum continuous power and to store energy for the whole mission [2]. We start the discussion by considering the simpler case of an all-electric aircraft, to later extend the approach to the hybrid electric case, where the solution will directly depend upon the selected propulsive architecture.

A possible method is proposed by Riboldi and Gualdoni [31]. The mission profile is divided in three phases, namely climb, cruise and loiter, under the assumption of a glided descent; for each phase required power and energy are evaluated.

- Climb: given a rate of climb RoC, an average value of air density ρ_{CL} [1] and constant airspeed V_{CL}, it is possible to evaluate needed power:

$$P_{CL} = \frac{1}{2}\rho_{CL} V_{CL}^3 S C_{D_{CL}} + W_{TO} RoC \tag{3.1}$$

  The overall time to climb T_{CL} is simply calculated as follows:

$$T_{CL} = \frac{Z_{CR}}{RoC} \tag{3.2}$$

  where Z_{CR} is the selected cruise altitude. The total energy needed in this phase is simply:

$$E_{CL} = P_{CL} T_{CL} \tag{3.3}$$

[1] Due to altitude variation we would have to consider density reduction; this level of accuracy is not greatly affecting the final result, thus an average density value can be considered starting from values at sea level and cruise altitude.

- Cruise: similar considerations can be made for cruise phase, with the great simplification of constant air density and weight, since all-electric aircraft do not experience mass losses due to no fuel burn. Needed power is simply:

$$P_{CR} = \frac{1}{2}\rho_{CR} V_{CR}^3 S C_{D_{CR}} \tag{3.4}$$

  Cruise time depends on the required range R and on cruise speed:

$$T_{CR} = \frac{R}{V_{CR}} \tag{3.5}$$

  and the needed energy as before is:

$$E_{CR} = P_{CR} T_{CR} \tag{3.6}$$

- Loiter: as for cruise phase we will consider power and energy, with the only major difference that loiter time will be a requirement and thus will be a known value; needed power and energy are thus respectively:

$$P_{LT} = \frac{1}{2}\rho_{LT} V_{LT}^3 S C_{D_{LT}} \tag{3.7}$$

$$E_{LT} = P_{LT} T_{LT} \tag{3.8}$$

  where loiter speed V_{LT} should be selected in such a way to maximize aircraft endurance.

Once power and energy requirements are computed for each phase, battery mass can be computed as follows:

$$M_B = \frac{1}{\eta_P} \max\left[\frac{E_{CL} + E_{CR} + E_{LT}}{e}, \frac{\max[P_{CL}, P_{CR}, P_{LT}]}{p}\right] \tag{3.9}$$

where η_P is propeller efficiency, always less than 1, and e and p are battery specific energy and power respectively. The resulting battery mass is needed to satisfy requirements given an aircraft weight W_{TO} and this procedure must be iterated by considering the following relation:

$$W_{TO} = W_E(W_{TO}) + W_{PL} + W_B + W_M \tag{3.10}$$

where W_E is aircraft empty weight as a function of takeoff weight, W_{PL} is payload weight, fixed by the requirements, battery weight is calculated as $W_B = M_B g$ and W_M is electric motor(s) weight, usually as a function of maximum power, and thus indirectly a function of maximum takeoff weight, since its value will be fixed by selecting a proper design point to satisfy all requirements.

This simplified method can be schematized in figure 3.1, where requirements are met through an iterative procedure taking into account statistical regression for empty - takeoff weight and motor power - mass relationships, as well as battery specific power and energy. The procedure considers a simplified flight mechanics model as shown

before, considering basic aerodynamic data to build polar curves used to evaluate drag coefficients in various phases, obtained as usually as:

$$C_{D_{PH}} = C_{D0} + \frac{C_{L_{PH}}^2}{\pi e \lambda} \tag{3.11}$$

where parasite drag coefficient C_{D0} and Oswald efficiency factor e can be estimated from statistical regression and lift coefficient for the generic flight phase PH is simply obtained from vertical equilibrium:

$$C_{L_{PH}} = \frac{2W_{TO}}{\rho_{PH} V_{PH}^2 S} \tag{3.12}$$

A better battery sizing can be carried out by considering design point position in sizing matrix plot analysis, by adding in maximum power comparison in equation 3.9 the term $P_{SMP} = W_{TO} / \left(\frac{W_{TO}}{P}\right)$ to satisfy all constraints.

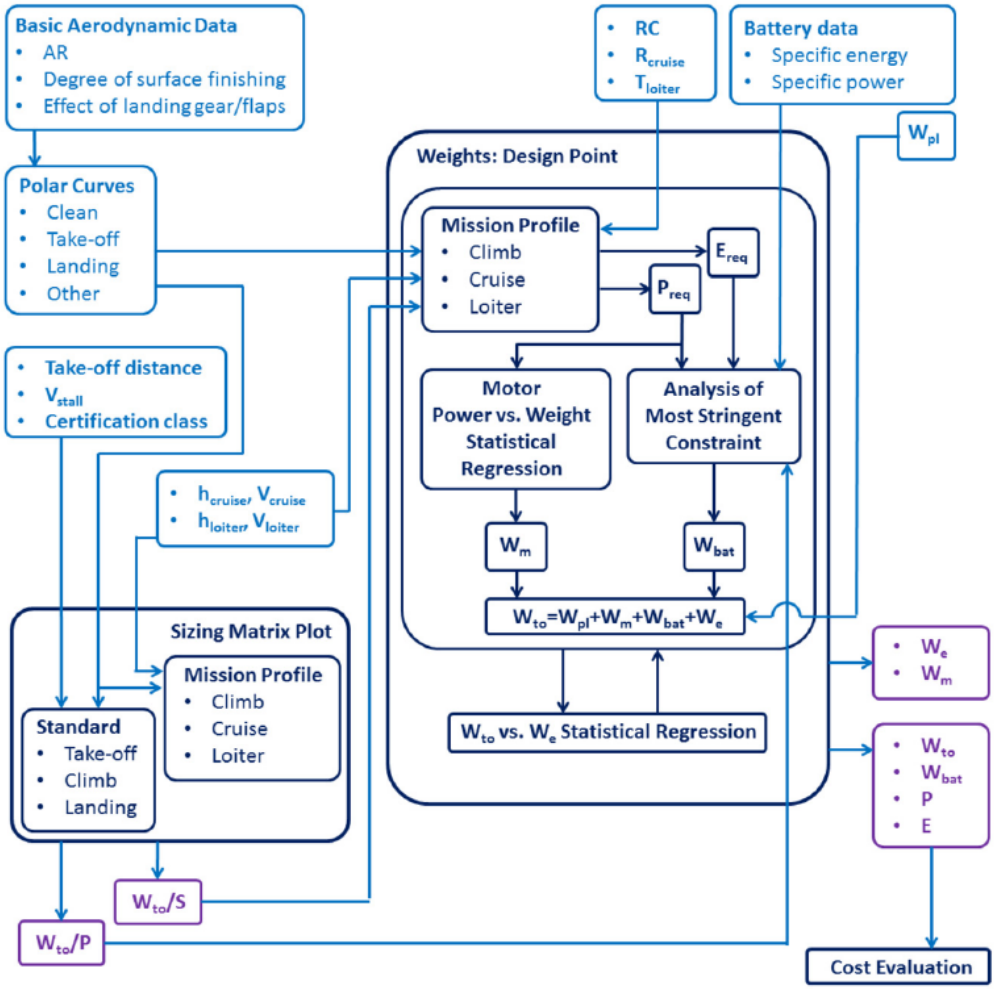

Figure 3.1: Complete flowchart of all-electric aircraft sizing, from [31].

3.2 Hybrid-Electric Design Approach

In previous section a method to size battery mass was presented for an all-electric aircraft. Despite the technological differences with conventional aircraft, the sizing procedure is rather close to traditional design: energy requirement is estimated from flight profile definition and each phase is analyzed, by considering performance indicators as rate of climb, range and loiter time. Battery data and motor specific power are estimated as usually done in case of thermal engine specific fuel consumption; the major difference with traditional design lies in the need to add an extra constraint to battery sizing, since power requirement has to be taken into account, while fuel mass assessment in conducted only from an energetic point of view.

3.2.1 Degrees of Hybridization

Hybrid-electric design adds extra degrees of freedom to our analysis: first of all, we must define *how much* of the overall energy and power will be provided by electric source and by thermal one, and then we must consider a wide variety of possible hybrid propulsion architectures, which in general depend on the available technology, and thus the entry into service date of the aircraft under study.

The key hybrid electric descriptors are the so called *degrees of hybridization*, defined as follows [25] [33]:

- Energy degree of hybridization, H_E, measuring the extent of electrical energy on the overall stored one:
$$H_E = \frac{E_E}{E_E + E_F} \tag{3.13}$$
where E_E is electrical energy and E_F is fuel energy.

- Power degree of hybridization, H_P, measuring the amount of power provided by electric motors on the overall installed one:
$$H_P = \frac{P_E}{P_E + P_T} \tag{3.14}$$
where P_E is electric motor(s) power and P_T is thermal engine(s) power.

Using the above notation, we can distinguish several limit cases [25]:

- Conventional aircraft; with 100% thermal engines fed by fuel tanks, degrees of hybridization will be zero, thus: $H_E = 0$ and $H_P = 0$
- Full Turbo-Electric aircraft; all power is provided by electric motors fed by fuel-based generators: $H_E = 0$ and $H_P = 1$
- All-Electric aircraft; all power is provided by electric motors and all energy is provided by batteries: $H_E = 1$ and $H_P = 1$

As the previous discussion about available and forecast technology suggests, we can investigate the feasibility of electric and hybrid-electric solutions at various power levels in time as in figure 3.2 from Safran group [25].

We can identify 5 aircraft categories based on installed power:

- P $<$ 1 MW: general aviation;
- 1 MW $<$ P $<$ 2 MW: commuters, helicopters and UAVs;
- 2 MW $<$ P $<$ 5 MW: turboprop regional airliners (50-100 PAX), business jets;
- 5 MW $<$ P $<$ 10 MW: turbofan regional airliners (100-150 PAX);
- P $>$ 10 MW: turbofan standard airliners (200-300 PAX).

Safran identifies 5 main working areas:

- Multi-source non propulsive energy; $H_P < 0.05$. Non-Propulsive Systems (NPS) are electric or hybrid-electric systems studied to reduce fuel consumption or to increase overall efficiency in certain key mission phases, such as taxiing with wheel electric motors [32], or to reduce risks during emergencies.
- Electrically Assisted Gas-Turbine; $H_P < 0.10$. A possible way to increase efficiency on the whole mission is to equip standard thermal engines with electric systems able to reduce thrust specific fuel consumption by increasing power during transient phases or emergencies. These systems are currently too heavy to be of practical application.
- Parallel Hybrid or Partially Electric Propulsion; $H_P = 0.20 \div 0.50$. Use of electric motors to partially propel the aircraft in parallel with thermal engines to reduce overall emissions, but at the expense of higher overall weight and thus cost.
- Series Hybrid or Turboelectric; $H_P = 1$, $H_E < 1$. Only electric motors are used to propel the aircraft and thermal engines are used only to provide energy storage.
- Full-Electric; $H_P = 1$, $H_E = 1$. Electric motors power the aircraft and are fed by batteries.

Referring to figure 3.2, where analyses have been carried out in 2015, we can see that with current technology only general aviation airplanes can be fully or partially powered by electric motors, in agreement with previous state-of-art discussion, where the most powerful aircraft, Extra 330LE, was equipped with a 260 kW motor.

Considering a time span up to 2035, meaning +20 years in figure, we can see how full electric power could be employed only in general aviation and in some commuter or UAV applications, while partially electric propulsion would be needed to power commuters and regional propeller-driven airplanes. Turbofan aircraft would at most benefit from assisted electric power, provided that a trade-off could be made between engine mass increase and fuel consumption, noise and pollutant emissions decrease; only *more electric aircraft* tendency is thus expected.

Moving to a larger time span, up to 2050 (+35 years), we can expect to have advanced enough batteries to grant high performance to enable full electric power sources even to standard 200-300 PAX airliners. This possibility to extend this technology to large aircraft by 2050 is affected by heavy uncertainty and requires large improvements in terms of power-to-weight ratio of electric motors and electro-mechanical conversion, cooling systems, wiring and, of course, on batteries.

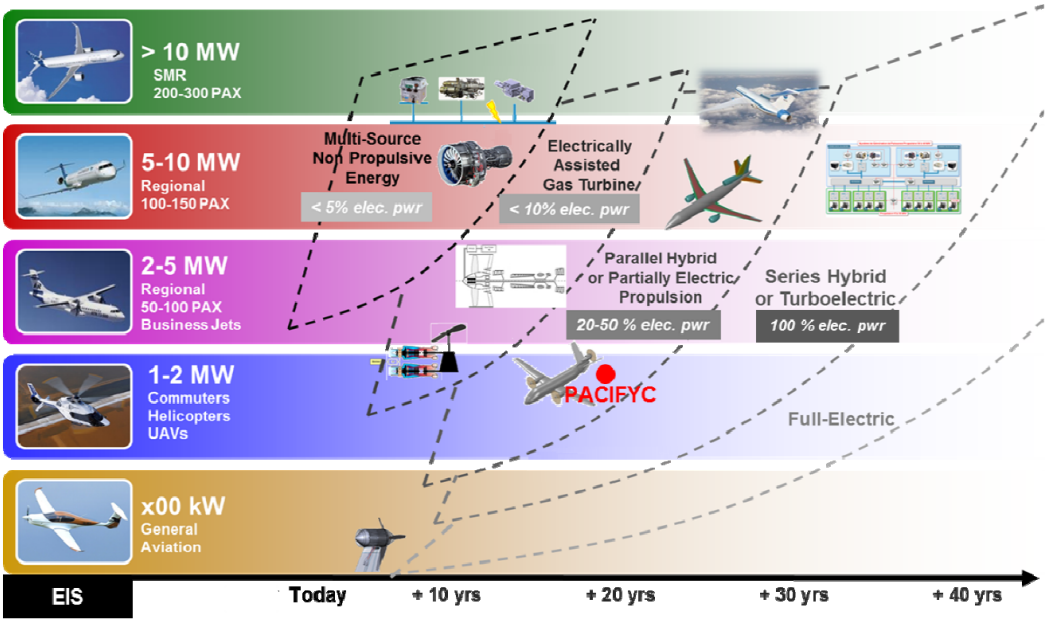

Figure 3.2: Trends of possible aircraft hybrid architectures at different installed power, from [25]. We can identify PACIFYC aircraft, in section 3.3.2, time-power location.

Concerning fuel burn reduction, we can observe in figure 3.3 from [34] a study of potential trend for commercial aircraft. Taking year 2000 as a reference, as considered by Flightpath 2050 program, we can expect an improvement due to hybrid electro-mobility starting around 2025, with fuel saving around 25-30% due to advanced turbofan studies, while further improvements are subjected to large uncertainties.

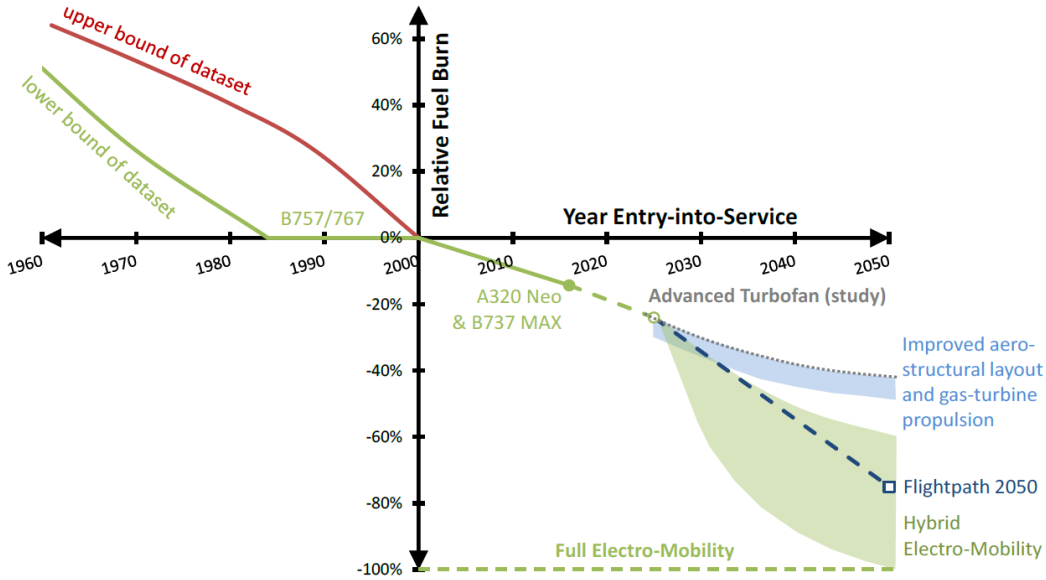

Figure 3.3: Fuel burn reduction expectation with respect to year 2000, from [34].

3.2.2 Hybrid propulsion architectures

With focus on propulsive applications of electric motors in aviation, thus excluding both non-propulsive energy and electrically assisted gas turbines, we focus on the possible architectures of hybrid-electric propulsive systems.

A possible classification of hybrid architectures is presented by Chau et al. [35] while discussing possible solutions for hybrid-electric vehicles (HEVs); although aircraft solution may be more complex, we consider this analysis as a starting point. Consider a user, denoted in figure 3.4 as T: since discussion regards HEVs, the user is considered to be the transmission, then connected to wheels; in our case T represents the propeller or the set of propellers driving the aircraft.

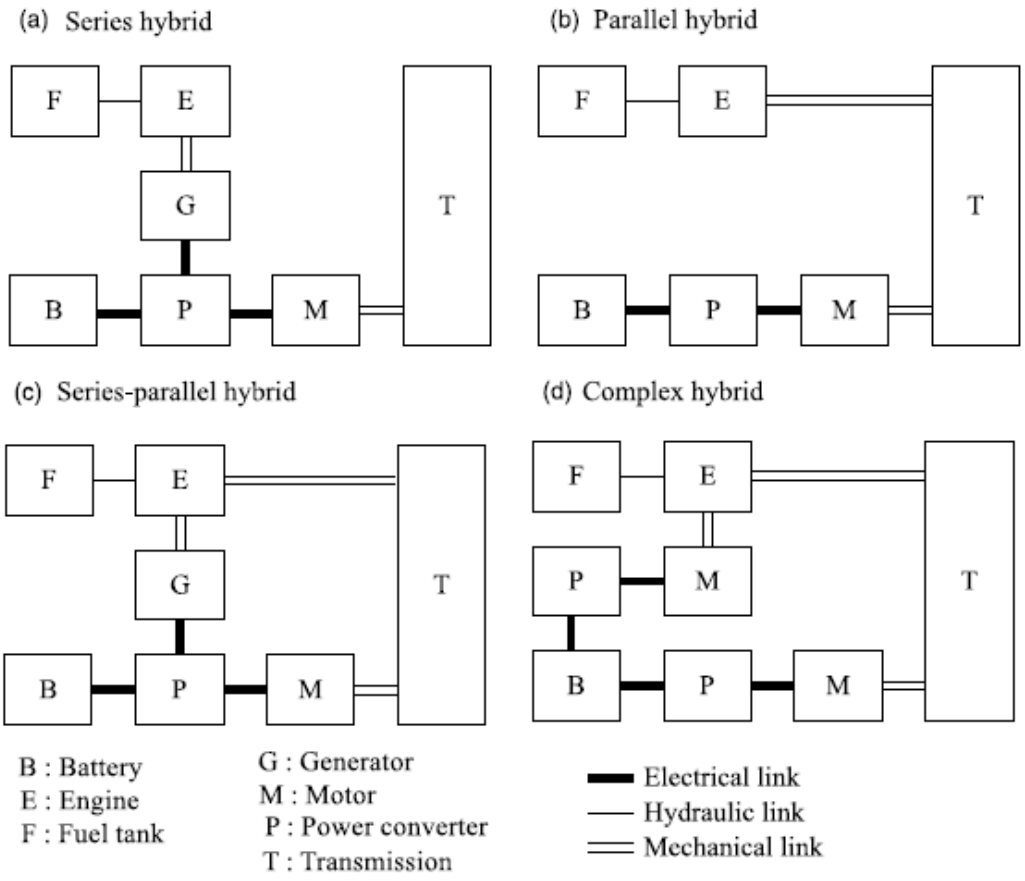

Figure 3.4: Classification of possible architectures for hybrid-electric vehicles, from [35].

Chau et al. identify four main hybrid architectures, summarized as follows:

- Series hybrid: an electric motor drives the transmission, powered either by a battery or a generator fed by a thermal engine; a power converter, equipped with a proper power control unit (PCU) delivers the proper electric current to the motor.
- Parallel hybrid: the user is driven by an electric motor, powered by batteries, and a thermal engine; these lines are decoupled.

- Series-parallel hybrid: the user is driven by an electric motor, powered either by a battery or a generator, and by a thermal engine; the two lines are connected by a generator, making this solution more complex and heavy.
- Complex hybrid: an evolution of the previous architecture, where thermal and electric lines are connected by an electric motor, providing power flow bidirectionality; this motor can be either used as a generator to charge the battery or as a booster do the thermal engine.

Another point of view on possible global architectures is given by [36] as presented in figure 3.5, where *fans* can be also extended to propellers, since at this level we are mainly interested in comparing generic architecture solutions and we are not restricting our view on one particular type of aircraft.

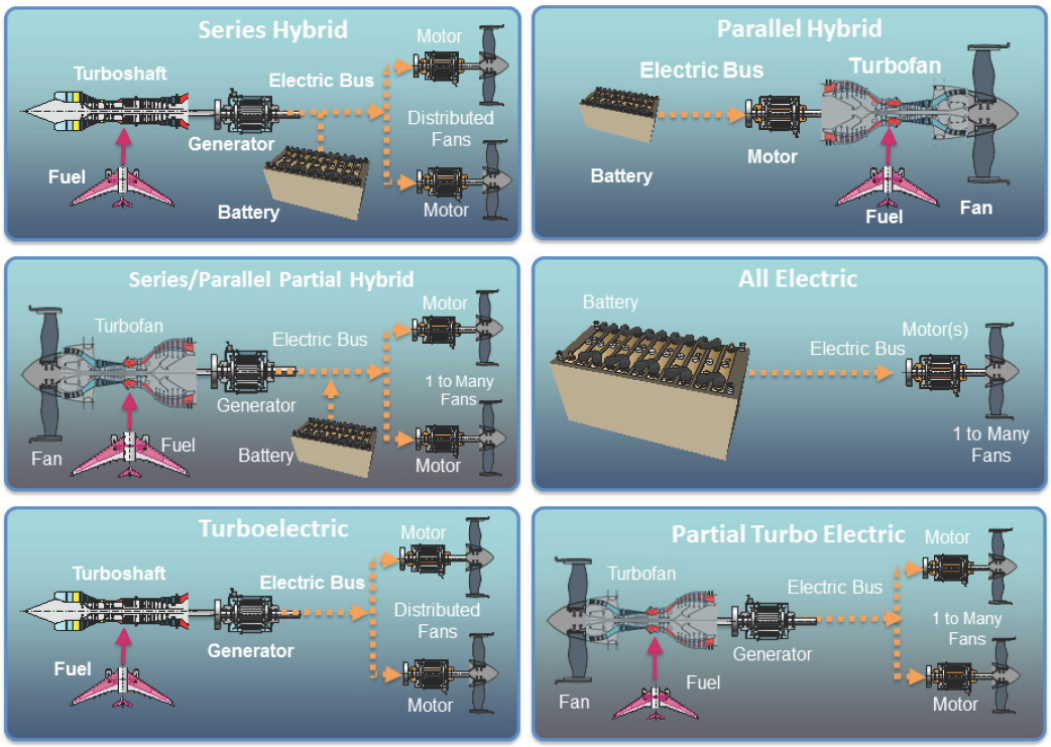

Figure 3.5: Electric aircraft propulsion architecture classifications, from [36].

As we can observe, we have five hybrid solutions:

- Series hybrid: the electric motors are driving propellers/fans and are powered either by a turboshaft plus generator system (or a set of systems) or a battery, which is also charged by the generator if needed.
- Turboelectric: similar to series hybrid solution but without a battery; the electric motors driving propellers/fans are powered by a generator driven by a turboshaft engine.
- Partial turboelectric: as for turboelectric solution, but in this case the thermal engine is not delivering all power to a generator but is providing extra power/thrust being a turboprop or turbofan;

- Parallel hybrid: the electric motors fed by batteries are providing extra power to the thermal engines;
- Series/Parallel hybrid: as for series hybrid, but in this case the thermal engine is not a turboshaft delivering all power to a generator but is providing extra power/thrust being a turboprop or turbofan.

As we can observe from the two discussions above there are several possible architectures, confirming the high levels of flexibility granted by hybrid-electric solution. This flexibility is not allowing for a general a priori analysis of which solution is the most suitable one without an in-depth comparison between architectures, as shown in section 3.3.2. Referring to figure 3.2, only a preliminary selection of candidates can be made, based on required power and entry-into-service year.

3.3 Design Examples

A set of conceptual design examples from literature is here presented, as a summary of what discussed so far and to show different sizing techniques used by different authors. In particular, three examples will be considered, one per aircraft class: an ultralight aircraft, a commuter and an airliner.

3.3.1 Ultralight aircraft

A possible application of today's hybrid-electric propulsion systems (HEPS) is in ultralight aircraft field. Friedrich and Robertson [37] studied the application of hybrid electric propulsion to UK's single seat de-regulated (SSDR) microlight category, with a maximum 115 kg airframe. Due to aforementioned weight restrictions, their analysis involved the use of parallel HEPS: serial hybrid architecture requires both electric motor and thermal engine to be sized to maximum power [2], increasing weight; for such a small application the serial hybrid solution is considered to be too heavy.

Figure 3.6: Standard SONG ultralight aircraft, from [37].

Criteria	SOUL aircraft value
Wing area	10.3 m^2
Wing span	11.2 m
Length	5.6 m
Height	1.9 m
Airframe Mass	78 kg
Empty Mass	103 kg
Takeoff Mass	235 kg
Tank volume	25 L
Cruise speed	80-110 km/h
Maximum speed	143 km/h

Table 3.1: SOUL aircraft properties, from [37].

[2] Usually electric motor provides maximum takeoff power, while the generator is optimized for maximum cruise power.

Authors considered 16 kg of LiPo batteries characterized by 144 Wh kg^{-1} specific energy and simulated aircraft performance with a Matlab™/Simulink - X-Plane connection for the two flight profiles in figure 3.7, obtaining values found in tables 3.2 and 3.3.

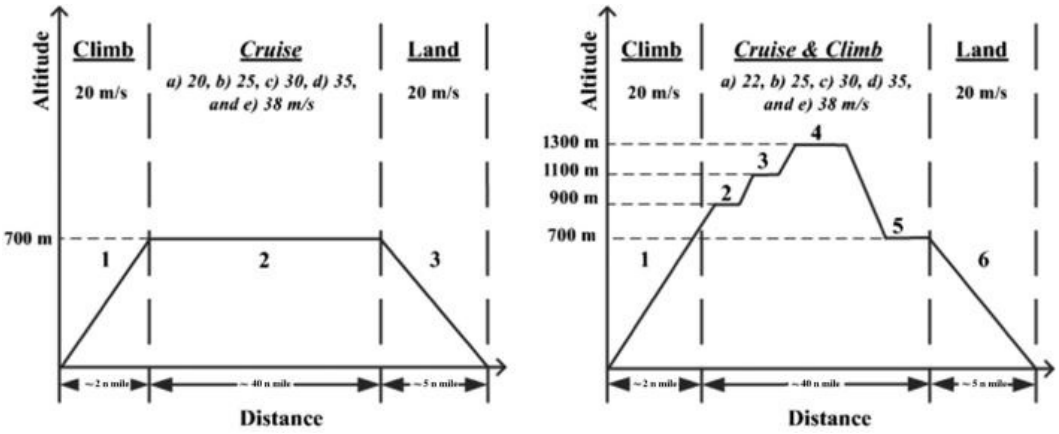

Figure 3.7: Mission profiles used to compare SOUL aircraft with conventional solution, from [37].

	Parallel HEPS		Conventional ICE	Total saving	
Speed [m/s]	Fuel [kWh]	Battery [kWh]	Fuel [kWh]	Fuel	Energy
20	19.7	0.0	28.6	31.1%	31.1%
25	19.0	0.0	26.8	29.1%	29.1%
30	23.7	0.0	29.1	18.6%	18.6%
35	26.7	0.4	34.0	21.5%	18.2%
38	27.1	1.1	42.2	35.8%	28.4%

Table 3.2: SOUL performance for mission profile 1, from [37].

	Parallel HEPS		Conventional ICE	Total saving	
Speed [m/s]	Fuel [kWh]	Battery [kWh]	Fuel [kWh]	Fuel	Energy
22	20.6	0.0	26.2	21.4%	21.4%
25	20.8	0.0	25.2	17.5%	17.5%
30	24.7	0.0	28.1	12.1%	12.1%
35	26.4	0.6	34.8	24.1%	19.3%
38	26.8	1.2	42.8	37.4%	29.4%

Table 3.3: SOUL performance for mission profile 2, from [37].

3.3.2 Commuter aircraft

The commuter class is covered by an extended investigation done by Fefermann et al. [7], who studied a hybrid-electric aircraft capable of respecting 2030 ACARE Strategic Research and Innovation Agenda 55% target for that year. The resulting aircraft, named PACIFYC (Propulsive ArChItecture For hYbrid Commuters), is a 19-seats hybrid commuter aiming at providing an environmentally friendly airplane able to complete any city-pair operations within a maximum range of 700 nm. The study takes as a state-of-art reference (SoAR) aircraft the Beech 1900D and predicts an improved 2030 version which different solutions, depending on the chosen hybrid architecture, are compared to, with general aircraft top-level requirements listed in table 3.4.

A multi-objective block fuel reduction problem was set, to assess fuel savings at 150 nm, 430 nm and 700 nm; the second range is representing of the 85% life-cycle departures, thus a 20% block fuel reduction for this distance is required.

Four possible architectures are presented, as shown in figure 3.8:

- ARCH 1: twin turboprop engines with small generators and one small electrical booster;
- ARCH 2: twin electric motors with a turboshaft generator each;
- ARCH 3: electric motor plus turboprop engine, with exchangeable batteries;
- ARCH 4: as for ARCH 1, but the electric motor is here is intended to operate during the whole mission, not only to boost in emergencies.

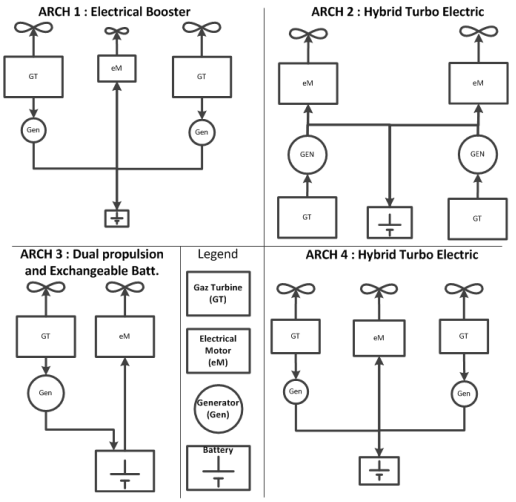

Figure 3.8: Proposed architectures for PACIFYC aircraft, from [7].

Entry-Into-Service year	2025/2030
Design Range	700 nm
Accommodation	19 passengers 102 kg/PAX 813 mm seat pitch
Emissions Reduction	-55% CO_2 -83% NO_X -53% noise
Takeoff field length	$\leq$ 1200 m at MTOW
Landing field length	$\leq$ 1100 m at MLW
Cruise speed	$\geq$ Mach 0.40
AEO cruise altitude	$\geq$ 25000 ft
OEI cruise altitude	$\geq$ 15000 ft

Table 3.4: PACIFYC study requirements, from [7], where AEO stands for All Engines Operative and OEI One Engine Inoperative.

As we can see from the set of considered architectures, the design procedure allows for a preliminary selection of possible candidates, which have to be considered together, and a final decision can be made only after a down-selection process. Referring to

figures 3.4 and 3.5 we can observe that ARCH 1, ARCH 3 and ARCH 4 correspond to series-parallel hybrid while ARCH 2 to series hybrid. An interesting aspect of this analysis is given by properties and performance of electrical components and energy storage, considering bus voltage at 540 V and Li-S batteries:

Property or Component	Value	Unit	Efficiency
Fuel Energy Density	11.8	kWh kg^{-1}	N/A
Battery Energy Density	500	Wh kg^{-1}	
Battery Power Density	1000	W kg^{-1}	
Battery Volumetric Density	500	Wh L^{-1}	
Battery Charger Power Density	15.0	kW kg^{-1}	97 %
Motor Power Density	9.0	kW kg^{-1}	95 %
Generator Power Density	5.0	kW kg^{-1}	90 %
Power Electronics Power Density	10.0	kW kg^{-1}	95 %
Aluminum Transmission	5.8	kg m^{-1}	100 %
Thermal System Penalty	1.5	kW kg^{-1}	N/A

Table 3.5: Properties and electrical component performance for PACIFYC aircraft, from [7].

Using these values, Fefermann et al. found that block fuel reduction of 39%, 25% and 10% are achieved for 150 nm, 430 nm and 700 nm mission respectively with respect to the 2030 reference aircraft, an improved version of the SoAR Beech 1900D, using the solution denoted as ARCH 4. A comparison between reference airplanes and the two best hybrid architecture is presented in table 3.6

Property or Component	SoAR	REF2030	ARCH 1	ARCH 4
Design max range [nm]	680	700	700	700
Maximum Takeoff Weight [kg]	7766	7880	8490	11020
Operational Empty Weight [kg]	4847	4962	5603	6331
Payload mass [kg]	1938	1938	1938	1938
Wing area [m^2]	29.08	29.50	31.78	41.26
Wing span [m]	17.4	18.8	19.5	22.3
Wing loading [N m^{-2}]	2620	2620	2620	2620
Total power [kW]	2x954	2x1012.5	2x840+295	2x840+1105
Cruise speed	M0.38 @FL230	M0.42 @FL250	M0.40 @FL250	M0.42 @FL250
Lift-to-Drag ratio	REF	+7.9%	+6.7%	+11.2%
Block fuel @ 150 nm	+19.4%	REF	-11.5%	-38.8%
Block fuel @ 430 nm	+34.3%	REF	-10.7%	-24.7%
Block fuel @ 700 nm	N/A	REF	-3.0%	-10.3%

Table 3.6: Comparison between present state-of-art, reference 2030 conventional aircraft and the two best PACIFYC architectures, from [7].

As we can observe, ARCH 4 is the solution granting the highest emissions reduction, although takeoff mass is increased by 30% with respect to 2030 reference aircraft, with an increased Cash Operating Cost (COC) of about 11.5%; architecture ARCH 1 is able to slightly reduce COC at -2.1% with little block fuel savings.

3.3.3 Airliner

The last example is a study conducted by Bauhaus Luftfahrt e.V. [24], about the investigation of the needed technologies to develop an all-electric airliner capable of covering European short-range routes with an entry into service in 2035. Market demand analysis in figure 3.9 showed that the optimal number of seats was between 180 and 200, with a cumulative percentage of about 80% of flights up to 900 nm. Analysis conducted at battery level returned a minimum required specific power of 1.2 kW kg^{-1} and specific energy of 1.7 kWh kg^{-1} to satisfy propulsion needs only; subsystems power supply, alternate airport approach and high-safety requirements led to a battery performance target of 2 kW kg^{-1} and 2 kWh kg^{-1}.

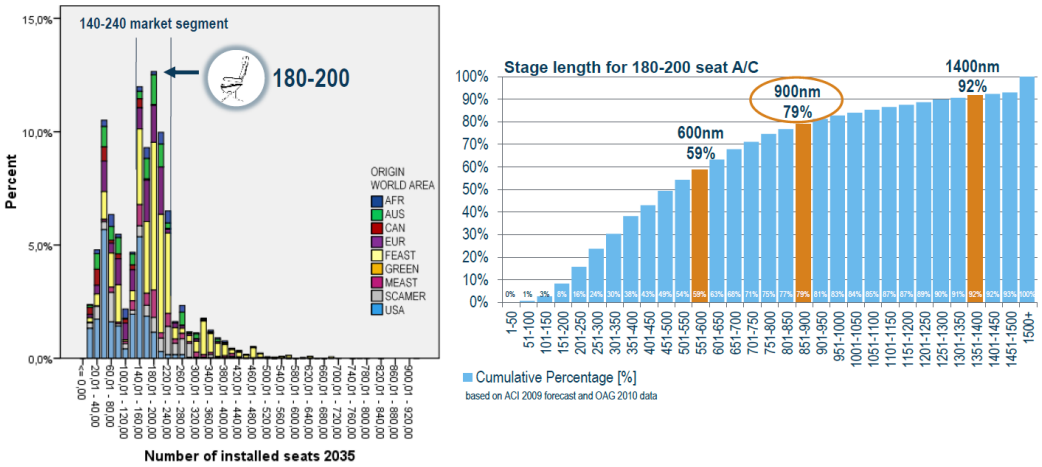

Figure 3.9: Market analysis for medium-range European airliner, from [24].

The innovative concept shown in figure 3.10, with C-shaped self-trimming wing and SAFE electro-fans previously shown in figure 2.10 is thus compared to a hypothetical improved version of Boeing 787 aircraft in table 3.7.

Although Ce-Liner is much heavier than its conventional counterpart, studies show that Cash Operating Cost (COC) is virtually unaltered (+0.1%), mainly because lack of costs related to Emission Trading Scheme (ETS) charge, since no emissions are generated by the aircraft. This investigation shows that, provided large improvement in battery performance, it could be possible to obtain a practical airliner for European medium-range air transport.

Aircraft Property	Unit	Ce-Liner	REF B787-3+	Δ
Maximum Takeoff weight	kg	109300	73700	+49.1%
Maximum Landing weight	kg	109300	70360	N/A
OEW/MTOW	-	0.544	0.654	-16.8%
OEW/PAX	kg/PAX	314	253	+24.0%
Max. energy mass fraction	-	0.275	0.243	+13.2%
Wing reference area	m^2	172.3	115.2	+49.6%
Power-to-weight ratio	kW/kg	0.407	N/A	N/A
Thrust-to-weight ratio	-	0.233	0.310	-24.8%
Takeoff field length	m	2245	1830	+22.7%
Landing field length	m	1875	1770	+5.9%
Approach speed	kn	149	146	+2.1%
Maximum L/D ratio	-	20.5	18.4	+11.4%
ESAR @ 900 nm	km/kWh	0.0473	0.0374	+26.4%

Table 3.7: Comparison between Ce-Liner and reference Boeing 787-3+ version, from [24].

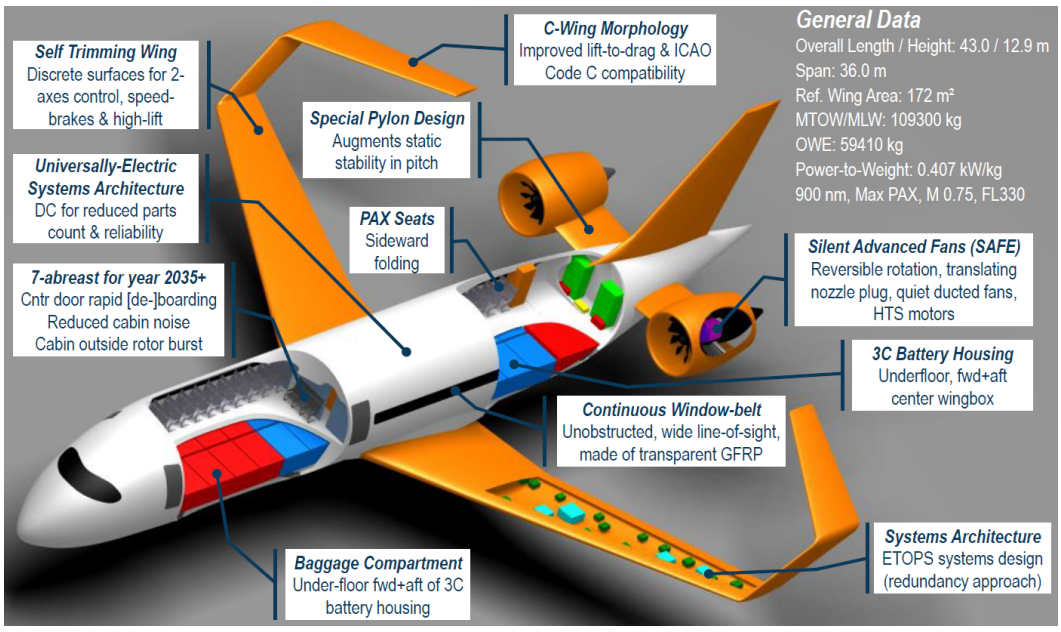

Figure 3.10: Overview on Ce-Liner, from [24].

Chapter 4

Design and Simulation Procedure

An overview on technologies, hybrid architectures and design examples has been discussed in previous chapters; in the following, the procedure used throughout the present work is presented, starting from working assumptions and leading to design procedure and simulation framework. A discussion on the implemented *Hyperion* program is presented, by analyzing its working principle.

4.1 Working Assumptions

As seen in Chapter 3, there is no general description of hybrid-electric architecture, and even within a given one there is no general way to compare different solution a priori; as for PACIFYC aircraft in Section 3.3.2, even considering serial/parallel hybrid solution, authors were unable to select the proper sub-architecture until the very end of the project: was it better to have an electric booster, a third-electric-motor, two motors driving propellers and two turboshaft generators?

An answer is mainly related to considered technology: the more advanced battery and generator technologies the different the architecture will be, more and more towards an all-electric airplane. As observed in previous examples, very different values of battery specific power and energy were considered and they were the key point in determining the overall hybrid architecture: series or series/parallel hybrid electric systems could be employed either in small aircraft applications or with optimistic battery data, parallel or partial parallel hybrid for high-performance aircraft with close entry-into-service date, and even all-electric airliners if very high-performance batteries were available.

To develop a general procedure that can be suitable for all battery values and grants relatively high flexibility a choice is made: selected architecture will be **serial hybrid** or at most **turboelectric** referring to figure 3.5; in this way, as discussed later, we will be able to consider full-electric propulsion by excluding a generator, turboelectric solution by considering *infinitely* powerful batteries, a solution that allows to model the limit-case of a conventional aircraft, and serial hybrid propulsion. Parallel architectures, as seen in examples, are too case-sensitive to be analyzed in a general way: serial hybrid propulsion will thus be considered to assess its feasibility and limitations. A series (or serial) hybrid architecture allows to consider a wide range of possible solutions: since the thermal engine is decoupled from the propellers, we can consider a single powerful

generator – which location may be in the most suitable part of the fuselage – and a set of electric motors; we could consider a limited amount of high-power motors or also distributed propulsion, using many low-power motors. Aerodynamic effects of distributed propulsion are not considered though, since the complexity of the topic, which is beyond the scope of the present work.

Another assumption is, as anticipated, the **use of propellers**: in our model we will consider that motors are providing mechanical power, which will be converted into traction force by a propeller, described by its efficiency η_P, treated as a constant value during the whole mission since the lack of $\eta_P - J$ performance charts at this level of design. The use of propellers allows also for **windmilling**: although no specific energy-harvest system is designed, during the descent phase it is possible to recover energy if vertical speed is high enough, extending mission duration.

Batteries will be characterized by the two performance parameters widely used in above discussion: specific power, denoted as W_{SP} and expressed in W kg^{-1}, and specific energy, denoted as E_{SP} and expressed in Wh kg^{-1}, will be the only needed data during sizing procedure. No particular technology is selected though: virtually any couple of $W_{SP} - E_{SP}$ may be employed in our analyses, allowing for a greater flexibility; the drawback of this assumption is, of course, that actual feasibility of the solution must be assessed separately.

Power generators that are here considered are **turboshaft** and **four-stroke reciprocating engines**, which thermodynamic cycle will be simulated at every given altitude. In this way we will be able, with proper efficiencies as we will discuss in the following sections, to characterize and simulate a real thermal engine and to analyze its performance in different working envelopes. The generators will be sized to satisfy aircraft power needs and thus are considered to operate in an optimal working regime to grant low fuel consumption. The considered **mission profile** is defined as follows:

- Takeoff: this maneuver is simulated to have a realistic power requirement and energy consumption, by considering the two phases of ground run and airborne acceleration.

- Climb: the aircraft climbs from airport altitude to cruise altitude and accelerates from takeoff to cruise speed. The climb strategy will be discussed in following sections, but involves keeping horizontal either at a constant true airspeed (TAS) or equivalent airspeed (EAS).

- Cruise: this phase is carried out at a constant altitude and true airspeed; as we will see, total range is not covered only in this phase, but also in climb and descent ones. The horizontal distance covered in these phases will be added to the cruise one, thus its actual duration will be estimated and then corrected starting from the other two.

- Descent: the dual of climb phase, it starts at cruise speed and altitude and ends at loiter speed and altitude, using the same strategy considered for climb; windmilling is possible if descent rate is such that equilibrium power is negative.

- Loiter: this phase is considered both for possible deviations and for actual hold above the destination airport; horizontal distance covered in this phase will not be included in final range.

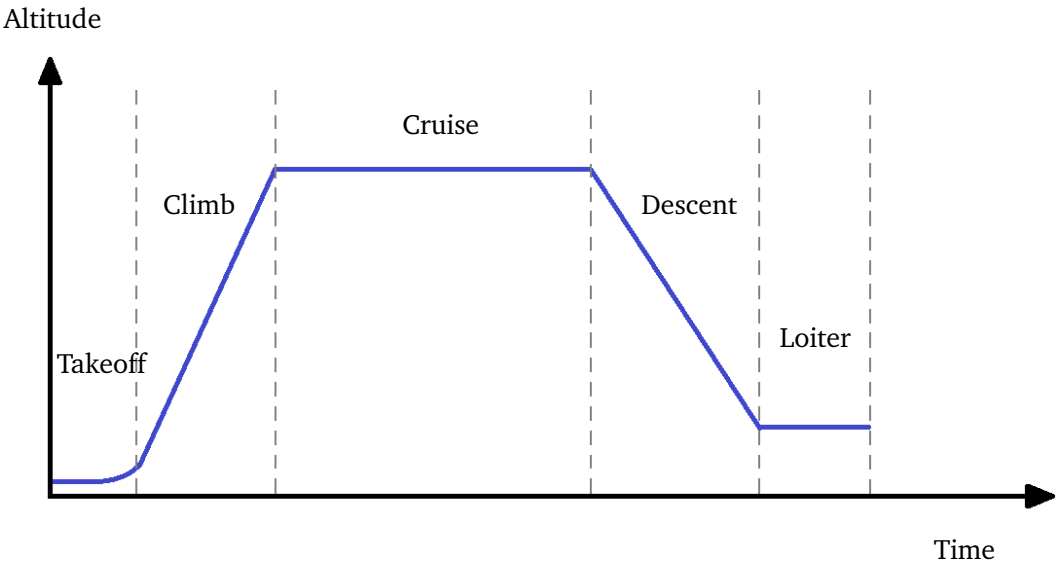

Figure 4.1: Considered mission profile. We can distinguish between two sub-phases of takeoff maneuver, the ground run and airborne phase, then climb, cruise, descent and loiter phase, at a higher altitude than takeoff. Landing phase is not considered, being short in time and characterized by low-power engine settings.

4.2 Sizing Procedure

The selected preliminary sizing procedure is here discussed. The first step is to determine payload mass, where crew is included in payload to consider a uniform notation for small aircraft; considering a distinction between pilot/crew and passengers, that are carrying luggage, the payload mass, expressed in kg, is obtained as:

$$M_P = N_{crew} \cdot 78 + N_{pax} \cdot 102 \tag{4.1}$$

The generic *weight breakdown* at this level is in the form:

$$M_{TO} = M_E + M_B + M_F + M_G + M_P \tag{4.2}$$

where takeoff (TO) mass is equal to the sum of, from left to right, empty (E) mass, batteries (B), fuel (F), generator (G) and payload (P). To treat empty mass in an uniform way with conventional aircraft design techniques, batteries are considered as fuel at this level, thus empty mass is corresponding to structure-plus-systems mass. As a first guess of maximum takeoff mass we will consider $M_0 = 4M_P$, under the assumption that payload mass is generally around 25% of maximum value; this is not true in case of specific aircraft, such as a hypothetical surveillance drone carrying only a small payload: in this case a proper suitable guess will be used. Once payload mass and guess starting maximum takeoff mass are estimated, an iterative loop on takeoff mass is needed to properly size all components; in the following subsections all the steps per loop are presented.

4.2.1 Aerodynamic data estimation

Starting from a required stall speed, that may be set either by certifications or by the designer, and an expected maximum landing-flap lift coefficient, the maximum wing loading is evaluated:

$$\left(\frac{W}{S}\right)_{max} = \frac{\rho_0 V_{ST}^2}{2C_{L_{max}}} \tag{4.3}$$

where ρ_0 is density at sea level and V_{ST} and $C_{L_{max}}$ are the aforementioned minimum stall speed and maximum flaps-down lift coefficients. The actual wing loading will be lower than the maximum one, to grant a little flexibility to the obtained solution; we can relate the final wing loading with the maximum one through a coefficient:

$$\left(\frac{W}{S}\right) = \eta_{WS}\left(\frac{W}{S}\right)_{max} \tag{4.4}$$

where unless specified otherwise a value of $\eta_{WS} = 0.98$ will be used. Wing reference surface will easily be obtained as:

$$S = \frac{M_{TO}g}{\left(\frac{W}{S}\right)} \tag{4.5}$$

and the wing span is obtained from aspect ratio λ, selected before the analysis, as $b = \sqrt{\lambda S}$; from the wing span a reference chord is calculated as $C_{ref} = S/b$, since at this stage we have no other geometrical information about the wing.

To evaluate parasite drag coefficient the method proposed by Roskam [38] is used: since the zero-lift drag coefficient C_{D_0} is related to parasite area f, its value may be obtained by a statistical regression relating f and the so called wetted area S_{wet}, which in turn can be related to takeoff mass. The set of equation is thus:

$$C_{D_0} = \frac{f}{S} \tag{4.6}$$

$$Log_{10}f = a + bLog_{10}S_{wet} \tag{4.7}$$

$$Log_{10}S_{wet} = c + dLog_{10}W_{TO} \tag{4.8}$$

where a, b, c and d are regression values depending on the type of aircraft; all areas are measured in square feet (ft^2) and takeoff weight in pounds (lb). Combining the previous equation together with proper conversion to S.I. units, the parasite drag coefficient is in the form:

$$C_{D_0} = \frac{0.3048^2}{S} 10^{a+b[c+dLog_{10}(2.2M_{TO})]} \tag{4.9}$$

Parameters a and b are related to aircraft friction coefficient c_f as in table 4.1, thus an estimate from Reynolds number is required and can be computed as:

$$C_f = \frac{0.1488}{Re_C^{0.2}} \tag{4.10}$$

c_f	0.0090	0.0080	0.0070	0.0060	0.0050	0.0040	0.0030	0.0020
a	-2.0458	-2.0969	-2.1549	-2.2218	-2.3010	-2.3979	-2.5229	-2.6990
b	1.0000	1.0000	1.0000	1.0000	1.0000	1.0000	1.0000	1.0000

Table 4.1: Correlation coefficients for parasite area, from [38].

where Re_C is the Reynolds number evaluated at cruise speed and altitude, using the previously obtained reference chord C_{ref}.

The analysis is completed by considering aircraft class, taking from 4.2 proper values for c and d. Once zero-lift drag coefficient has been estimated, polar drag relations can be written for clean and takeoff configurations as:

$$C_D = C_{D_0} + \frac{C_L^2}{\pi\lambda e} \tag{4.11}$$

$$C_{D_{TO}} = C_{D_0} + \Delta C_{D_{gear}} + \Delta C_{D_{flap}} + \frac{C_L^2}{\pi\lambda e_{TO}} \tag{4.12}$$

4.2.2 Empty mass estimation

Using statistical regression proposed by Roskam it is possible to estimate empty mass from takeoff mass as:

$$Log_{10}W_{TO} = A + BLog_{10}W_E \tag{4.13}$$

where coefficients A and B are taken from table 4.2.

Aircraft Type	A	B	c	d
Homebuilt	0.3411	0.9519	1.2362	0.4319
Single-Engine Propeller Driven	-0.1440	1.1162	1.0892	0.5147
Twin-Engine Propeller Driven	0.1063	1.0351	0.8635	0.5632
Agricultural	-0.4398	1.1946	1.0447	0.5326
Business Jet	0.2678	0.9979	0.2263	0.6977
Regional Turboprop	0.3874	0.9647	-0.0866	0.7699
Transport Jet	0.0833	1.0383	0.0199	0.7531
Military Bomber, Transport, Patrol	-0.2009	1.1037	0.1628	0.7316

Table 4.2: Statistical regression values relating empty weight and wetted surface to takeoff weight, from [38].

4.2.3 Performance estimation

Each phase is here characterized by an estimation on the average power needed, time and thus total required energy, that will be used to size electric motors, batteries and generator if present.

Takeoff

The takeoff maneuver is divided in two parts, namely ground run and airborne: in both cases power is an unknown value and implicit equations must be solved to obtain the required power to ensure to cover the required distance. Total takeoff run is divided in [38] as:

$$L_{TO} = L_{GR} + L_{AB} \tag{4.14}$$

where we consider that $L_{TO} = 1.66 L_{GR}$. In this way, we calculate the needed power during ground run, P_{GR}, by finding a value of P such that:

$$L_{GR} = \int_0^{V_{TO}} \frac{M_{TO} V}{\frac{P}{V_{TO}} - \frac{1}{2}\rho_{TO} V^2 S C_{D_{TO}}(C_{L_{TO}}) - \mu\left(Mg - \frac{1}{2}\rho_{TO} V^2 S C_{L_{TO}}\right)} \mathrm{d}V \tag{4.15}$$

where we consider that the maximum propeller traction is found at takeoff speed, since at low speed the ratio $\frac{P}{V}$ would lead to unrealistic values. The takeoff speed is considered to be such that vertical equilibrium is granted for a scaled [38] lift coefficient with respect to the chosen one [1]:

$$V_{TO} = \sqrt{\frac{2Mg}{\rho_{TO} S \frac{C_{L_{TO_{max}}}}{1.21}}} \tag{4.16}$$

The airborne phase is considered to be carried out on an arc characterized by a radius R and a climb angle γ satisfying the relations:

$$L_{AB} = R \sin\gamma \tag{4.17}$$

$$h_{AB} = R(1 - \cos\gamma) \tag{4.18}$$

where h_{AB} is the obstacle height, with a value of 35 ft for CS-25 certified aircraft and 50 ft for CS-23 certified ones. The climb angle γ is used to obtain required power with the explicit relation:

$$P_{AB} = \frac{1}{2}\rho_{TO} V_{TO}^3 S C_{D_{TO}}(C_{L_{TO}}) + M_{TO} g V_{TO} \sin\gamma \tag{4.19}$$

The takeoff power P_{TO} is thus the maximum value between P_{GR} and P_{AB}. Concerning takeoff time, a simple estimation can be carried out by considering to cover the whole distance at takeoff speed, thus:

$$T_{TO} = \frac{L_{TO}}{V_{TO}} \tag{4.20}$$

The required energy is obtained by multiplying takeoff time, scaled in hours, with takeoff power:

$$E_{TO} = P_{TO} \frac{T_{TO}}{3600} \tag{4.21}$$

[1] Maximum lift coefficient with flaps in takeoff position, generally it differs from landing value.

Climb

The climb phase is characterized by two constraints: All Engine Operative (AEO) and One Engine Inoperative (OEI), unless a single-engine aircraft is considered. Climb power is obtained by considering an average density at midway altitude between takeoff and cruise:

$$P_{CL} = \frac{1}{\eta_P}\left[\frac{1}{2}\rho_{CL}V_{CL}^3 S C_D(C_{L_{CL}}) + V_{V_{CL}} M_{TO} g\right] \tag{4.22}$$

where we considered maximum takeoff mass in our calculations to be conservative in estimating the needed power and thus energy; climb lift coefficient is calculated as usual by enforcing vertical equilibrium.

In case of one engine inoperative, we apply CS-23 certification [2] and consider a minimum rate of climb of $0.027V_{ST}^2$, where horizontal speed is in knots and rate of climb in feet per minute; in S.I. units the required power is:

$$P_{CL_{OEI}} = \frac{N_E}{N_E - 1}\frac{1}{\eta_P}\left[\frac{1}{2}\rho_{OEI}V_{TO}^3 S C_D(C_{L_{TO}}) + 3.6 \cdot 10^{-4} V_{ST}^2 M_{TO} g\right] \tag{4.23}$$

where an altitude of 5000 ft is considered from certifications. The needed time to climb is calculated from AEO rate of climb, as:

$$T_{CL} = \frac{Z_{CR} - Z_{AIR}}{V_{V_{CL}}} \tag{4.24}$$

where Z_{CR} and Z_{AIR} are cruise and airport altitude respectively. The overall required energy is simply:

$$E_{CL} = P_{CL}\frac{T_{CL}}{3600} \tag{4.25}$$

The covered distance during climb phase may be calculated using average climb speed, thus:

$$R_{CL} = V_{CL} T_{CL} \tag{4.26}$$

Descent

We can consider descent as for climb phase, without the requirement on one engine inoperative case; power, time, energy and covered distance are respectively:

$$P_{DS} = \frac{1}{\eta_P}\left[\frac{1}{2}\rho_{DS}V_{DS}^3 S C_D(C_{L_{DS}}) + V_{V_{DS}} M_{TO} g\right] \tag{4.27}$$

$$T_{DS} = \frac{Z_{LT} - Z_{CR}}{V_{V_{DS}}} \tag{4.28}$$

where Z_{LT} is the loiter altitude; we consider vertical speed to be negative, since we are descending.

$$E_{DS} = P_{DS}\frac{T_{DS}}{3600} \tag{4.29}$$

$$R_{DS} = V_{DS} T_{DS} \tag{4.30}$$

[2] We simplify the problem by only considering CS-23 environment since CS-25 certifications are posing requirements on climb gradients, which are more complex to handle.

Cruise

The needed power during cruise phase is obtained by:

$$P_{CR} = \frac{1}{\eta_P}\left[\frac{1}{2}\rho_{CR}V_{CR}^3 S C_D(C_{L_{CR}})\right] \tag{4.31}$$

Cruise time depends on the needed distance to cover in this phase, which in turn depends on covered distance during climb and descent phases:

$$R_{CR} = R_{REQ} - R_{CL} - R_{DS} \tag{4.32}$$

where R_{REQ} is the total required range; thus cruise time is:

$$T_{CR} = \frac{R_{CR}}{V_{CR}} \tag{4.33}$$

Cruise energy is obtained as usual from power:

$$E_{CR} = P_{CR}\frac{T_{CR}}{3600} \tag{4.34}$$

Loiter

The loiter phase is carried out for a requested amount of time at the most favorable aircraft attitude; [39] shows that, for a propeller-driven aircraft, the most favorable attitude to maximize aircraft endurance is the one maximizing the quantity $C_L^{1.5}/C_D$. This is true for airplanes using conventional propulsion, but it has been observed that this relation holds also for electric aircraft, since overall required power at maximum $C_L^{1.5}/C_D$ is found to be lower than at maximum aerodynamic efficiency C_L/C_D. Loiter speed is thus obtained by finding the lift coefficient at maximum $C_L^{1.5}/C_D$, considering a polar $C_D - C_L$ relationship up to takeoff lift coefficient, and comparing the result with stall speed:

$$V_{LT} = \max\left[\sqrt{\frac{2M_{TO}g}{\rho_{LT}SC_{L_{LT}}}}, V_{ST}\right] \tag{4.35}$$

Required power and energy are thus

$$P_{LT} = \frac{1}{\eta_P}\left[\frac{1}{2}\rho_{LT}V_{LT}^3 S C_D(C_{L_{LT}})\right] \tag{4.36}$$

$$E_{LT} = P_{LT}\frac{T_{LT}}{60} \tag{4.37}$$

where we consider loiter time in minutes.

4.2.4 Generator model

Before analyzing sizing procedure for batteries a description of the used generators is needed: for the hybrid-electric case, as discussed in next section, we will split energy requirement between batteries and fuel, depending on generator efficiency. Two different generators have been considered: turboshaft and four-stroke gasoline reciprocating engines.

Turboshaft

The thermodynamic cycle of a turboshaft engine is modeled as suggested by Hill-Peterson [40]; starting from Mach number at given altitude, we can analyze total pressure and total temperature in each phase:

1. Intake: air enters at atmospheric pressure and temperature at given altitude in the diffuser (D)

$$T_{01} = T_1\left(1 - \frac{\gamma_D - 1}{2} M_1^2\right) \tag{4.38}$$

$$P_{01} = P_1\left[1 + \eta_D\left(\frac{T_{01}}{T_1} - 1\right)^{\frac{\gamma_D}{\gamma_D - 1}}\right] \tag{4.39}$$

2. Compression: air is compressed by the compressor (C)

$$T_{02} = T_{01}\frac{\Pi^{\frac{\gamma_C - 1}{\gamma_C}}}{\eta_C} \tag{4.40}$$

$$P_{02} = P_{01}\Pi \tag{4.41}$$

   where pressure ratio Π is fixed as an engine required parameter.

3. Combustion: air and fuel are mixed in the burner (B)

$$T_{03} = T_{02}\frac{f\,\eta_B Q_f + c_p T_{02}}{c_p(1+f)T_{02}} \tag{4.42}$$

$$P_{03} = P_{02}\eta_B \tag{4.43}$$

   where Q_f is fuel Low Heat Value (LHV) expressed in kJ kg^{-1} and f is fuel-to-air overall mass flow rate ratio, fixed at 0.02 [40].

4. Expansion: exhaust gases are expanded down to atmospheric pressure in the turbine (T) section

$$P_{04} = P_{01} \tag{4.44}$$

$$T_{04} = T_{03}\frac{\frac{P_{03}}{P_{04}}^{\frac{\gamma_T - 1}{\gamma_T}}}{\eta_T} \tag{4.45}$$

Efficiency η_i and air specific heat ratio γ_i for the generic i-th phase are taken from ref [40] and shown in table 4.3:

	Diffuser D	Compressor C	Burner B	Turbine T
Efficiency η	0.97	0.90	0.96	0.90
Specific heat ratio γ	1.4	1.37	N/A	1.33

Table 4.3: Experimental values used for turboshaft model, from [40].

The overall power is obtainable from fuel mass flow rate m_f:

$$P = \frac{m_f}{f}\eta_A c_p \left[(1+f)(T_{03}-T_{04})-(T_{02}-T_{01})\right] \tag{4.46}$$

where $\eta_A = 0.87$ from [40]; considering that in our calculations we will fix required power from flight mechanics simulation, we will manipulate the previous equation to obtain m_f for a given required power P. Overall efficiency is found as:

$$\eta = \frac{(T_{03}-T_{04})-(T_{02}-T_{01})}{T_{03}-T_{02}} \tag{4.47}$$

Reciprocating Engine

Four-stroke reciprocating engine performance is simulated as for turboshaft case by considering the evolution of temperature, pressure and specific volume of air or air-fuel mixture in each phase of the thermodynamic cycle, as follows:

1. Pre-Compression: a turbocharger pre-compresses incoming air up to maximum achievable pressure or design pressure, depending on altitude

$$\Pi = \min\left[\frac{P_D}{P_0}, \Pi_{max}\right] \tag{4.48}$$

   where P_D is design pressure, P_0 external pressure at given altitude and Π_{max} the maximum allowed pressure ratio. Temperature, pressure and specific volume are:

$$T_1 = T_0 \Pi^{\frac{\gamma-1}{\gamma}} \tag{4.49}$$

$$P_1 = P_0 \Pi \tag{4.50}$$

$$v_1 = R\frac{T_1}{P_1} \tag{4.51}$$

2. Compression: real compression is considered starting from ideal volume ratio τ;

$$v_2 = \frac{v_1}{\tau}[x_R(\tau-1)+1] \tag{4.52}$$

   where $x_R = 0.1$; real volume ratio is $r = \frac{v_2}{v_1}$. Temperature and pressure are:

$$T_2 = T_1 r^{\gamma-1} \tag{4.53}$$

$$P_2 = P_1 r^{\gamma} \tag{4.54}$$

3. Combustion: real combustion is considered starting from the corrected volume:

$$v_c = \frac{2}{3}\left(v_2 - \frac{v_1}{\tau}\right) \tag{4.55}$$

Combustion temperature is:

$$T_3 = \frac{\frac{\eta_B Q_f}{1+\alpha} + \nu_c P_2 + c_\nu T_2}{c_\nu + \frac{\nu_c R}{\nu_1}} \tag{4.56}$$

where $\alpha = 14.8$ as air-to-fuel ratio for optimal low fuel consumption operation, and $\eta_B = 0.70$ is burner efficiency.

4. Expansion: only exhaust temperature is needed and calculated as:

$$T_4 = T_3 r^{1-\gamma} \tag{4.57}$$

Total and turbocharger work can be computed as:

$$W_T = \frac{\eta_B Q_f}{1+\alpha} - c_\nu (T_4 - T_1) \tag{4.58}$$

$$W_C = c_p \frac{T_0}{\eta_C} \left[\Pi \left(1 - \frac{1}{\gamma} \right) \right] V \rho_0 \tag{4.59}$$

where V is engine displacement and $\eta_C = 0.95$ is turbocharger efficiency. At this stage it is possible to evaluate engine efficiency as a function of rotational speed, which is a function of a set of efficiencies: thermal η_T, real work η_0 and real power λ_ν. Thermal efficiency is estimated as:

$$\eta_T = 1 - V^{1-\gamma} \tag{4.60}$$

thus we define η_R as:

$$\eta_R = \frac{W_T}{\eta_T \frac{Q_f}{1+\alpha}} \tag{4.61}$$

overall power efficiency as a function of engine RPM N is:

$$\eta_P(N) = \eta_R \eta_0(N) \lambda_\nu(N) \tag{4.62}$$

where $\eta_0 - N$ and $\lambda_\nu - N$ relationship have been interpolated from experimental data. Overall engine efficiency will be:

$$\eta(N) = \eta_R \eta_0(N) \eta_T \lambda_\nu(N) \tag{4.63}$$

While total power is:

$$P(N) = \frac{N}{120} \left[\eta_P(N) \eta_T \frac{Q_f}{1+\alpha} \frac{V}{\nu_1} - |W_C| \right] \tag{4.64}$$

where the number of power strokes per second is considered [3] and turbocharger work W_C is subtracted to the total effective work. As for the case of turboshaft engine, power is an input, while fuel mass flow rate is an unknown: in our solution we will have to obtain both rotational speed N and fuel consumption m_f considering the following relationship between the two:

$$m_f = \frac{N}{120} \frac{V}{\nu_1 \alpha} \tag{4.65}$$

[3] Out of N rotations only $N/2$ are power strokes.

4.2.5 Motor and battery sizing

Once all phases have been analyzed, we can fix both power and energy requirements:

$$P_{max} = \max\left[P_{TO}, P_{CL}, P_{CL_{OEI}}, P_{CR}, P_{DS}, P_{LT}\right] \tag{4.66}$$

$$E_{tot} = E_{TO} + E_{CL} + E_{CR} + E_{DS} + E_{LT} \tag{4.67}$$

maximum motor power is then scaled as done for wing loading case: $P_{mot} = \frac{P_{max}}{\eta_{WP}}$, where $\eta_{WP} = 0.98$ unless specified otherwise. A distinction in further procedure is made, depending on the type of aircraft under study: we shall distinguish between all-electric, hybrid-electric and simulated conventional aircraft.

All-Electric

As done by [31], batteries are simply sized by power and energy requirements as follows:

$$M_B = \max\left[\frac{P_{mot}}{W_{SP}}, \frac{E_{av}}{E_{SP}}\right] \tag{4.68}$$

where $E_{av} = \frac{E_{tot}}{1-\zeta_{emer}}$, considering the emergency battery fraction ζ_{emer} we wish to spare.

Hybrid-Electric

In case of serial hybrid-electric propulsion only power requirement holds while sizing battery mass: the total energy is split between batteries and fuel; the selected procedure is as follows:

- Generator is sized considering cruise power:

$$P_{gen} = P_{CR}\frac{\chi_G}{\eta_{alt}} \tag{4.69}$$

  where η_{alt} is alternator efficiency and χ_G the ratio between ideal generator power and cruise power. Generator mass is then obtained from power and the selected power-to-weight ratio, depending on the used engine.

- Available mass for *energy system* is then computed from masses calculated so far:

$$M_{ES} = M_{TO} - M_E - M_P - M_G \tag{4.70}$$

- We seek for a solution that allows to cover all energy with a battery-fuel combination that does not exceed available mass, thus a solution satisfying the two constraints:

$$\begin{cases} M_B + M_F = M_{ES} \\ E_B + E_F = E_{tot} \end{cases} \tag{4.71}$$

  the second equation can be manipulated such that both battery and fuel energy are a function of corresponding mass. First of all we consider that we may wish to store some extra energy in batteries, thus a scaling factor on specific energy shall be considered; then we must estimate generator efficiency, by running a

simulation at a given flight condition, i.e. cruise phase. The second equation becomes:

$$M_B E_{SP_B}(1-\zeta_{min}) + M_F E_{SP_F}\eta_G\eta_{alt} = E_{tot} \tag{4.72}$$

where both generator and alternator efficiencies are considered. The system can be written in matrix form as:

$$\begin{bmatrix} 1 & 1 \\ E_{SP_B}(1-\zeta_{min}) & E_{SP_F}\eta_G\eta_{alt} \end{bmatrix} \begin{bmatrix} M_B \\ M_F \end{bmatrix} = \begin{bmatrix} M_{ES} \\ E_{tot} \end{bmatrix} \tag{4.73}$$

- Battery mass is thus estimated from:

$$M_B = \max\left[\frac{P_{mot}}{W_{SP}}, M_{B_{sys}}\right] \tag{4.74}$$

where $M_{B_{sys}}$ is battery mass calculated solving the system from the previous step.

At this point two considerations can be made: first of all, battery mass coming from these results may be too large to lead to a solution to the iterative process, and then we are not granted that available *energy system* mass is enough to lead to a solution of the previous system of equations. For these reasons a check is made on battery mass fraction, to be between prescribed bounds.

4.2.6 Fuel mass sizing

As discussed above, a proper analysis on needed fuel, if present, is made once battery mass is fixed. First of all, we consider required fuel energy, as:

$$E_F = \frac{E_{tot} - M_B E_{SP_B}(1-\zeta_{min})}{1-\xi_{min}} \tag{4.75}$$

where ζ_{min} is the minimum battery energy fraction that we want to save and ξ_{min} the minimum fuel level that we want to spare. At this point, the needed fuel mass is:

$$M_F = \frac{E_F}{E_{SP_F}\eta_G\eta_{alt}} \tag{4.76}$$

In case of a simulated conventional aircraft, all energy is considered to be provided by fuel, while a fictitious battery with unrealistic values of specific power and energy of 10^8 W kg^{-1} and 10^8 Wh kg^{-1} respectively is sized following hybrid-electric procedure.

4.2.7 Weight correction

Since previously considered empty weight estimation was based on a population of conventional aircraft, a correction must be provided. A suitable population of electric motors is reported in table 4.4; we can consider a linear relationship resulting from the regression as:

$$M_{EM} = 1.9309 + 0.1933 \cdot P \tag{4.77}$$

where P is expressed in kW and M_{EM} in kg. Concerning thermal engines, Roskam [38] shows that a suitable relationship is:

$$M_{TE} = 0.1860 \cdot P \tag{4.78}$$

Electric Motor	Aircraft	Power [kW]	Mass [kg]
Siemens SP260D	Extra 330LE	260	50
Emrax 348	N.Av.	170	40
N.Av.	Pipistrel Alpha Electro	85	14
N.Av.	Pipistrel Taurus Electro	40	11

Table 4.4: Electric motors population.

again where P is expressed in kW and M_{TE} in kg. We can plot the two lines in figure 4.2 and observe that Siemens' statement of scalable motor performance holds. At this point we simply subtract the resulting mass from thermal engines, embedded in the regression on empty weight fraction, and add the corresponding motor mass. Error is computed on empty mass fraction, as:

$$err = m_E - (1 - m_P - m_B - m_F) \tag{4.79}$$

where $m_{()} = \frac{M_{()}}{M_{TO}}$. Guess takeoff mass is updated as $M_{TO} = M_{TO_{old}}(1 + err)$.

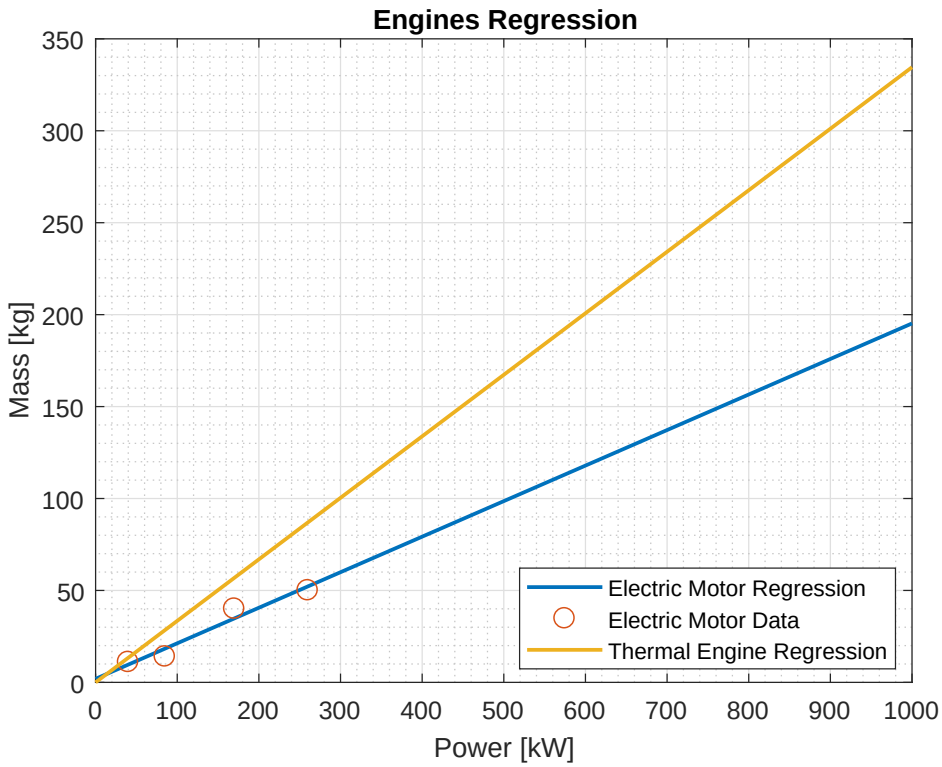

Figure 4.2: Mass-Power regression for electric motors and thermal engines.

4.3 Flight Simulation

A realistic estimation of energy consumption requires a detailed simulation of each flight phase, allowing to track step-by-step the required power, and thus energy, and also to consider a charging strategy for the generator. Since we are interested in analyzing different possible strategies, both from the point of view of the generator and flight profile, the most general procedure is considered.

Starting from preliminary sizing of aircraft conducted following the above procedure, performance is simulated by considering the following variables:

#	Variable	Symbol	Unit
1	Time	T	[s]
2	Horizontal Distance	X	[m]
3	Vertical Distance	Z	[m]
4	Horizontal Speed	V	[m s^{-1}]
5	Engine Power	P	[W]
6	Consumed Motor Energy	E	[Wh]
7	Horizontal Acceleration	a	[m s^{-2}]
8	Vertical Speed	V_v	[m s^{-1}]
9	Lift Coefficient	C_L	[-]
10	Specific Excess Power	SEP	[m/s]
11	Generator Temperature	T_G	[K]
12	Generator Energy	E_{gen}	[Wh]
13	Equivalent Specific Fuel Consumption	$ESFC$	[kg kWh^{-1}]
14	Battery Energy	E_{batt}	[Wh]
15	Battery Level	l_B	[-]
16	Tank Level	l_F	[-]
17	Throttle Level	δ_G	[-]

Table 4.5: Set of simulation variables.

Each main flight phase is then simulated step-by-step by considering the evolution of all these parameters, starting from information regarding the previous phase. The mission envelope is thus described as:

- Takeoff: the simulation is initialized by considering takeoff time, speed, altitude and power and overall energy consumed in this phase;
- Climb: regardless of the strategy, climb ends when both cruise speed and altitude are reached;
- Cruise: the cruise phase is conducted until the required range is covered, considering that the cumulative horizontal distance shall be

$$\bar{X}_{CR} = R_{req} - R_{DS} \tag{4.80}$$

where $\bar{X}_{CR} = X_{DS} + X_{CR}$ is the cumulative distance up to cruise phase, R_{req} the required total range and R_{DS} the estimated range that will be covered during the

descent phase. Cruise will thus end either when battery levels drop below a safety threshold or when wanted cruise range is covered.

- Descent: same as for climb, this phase ends when both loiter speed and distance are covered;
- Loiter: the loiter phase is conducted at fixed loiter speed for the given amount of time.

Once the simulation of the mission envelope is completed, ending battery and tank levels are verified and if they do not satisfy the prescribed requirements ζ_{min} and ξ_{min} as discussed above, a correction will be provided and simulation restarted, as shown in following sections.

4.3.1 Flight phase simulation

All phases, with the exception of takeoff one where we consider only the ending time instant to initialize climb, are simulated using the same framework for the sake of generality. Considering a fixed time step Δt, at a generic time instant t we can write:

$$W_t = \left[M_{TO} - (1 - l_{F_t})M_F\right] g \tag{4.81}$$

where aircraft weight at time t is obtained by subtracting the amount of burned fuel up to that instant. Atmospheric parameters are obtained by International Standard Atmosphere (ISA) data at given altitude Z_t such that aerodynamic coefficients may be evaluated:

$$C_{L_t} = \frac{2W_t}{\rho_{Z_t} V_t^2 S} \tag{4.82}$$

$$C_{D_t} = C_{D_0} + \frac{C_{L_t}^2}{\pi \lambda e} \tag{4.83}$$

The maximum Specific Excess Power (SEP) is thus:

$$SEP_{max_t} = \frac{1}{W_t}\left(P_{max} - \frac{1}{2}\rho_{Z_t} V_t^3 S C_{D_t} \frac{1}{\eta_P}\right) \tag{4.84}$$

At this point the generator performance, if present, may be computed given the required performance with current power requirement. Considering a generic strategy, we compute generator throttle δ_G as a function of simulation variables, namely aircraft altitude and battery/tank levels, and target charge settings, depending on the strategy. The required generator power is, thus:

$$P_{G_t} = P_{G_{max}} \delta_G(Z_t, l_{B_t}, l_{F_t}, s) \tag{4.85}$$

where s includes strategy charge settings. Generator fuel mass flow rate, efficiency and exhaust gas temperature are then computed by solving the cycle corresponding to selected engine described in section 4.2.4. We can evaluate specific fuel consumption and energy transferred to batteries as:

$$ESFC_t = \frac{3.6 m_{f_t}}{\delta_{G_t} P_{G_{max}}} \tag{4.86}$$

$$\dot{E}_{G_t} = m_{f_t} E_{SP_F} \eta_G \eta_{alt} \tag{4.87}$$

where conversion to kg kWh^{-1} is provided for ESFC. Variables evolution is carried on by considering requested horizontal and vertical speed, depending on the flight strategy and phase. Since our discussion considers a general procedure, these targets will be taken from a given flight strategy, thus allowing investigation of possible new strategies not involving, for example, constant speed/altitude cruise.

Given the generic strategy we can thus get target speed V_{req} and $V_{v_{req}}$; vertical speed is considered to be reachable in a quasi-static manner, thus not considering vertical acceleration, while horizontal speed target is met by considering horizontal acceleration. Real aircraft application involve flight control system with sophisticated control strategies to minimize fuel burn, which is far beyond the scope of this work; we consider a fictitious PD controller working on horizontal speed error $e_V = V_{req} - V$ as;

$$a = K_P e_V + K_D \frac{\Delta e_V}{\Delta t} \tag{4.88}$$

where values of 0.05 [s^{-1}] and 0.1 [-] for proportional and derivative coefficients have been used. A saturation on maximum positive and negative acceleration is taken into account to avoid unwanted and unrealistic overshoots.

To assess actual variables evolution we start by considering previously computed maximum Specific Excess Power; for a generic aircraft during climb in horizontal accelerated flight, horizontal equilibrium may be computed as:

$$T = D + M\dot{V} + Mg\sin\gamma \tag{4.89}$$

switching from forces to powers by multiplying both members by airspeed V and rearranging we obtain:

$$P = P_{req} + Mg\left(\frac{\dot{V}}{g}V + V\sin\gamma\right) \tag{4.90}$$

where $V\sin\gamma$ is vertical speed. Thus the term in brackets can be rewritten as:

$$\frac{a}{g}V + V_v = SEP \tag{4.91}$$

From computed acceleration a, required vertical speed and maximum SEP, we can here verify if we have enough power to satisfy above requirements. If not, SEP is split between vertical speed and horizontal acceleration:

$$V_{v_t} = \chi_{RC} \cdot SEP \tag{4.92}$$

where $\chi_{RC} = 0.75$ unless specified otherwise; acceleration is eventually obtained by manipulating equation 4.91.

The evolution of variables is thus:

- Horizontal distance:

$$X_{t+\Delta t} = X_t + V_t \Delta t \tag{4.93}$$

- Altitude:

$$Z_{t+\Delta t} = Z_t + V_{v_t} \Delta t \tag{4.94}$$

- Horizontal speed:
$$V_{t+\Delta t} = V_t + a_t \Delta t \tag{4.95}$$
- Motor power:
$$P_{t+\Delta t} = \frac{1}{2}\rho_{Z_t} V_t^3 S C_{D_t} \frac{1}{\eta_P} + W_t \left(\frac{a_t}{g} V_t + V_{v_t} \right) \tag{4.96}$$
- Motor cumulative energy:
$$E_{t+\Delta t} = E_t + P_t \frac{\Delta t}{3600} \tag{4.97}$$
- Battery charge:
$$E_{batt_{t+\Delta t}} = E_{batt_t} + \left(\dot{E}_{G_t} - \frac{P_t}{3600} \right) \Delta t \tag{4.98}$$
where $\dot{E}_{G_t}$, as we defined it, is an energy rate, thus expressed in Wh s^{-1}.
- Fuel level:
$$l_{F_{t+\Delta t}} = l_{F_t} - \frac{\dot{m}_F \Delta t}{M_F} \tag{4.99}$$

4.3.2 Flight envelope simulation

The overall envelope, as anticipated, is simulated by considering all the flight phases in chain, from takeoff initialization to loiter end. The final covered distance is compared to requested range and a correction is provided; this happens because descent phase is not carried out at constant fixed speed but the aircraft shall decelerate from cruise to descent speed: for this reason it has been observed that distance covered in descent phase is larger than predicted and thus overall distance is greater than needed.

After a second iteration to correct the total range battery and fuel levels l_B and l_F are checked and compared to requested values ζ_{min} and ξ_{min}. Correction on these values is based on the assumption that overall error is small and thus there is no need to re-design the aircraft: considering the 2% margin we took on both wing loading and power loading it is possible to add battery and/or fuel mass, depending on the case; we shall distinguish three cases, depending on the type of simulated airplane.

All-Electric

Only battery final energy is considered, due to lack of generator and fuel; if battery level at final time instant $l_{B_{tf}}$ is less than ζ_{min}, correction is provided. In this simple case, correction is:
$$\Delta M_B = M_B(\zeta_{min} - l_{B_{tf}}) \tag{4.100}$$
Aircraft mass, wing loading, power loading and battery energy are thus updated and a new envelope simulation is started.

Conventional

If a simulated conventional airplane is considered, the same above procedure is considered; the error tank level $l_{F_{tf}}$ is compared to ξ_{min} and correction is provided as before:
$$\Delta M_F = M_F(\xi_{min} - l_{F_{tf}}) \tag{4.101}$$

once again, all relevant aircraft parameters are updated.

Hybrid-Electric

As for airplane sizing, the hybrid-electric case generally involves the need to split correction both on batteries and on fuel: if both levels are below selected minimum threshold a correction is provided to rely on fuel as much as possible, so that mass increment is reduced. We define χ_B as the amount of battery error correction, thus:

$$\Delta M_B = M_B \chi_B (\zeta_{min} - l_{B_{tf}}) \tag{4.102}$$

$$\Delta M_F = M_F(\xi_{min} - l_{F_{tf}}) + \frac{E_B}{E_{SP_F}\eta_G\eta_{alt}}(1-\chi_B)(\zeta_{min} - l_{B_{tf}}) \tag{4.103}$$

where battery energy correction due to fuel is carried out by considering that the required energy is provided by the generator. As before, aircraft parameters are then updated.

4.3.3 Flight phase strategies

As anticipated in the prevous section the general considered procedure allows for flexible definition of both flight path, described in this section, and charging strategies, described in the next one. Two flight strategies have been considered: one where climb and descent phases are carried out at constant true airspeed (TAS) while the other at constant equivalent airspeed (EAS). Given the similarities between the two strategies a common description is provided:

- Climb: the final target is to reach both cruise speed and altitude. Until cruise altitude is not met, target vertical speed is set to prescribed rate of climb, while target horizontal speed depends on the two strategies:
  - Constant TAS: $V_{req} = V_{CL}$
  - Constant EAS: $V_{req} = \min\left[V_{CL}\sqrt{\frac{\rho_{SL}}{\rho}}, V_{CR}\right]$

  when cruise altitude is met, the required vertical speed is set to zero and the required horizontal speed is set to cruise speed.
- Cruise: target vertical speed is set to zero and target horizontal speed is cruise speed. The cruise phase lasts until cumulative covered distance reaches the estimated value $\bar{X}_{CR} = R_{req} - R_{DS}$ or when battery level drops below emergency threshold ζ_{emer}.
- Descent: as for climb phase, the final target is to reach both loiter speed and altitude. Vertical speed is set to the prescribed rate of descent, while horizontal speed depends on strategy:
  - Constant TAS: $V_{req} = V_{DS}$
  - Constant EAS: $V_{req} = \max\left[V_{DS}\sqrt{\frac{\rho_{SL}}{\rho}}, V_{LT}\right]$
- Loiter: being at a constant altitude, the required vertical speed is zero; target horizontal speed is set as previously calculated loiter speed. The loiter phase ends after prescribed time was covered or if batteries are depleted.

4.3.4 Generator control strategies

Regardless of the chosen generator type, a control strategy must be employed. Two different strategies have been considered; in both cases a transition below which generator operates only in emergency situations, when battery level is such that $l_B \leq \zeta_{emer}$.

- Steady strategy: it aims at keeping the battery at a constant maximum level ζ_{max} to start burning fuel as soon as possible, reducing aircraft mass early, thus requiring less energy. Generator stops when fuel level drops below a minimum threshold ξ_{min}: in this case the aircraft runs on battery power only, down to minimum threshold ζ_{min}; in this case the generator is turned on again to keep this battery level. Since final tank level will be below minimum wanted fraction, a new iteration of the flight envelope will be needed.
- Cyclic strategy aims at charging the battery up to a given level only when it drops down below a certain threshold. Since the generator is turned off at the beginning of the mission, it will start charging batteries when the state of charge drops below ζ_{min}, and stops when it reaches ζ_{max}, cycling in this way until fuel drops below ξ_{min}. In this case the generator mode will be as for the previous case.

Both strategies rely on a fictitious PID controller on battery level error to simulate realistic generator behavior; the controller is used to obtain generator throttle:

$$\delta_G = K_P e_P + K_I \int_0^t e_P(\tau)\mathrm{d}\tau + K_D \dot{e}_P \tag{4.104}$$

where $e_P = \bar{l}_B - l_B$ is the error between desired battery level $\bar{l}_B$ and actual one l_B. Saturation is considered if throttle value is above 1 or below 0 and the new error is recomputed accordingly. Used values for the coefficients are 15 [-], 0.075 [s] and 150 [s^{-1}] for proportional, integral and derivative coefficients respectively.

4.4 Implementation of *Hyperion* Program

This procedure has been implemented in the *Hyperion* (HYbrid PERformance simulatION) program, which will be used to obtain results and parametric analyses carried out in next chapters. A brief description of the overall procedure is here presented.

4.4.1 Input data

The required input data are provided by a text file written by the user or automatically by the program using the command window; five groups of values are considered: aircraft data, drag estimation, required performance, hybrid and battery data, and simulation settings.

- Aircraft: takeoff and landing maximum lift coefficients, aspect ratio, Oswald efficiency factor, propeller efficiency, number of crew and passengers, number of engines.
- Drag estimation: aircraft type, ΔC_{D_0} due to flaps at takeoff and landing gear, Oswald efficiency factor at takeoff.

- Performance: stall, cruise, descent and cruise speed, airport, loiter and cruise altitude, rate of climb and of descent, loiter time, takeoff field length, target range.
- Hybrid: propulsion type (all-electric, hybrid-electric or conventional), type of generator (GT or ICE), pressure/volume ratio (depending on the generator), generator power-to-weight ratio, alternator efficiency, ζ_{min}, ζ_{max}, ξ_{min}.
- Battery: specific power and specific energy, minimum and maximum weight fraction, ζ_{emer}.
- Settings: measurement units for length, horizontal speed and vertical speed.

4.4.2 Program overview

A brief overview on the program is presented. The analysis starts with `GetData` function, which collects previously described values either by an already existing file or a `.mat` variables set, or is written by the user through `WriteFile` function, where all fields are filled with aid of `messenger` function, providing questions and required help. The input file is read by `reader`, building all needed structures to start the sizing process; if a `.mat` file is used this process is not needed: the user may change all variables using a simple `keyboard` command.

Airplane preliminary sizing is conducted following procedure described in Section 4.2 through `AircraftSizing` function, using all information coming from input file and `ExtraSettings`, where all sizing and simulation settings are stored.

The simulation starts at the end of the takeoff phase: function `Takeoff` sets initial values and through function `initialize` the simulation starts. Each phase is simulated by the routine `FMS`, which uses vectors as input and output: to handle variables in a simple way, the whole *Hyperion* program uses structures, such that no array order has to be known to the user. To handle this, two simple functions, namely `Struct2Mat` and `Mat2Struct` provide data conversion. Each output is then used to initialize the subsequent phase.

When all flight phases have been analyzed, results are verified as discussed in Section 4.3.2 and, if a correction was needed, the simulation loop restarts. If convergence was achieved, the two functions `PostProcess` and `PlotResults` collects all results both in a text file and plot variables evolution respectively; if the user desires, a `.mat` file is then created, storing all results, with corresponding input data.

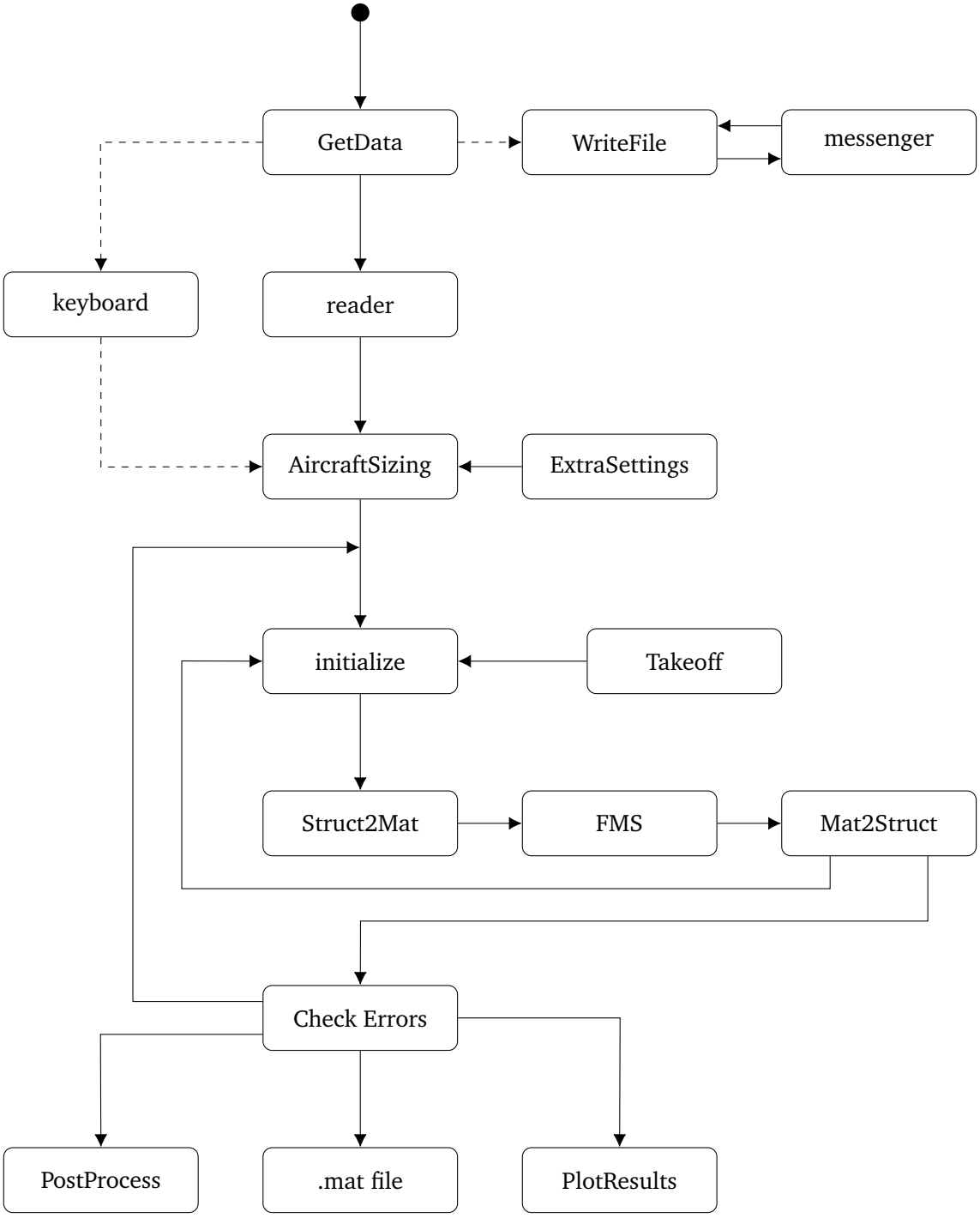

Figure 4.3: *Hyperion* program scheme.

Chapter 5

Results, Validation and Design Examples

Starting from the previously described procedure, results are now presented using the *Hyperion* program: after a proper validation using reference airplanes, some design examples are provided.

5.1 Results and Validation

The results are divided in two main categories: aircraft sizing and performance output, and a set of plots describing time evolution of all relevant quantities considered in flight simulation, with a special focus on three key parameters: battery and fuel tank levels, and generator throttle. The validation is conducted by comparing program's results with existing aircraft: due to lack of hybrid-electric airplanes for most of the classes, a simulated conventional aircraft will be considered.

This validation process will be carried out by considering reference data obtained from aircraft data-sheet, listed in table 5.1, while all other needed data, such as lift coefficients, landing gear and flap drag coefficients, and so on, are estimated.

	General aviation	Micro feeder	Commuter	Large regional	Unit
Takeoff run	530	580	1100	1340	m
Climb speed	130	120	170	170	kn
Rate of climb	1150	1500	2615	1350	ft min^{-1}
Cruise speed	175	190	280	275	kn
Cruise altitude	12000	10000	20000	25000	ft
Range	830	1200	1300	1530	km
Passengers	3	9	19	70	-
Pilots/Crew	1	2	2	4	-
Reference Aircraft	Panthera Hybrid	Tecnam P2012	Beech 1900D	ATR 72-600	

Table 5.1: Input data for validation processes.

5.1.1 General aviation

The selected general aviation aircraft is Pipistrel Panthera Hybrid, with estimated requirements taken from [56] and listed in table 5.1. Since this aircraft is a particular case of general aviation airplane, some clarifications are needed before proceeding: statistical population of general aviation aircraft is composed of a lot of braced-wing and fixed-gear aircraft, thus estimated zero-lift drag coefficient is pretty high. Panthera Hybrid is much different from this point of view, thus a proper estimation of C_{D_0} is needed; from [56], we obtain that maximum continuous power is 100 kW and maximum horizontal true airspeed is 203 kn, thus:

$$C_{L_{V_{max}}} = \frac{Mg}{\frac{1}{2}\rho V^2 S} = 0.228 \tag{5.1}$$

$$C_{D_0} = \frac{P_{max}}{\frac{1}{2}\rho V^3 S} - \frac{C^2_{L_{V_{max}}}}{\pi e \lambda} = 0.0164 \tag{5.2}$$

assuming density at 12000 ft, an Oswald efficiency factor of 0.90 and using the known aspect ratio of 10.5. A battery with 1500 W kg^{-1} and 150 Wh kg^{-1} of specific power and energy respectively was used, obtaining the following results:

	Variable	Panthera Hybrid	Simulated Aircraft	Unit
Mass	Takeoff	1315	1362	kg
	Empty	830*	868	
	Generator	95	95	
	Battery	120*	121	
	Fuel	53*	61	
	Payload	312*	312	
Aircraft	Wing Loading	1152	1144	N m^{-2}
	Power Loading	86	73.3	N kW^{-1}
	Wing Surface	11.2	11.7	m^2
	Wing Span	10.86	11.07	m
Power	Takeoff	200 max.	178	kW
	Climb	150 max.	118	
	Cruise	100 max.	86	
	Descent	N.Av.	3	
	Loiter	N.Av.	33	
	Generator	110	105	
Time	Climb	N.Av.	14.9	min
	Cruise		127.0	
	Descent		24.6	
	Loiter		0.0	
	Total		166.5	

Table 5.2: Results of general aviation aircraft validation. Values labeled with an asterisk are subjected to uncertainty since are estimated.

Values presented in table 5.2 show good accordance with real values: the reader should keep in mind that, first of all, reported generator mass is included in empty mass, while battery is excluded; then that real aircraft motor has two different conditions, namely maximum continuous (150 kW) and peak (200 kW) power, while we have one single value. The higher mass is due to empty mass errors from statistical population: error is below 10% [1], thus still acceptable; Panthera is a brand new aircraft, as already mentioned regarding aerodynamic data, thus structural optimization was possible.

The evolution of relevant parameters can be shown in figure 5.1; in the first block of plots we can observe aerodynamic data, aircraft performance and required power and energy. The largest plot shows the evolution of battery state of charge, fuel tank level and generator throttle: the selected strategy was steady charge strategy, where after climb phase, where the overall required power was higher than the available one from the generator and thus battery level decreases, state of charge is kept at 90% until fuel drops below 5%.

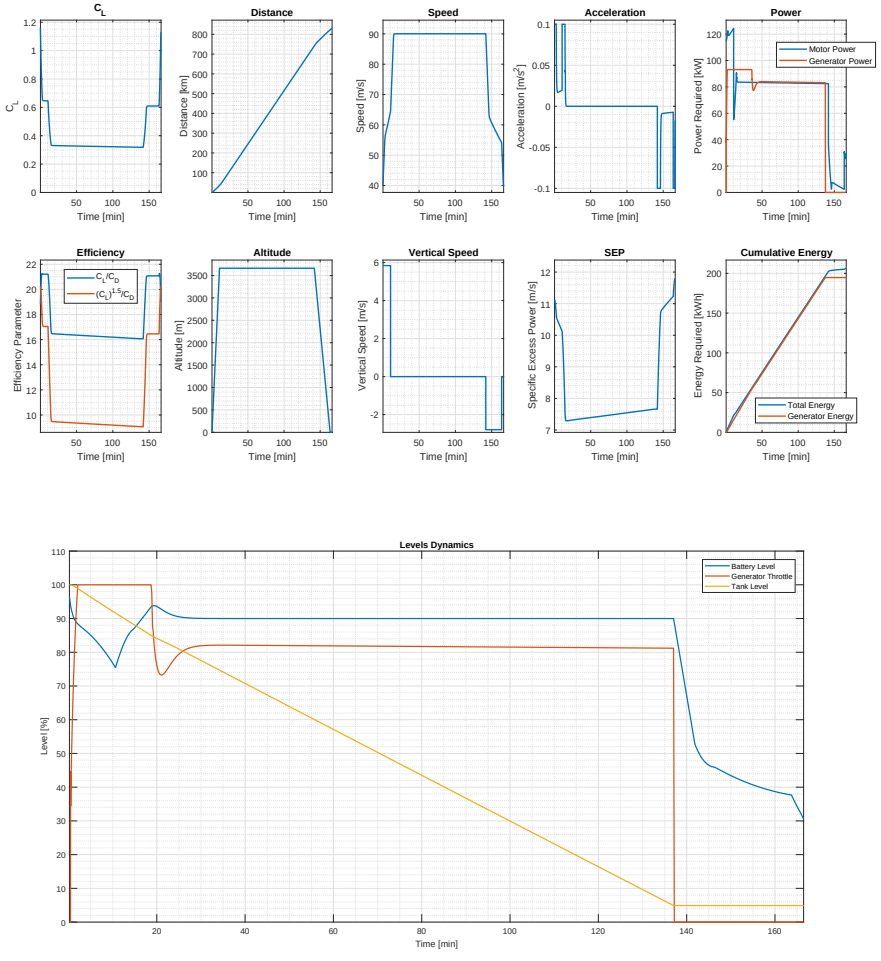

Figure 5.1: Variables evolution for Panthera Hybrid simulated aircraft.

[1] Roskam [38] considers that a ±10% confidence band should be taken into account.

5.1.2 Micro feeder

The micro feeder class is covered by the Italian Tecnam P2012 aircraft, propeller-driven powered by piston engines. Since it is a conventional airplane, we will expect our results to be different in terms of power: even if we can add a model for altitude power losses during design phase, the program does not include it in terms of simulation. In table 5.3 the obtained parameters are reported: with respect to the previous case only a small sub-set of data is presented, since there is little information about available power in flight phases, and there is no battery or generator. As for the Panthera Hybrid case, we can observe a smaller value for the empty weight, and, as predicted above, a lower maximum power.

	Variable	Tecnam P2012	Simulated Aircraft	Unit
Mass	Takeoff	3600	3327	kg
	Empty	2250	1927	
	Fuel	275	304	
	Payload	1075	1095	
Aircraft	Wing Loading	1390	1356	$N\ m^{-2}$
	Power Loading	63.1	73.6	$N\ kW^{-1}$
	Wing Surface	25.4	24.0	m^2
	Wing Span	14.0	14.6	m
	Maximum Power	560	443	kW

Table 5.3: Results of micro feeder aircraft validation.

5.1.3 Commuter

The commuter class is represented by Beechcraft Beech-1900D, considered to be the state-of-art [7] aircraft of this kind. Results shown in table 5.4 show that there is good agreement between real and simulated data, with lower fuel required, mostly due either to different ending mission fuel reserve (a value of 10% of fuel left was selected) or to lower fuel consumption due to more favorable generator operative condition.

	Variable	Beech-1900D	Simulated Aircraft	Unit
Mass	Takeoff	7764	7659	kg
	Empty	4732	4707	
	Fuel	894	814	
	Payload	2138	2138	
Aircraft	Wing Loading	2644	2663	$N\ m^{-2}$
	Power Loading	39.9	40.4	$N\ kW^{-1}$
	Wing Surface	28.8	28.2	m^2
	Wing Span	17.7	17.5	m
	Maximum Power	1910	1860	kW

Table 5.4: Results of commuter aircraft validation.

5.1.4 Large regional

One last simulation is considered to assess program performance with a large airplane: the ATR 72-600 version was selected as a reference, in its full payload - fuel up to MTOW configuration. We can see from results in 5.5 that there is excellent agreement between predicted and obtained data: as for the Beech-1900D we have less fuel, again mostly due to favorable generator performance. In this case we observe a higher required power: this was found to be related to climb phase.

	Variable	ATR 72-600	Simulated Aircraft	Unit
Mass	Takeoff	23000	22990	kg
	Empty	13500	13450	
	Fuel	2000	1920	
	Payload	7500	7615	
Aircraft	Wing Loading	3700	3650	$N\ m^{-2}$
	Power Loading	61.8	57.3	$N\ kW^{-1}$
	Wing Surface	61.0	61.8	m^2
	Wing Span	27.1	27.3	m
	Maximum Power	3650	3930	kW

Table 5.5: Results of large regional aircraft validation.

5.2 Design Examples

After validation process, a set of possible electric and hybrid-electric aircraft is presented for the above considered classes. Comparisons between some key features will be carried out, answering to different questions: what are the differences between an all-electric and a hybrid-electric aircraft doing the same mission? Is it better to employ a steady or a cyclic generator strategy? A lot of questions may be asked and some answers can be provided by considering a set parametric analyses, as covered in Chapter 6; in the following section we will obtain the reference airplanes for these sensitivity studies. The covered design examples are:

- General aviation: all-electric and hybrid-electric aircraft on the same mission;
- Micro feeder: all-electric and hybrid-electric aircraft on two missions at different range;
- Commuter: hybrid-electric aircraft with different generator strategy;
- Large regional: hybrid-electric aircraft with different generator strategy.

5.2.1 General aviation

An all-electric and a hybrid-electric aircraft, named *E-4P* and *H-4P* respectively, are compared, using input values listed in table 5.6 to cover a mission of 300 km, where a final state of charge of at least 25% and fuel tank level of 10% are required.

Variable	Value	Variable	Value	Unit
Takeoff lift coefficient	1.6	Stall speed	60	kn (TAS)
Landing lift coefficient	2.0	Cruise speed	160	kn (TAS)
Wing aspect ratio	10.5	Climb/descent speed	105	kn (EAS)
Oswald efficiency (clean)	0.90	Climb rate	500	ft min^{-1}
Oswald efficiency (takeoff)	0.85	Descent rate	-350	ft min^{-1}
Propeller efficiency	0.85	Takeoff field length	325	m
Number of engines	1	Cruise altitude	8000	ft
Number of passengers	3	Loiter altitude	1000	ft
Number of pilots	1	Loiter time	45	min
Landing gear ΔC_{D_0}	0.02	Battery specific power	1000	W kg^{-1}
Takeoff flaps ΔC_{D_0}	0.02	Battery specific energy	500	Wh kg^{-1}

Table 5.6: Common input values for general aviation all-electric and hybrid-electric design examples.

	Variable	E-4P	H-4P	Unit
Mass	Takeoff	1775	1328	kg
	Empty	985	841	
	Generator	N/A	81	
	Battery	478	144	
	Fuel	N/A	31	
	Payload	312	312	
Aircraft	Wing Loading	1144	1144	N m^{-2}
	Power Loading	91.4	90.7	N kW^{-1}
	Wing Surface	15.2	11.4	m^2
	Wing Span	12.6	10.9	m
Power	Takeoff	186	143	kW
	Climb	115	92	
	Cruise	156	136	
	Descent	39	35	
	Loiter	51	40	
	Generator	N/A	151	
Time	Climb	19.8	19.8	min
	Cruise	30.3	30.3	
	Descent	23.7	23.7	
	Loiter	45.0	45.0	
	Total	73.9 (118.9)	73.9 (118.9)	

Table 5.7: Results of general aviation design examples.

As we can observe from results listed in table 5.7, a difference of about 450 kg was found between the two different aircraft configurations, mainly due to a large difference between required battery mass. This is due to overall required energy for the mission, which has to be fully provided by batteries. From figure 5.2 we can see that the required energy is almost 180 kWh, while from figure 5.3 we can see a total value of 150 kWh, which is split between battery and fuel, roughly 35% and 65% respectively. To satisfy energy requirement of the hybrid case with a battery alone, we can compute the needed specific energy considering the available mass of 175 kg: 857 Wh kg^{-1} are required for the mission, while to end with a 25% SoC this value increases to 1140 Wh kg^{-1}.

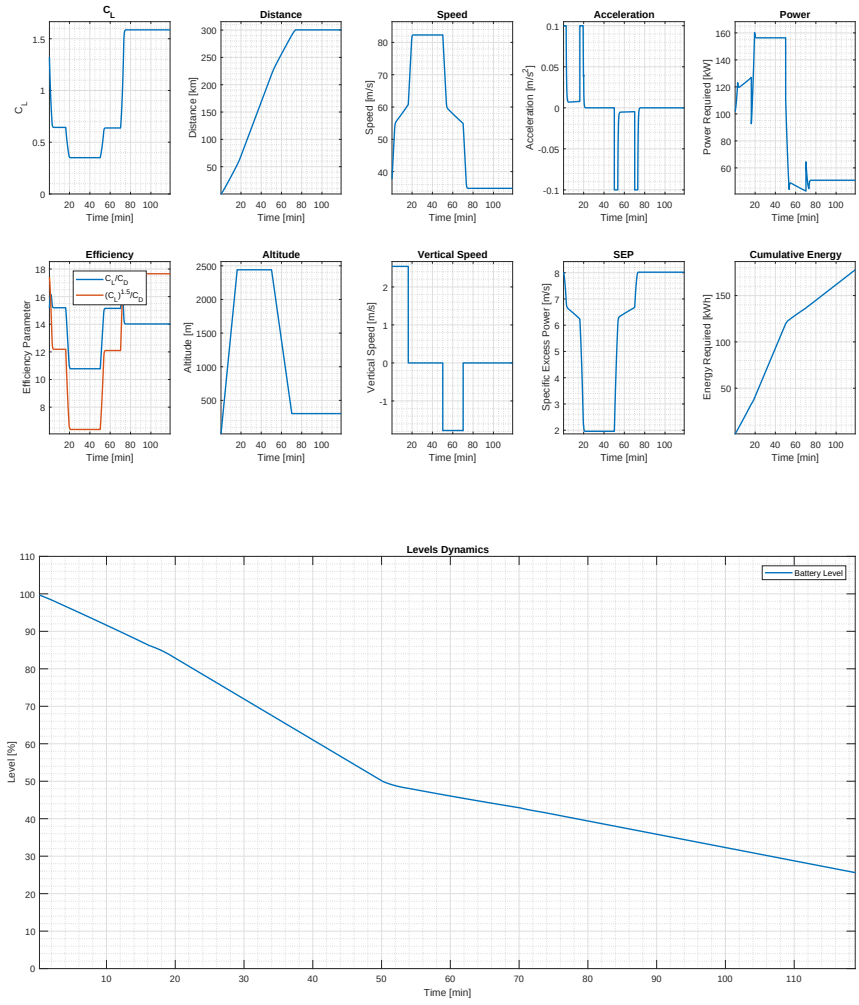

Figure 5.2: Parameters evolution for general aviation all-electric design example.

The hybrid-electric solution proves to be more suitable for this example: to fly 300 km for more than 1h at relatively high speed it is shown that a generator is required. A reciprocating engine with a 8:1 volume ratio was used and only 30 kg of avgas where

required, obtaining a final energy degree of hybridization of 40% [2]. From what we obtained in this example we can observe that, in general, fixing the same parameters for an all-electric and a hybrid-electric aircraft will lead to a heavy all-electric solution and a hybrid one characterized by very low fuel required. For this reason, we should either select different battery settings, seeking a high specific energy battery for the all-electric and a high specific power one for the hybrid, or imposing two different range requirements, in such a way that two similar airplanes may be found, carrying on different missions.

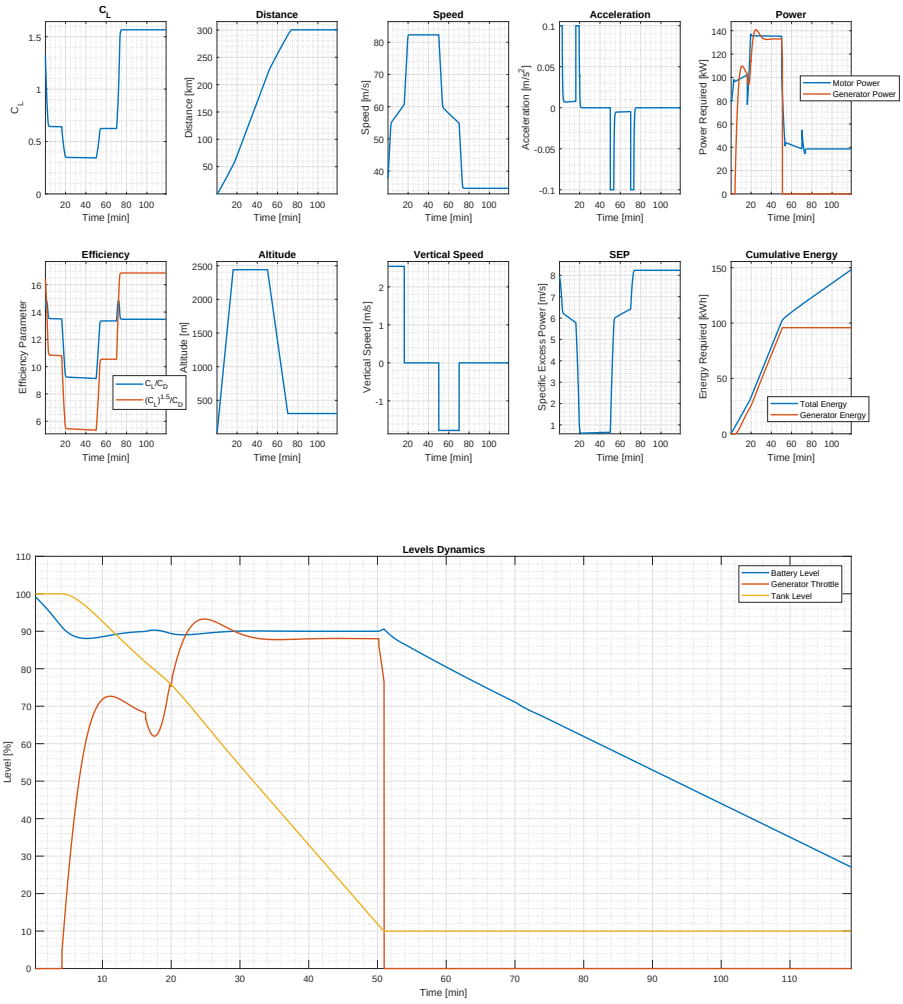

Figure 5.3: Parameters evolution for general aviation hybrid-electric design example.

[2]Consider that from an operative point of view we split energy requirement as 35% for batteries and 65% from fuel, but final levels were not the same: 25% of SoC was left against 10% fuel available.

Variable	Value	Variable	Value	Unit
Takeoff lift coefficient	2.0	Stall speed	60	kn (TAS)
Landing lift coefficient	2.6	Cruise speed	200	kn (TAS)
Wing aspect ratio	12	Climb/descent speed	150	kn (EAS)
Oswald efficiency (clean)	0.82	Climb rate	500	ft min^{-1}
Oswald efficiency (takeoff)	0.75	Descent rate	-500	ft min^{-1}
Propeller efficiency	0.85	Takeoff field length	325	m
Number of engines	2	Cruise altitude	8000	ft
Number of passengers	8	Loiter altitude	1000	ft
Number of pilots	1	Loiter time	45	min
Landing gear ΔC_{D_0}	0.015	Battery specific power	1000	W kg^{-1}
Takeoff flaps ΔC_{D_0}	0.030	Battery specific energy	500	Wh kg^{-1}

Table 5.8: Common input values for micro feeder all-electric and hybrid-electric design examples.

	Variable	E-8P	H-8P	Unit
Mass	Takeoff	3615	3609	kg
	Empty	2049	2123	
	Generator	N/A	77	
	Battery	653	407	
	Fuel	N/A	166	
	Payload	913	913	
Aircraft	Wing Loading	1144	1144	N m^{-2}
	Power Loading	87.0	87.0	N kW^{-1}
	Wing Surface	24.6	24.5	m^2
	Wing Span	17.2	17.2	m
Power	Takeoff	400	400	kW
	Climb	291	291	
	Cruise	367	367	
	Descent	111	111	
	Loiter	105	105	
	Generator	N/A	386	
Time	Climb	18.9	18.9	min
	Cruise	11.7	68.3	
	Descent	20.5	20.5	
	Loiter	45.0	45.0	
	Total	51.0 (96.0)	107.7 (152.7)	

Table 5.9: Results of micro feeder design examples.

5.2.2 Micro feeder

The micro feeder class is represented by two airplanes, an all-electric aircraft and a hybrid one, denoted as *E-8P* and *H-8P* respectively; they share most of the requirements, listed in table 5.8. Considering previous example, we choose to impose two different range values: 250 km for the all-electric version and 600 km for the hybrid one, using the steady charging strategy. As from table 5.9, we obtain two very similar airplanes: they can be considered two different variants of the same aircraft, sharing the same airframe and differing only due to batteries, generator and fuel tanks. The electric version is pushed up to a minimum SoC level of 10%, while a 25% SoC and 10% fuel was considered for the hybrid-electric version, with a 12:1 turboshaft generator. A variant of the hybrid-electric aircraft is possible by considering a different battery setting: using a higher specific power and a lower specific energy it is possible to further save mass, as shown in table 5.10; this latter aircraft will be considered as a starting point for sensitivity studies in the next chapter.

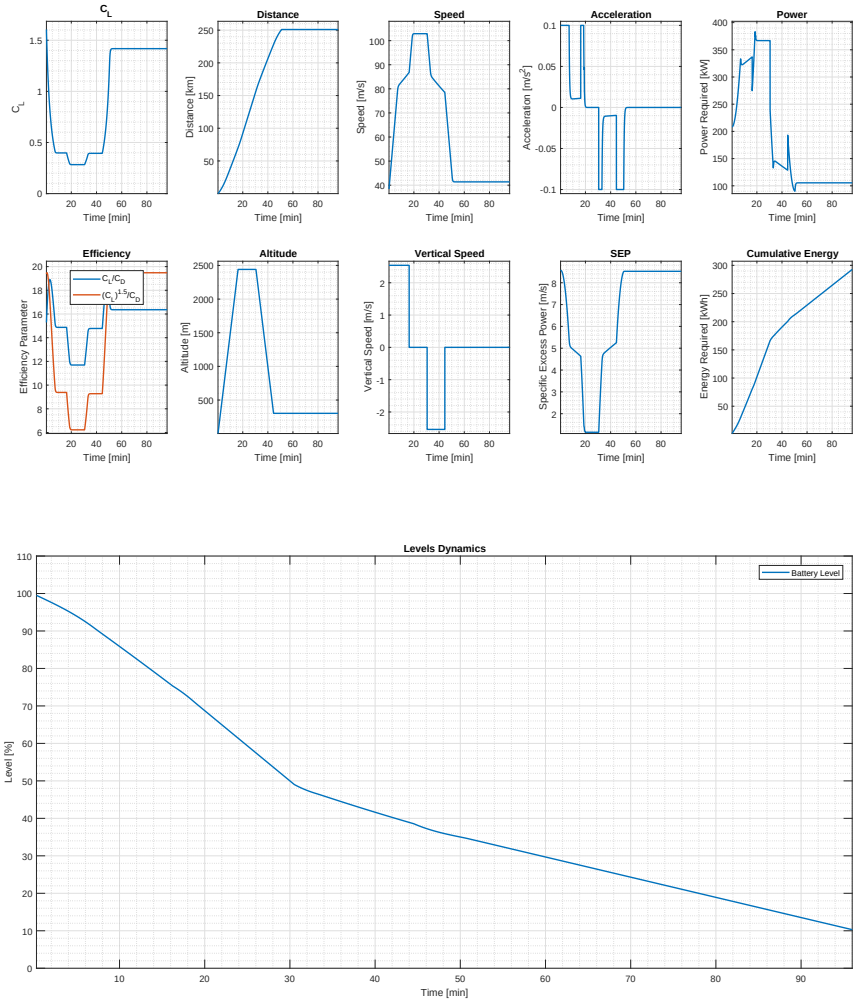

Figure 5.4: Parameters evolution for micro feeder all-electric design example.

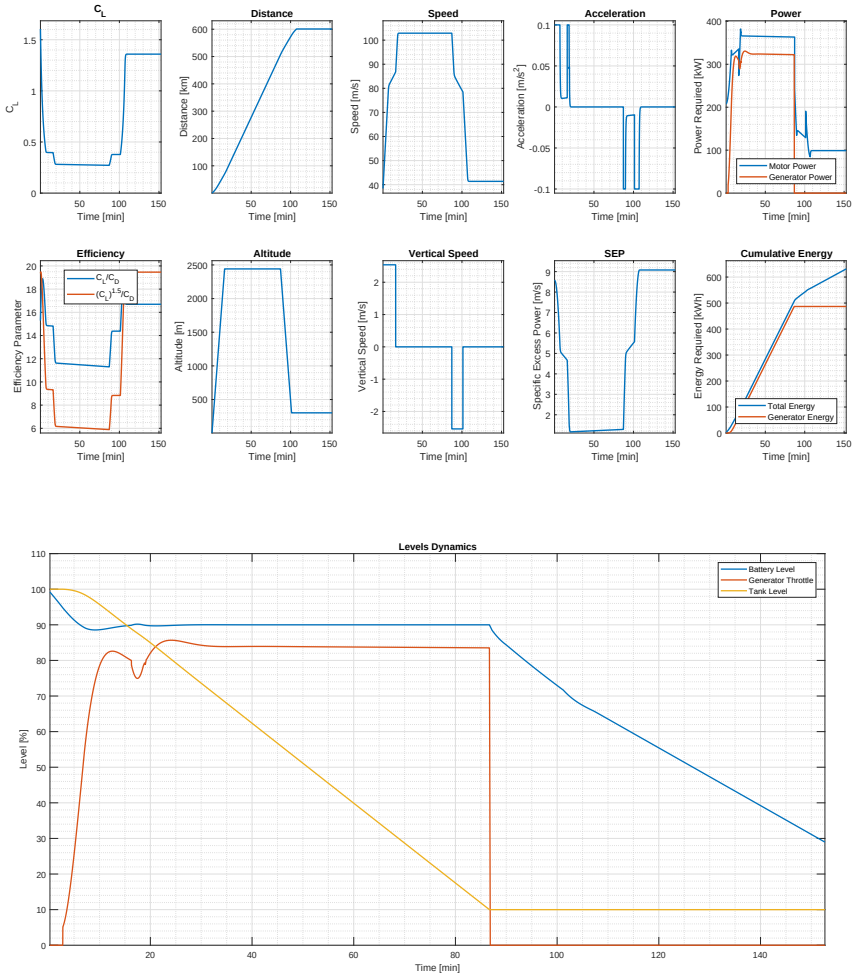

Figure 5.5: Parameters evolution for micro feeder hybrid-electric design example.

	Variable	H-8PA	H-8PB	Unit
Mass	Takeoff	3609	3382	kg
	Empty	2123	1980	
	Generator	77	75	
	Battery	407	323	
	Fuel	166	166	
Aircraft	Battery Specific Power	1000	1300	W kg^{-1}
	Battery Specific Energy	500	400	Wh kg^{-1}
	Degree of Hybridization	0.273	0.180	-
	Wing Surface	24.5	221	m^2
	Maximum Power	400	380	kW

Table 5.10: Comparison between hybrid-electric micro feeder variants.

Variable	Value	Variable	Value	Unit
Takeoff lift coefficient	2.0	Stall speed	85	kn (TAS)
Landing lift coefficient	2.6	Cruise speed	250	kn (TAS)
Wing aspect ratio	10.8	Climb/descent speed	145	kn (EAS)
Oswald efficiency (clean)	0.85	Climb rate	1500	ft min^{-1}
Oswald efficiency (takeoff)	0.75	Descent rate	-850	ft min^{-1}
Propeller efficiency	0.85	Takeoff field length	1100	m
Number of engines	3	Cruise altitude	25000	ft
Number of passengers	19	Loiter altitude	4000	ft
Number of pilots	2	Loiter time	45	min
Landing gear ΔC_{D_0}	0.01	Battery specific power	1300	W kg^{-1}
Takeoff flaps ΔC_{D_0}	0.03	Battery specific energy	400	Wh kg^{-1}

Table 5.11: Input values for commuter hybrid-electric design examples.

	Variable	H-19P(S)	H-19P(C)	Unit
Mass	Takeoff	8538	8366	kg
	Empty	4690	4690	
	Generator	282	282	
	Battery	1218	1027	
	Fuel	492	511	
	Payload	2138	2138	
Aircraft	Wing Loading	3052	2991	N m^{-2}
	Power Loading	62.7	61.4	N kW^{-1}
	Wing Surface	27.4	27.4	m^2
	Wing Span	17.2	17.2	m
Power	Takeoff	1309	1309	kW
	Climb	1094	1094	
	Cruise	805	805	
	Descent	128	128	
	Loiter	409	409	
	Generator	848	848	
Time	Climb	19.8	19.8	min
	Cruise	96.3	96.3	
	Descent	27.3	27.3	
	Loiter	45.0	45.0	
	Total	143.4 (188.4)	143.4 (188.4)	

Table 5.12: Results of commuter design examples.

5.2.3 Commuter

A 19-seats hybrid-electric commuter is presented with the aim to stay below 19000 lb, thus to stay in a CS-23/FAR-23 regulation environment, which is indeed more favorable in real aircraft application, due to lower certification costs. Since cost analysis is beyond the scope of this work, we will simply consider the mass limit of 8618.4 kg, that ensures more feasible aircraft solution. For this case, since we have a stringent mass limitation, we will not consider an electric case: we will compare two different charging strategies, namely steady and cyclic charging, for a 1000 km mission with a 15:1 turboshaft generator operating above 5000 ft to evaluate possible differences.

Referring to table 5.12 we can immediately see that, since empty mass, wing surface and power is found to be the same, the *starting* aircraft was the same. As discussed in Chapter 4, we size fuel mass by considering expected generator efficiency, but no strategy is required at this level: the strategy will affect the simulation and thus the final values of state of charge and fuel tank level.

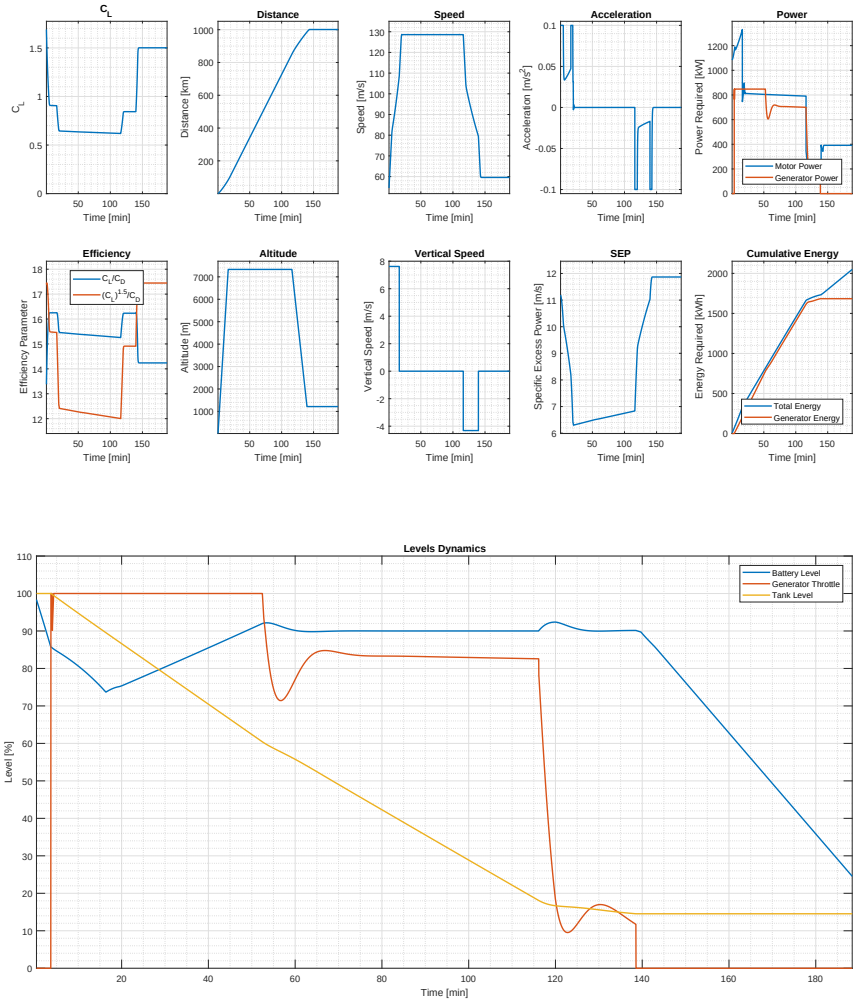

Figure 5.6: Parameters evolution for commuter steady charging design example.

The important result obtained here is that apparently a cyclic charging strategy allows for a reduction in takeoff mass of 172 kg, about 2%: this reduction is due to a lower battery mass of 191 kg, with an increase of fuel tank of 19 kg. These results show that a cyclic strategy allows for a somewhat better battery energy management; this might be explained as follows: the generator starts when battery level is low (25 % SoC), thus it will burn fuel at a higher rate, in such a way that overall required energy is lower. We also observe a final SoC of 55%, meaning that only 45% battery recharge will be needed on ground instead of 75%. The higher amount of required fuel is thus resulting in lower degree of hybridization and higher emissions.

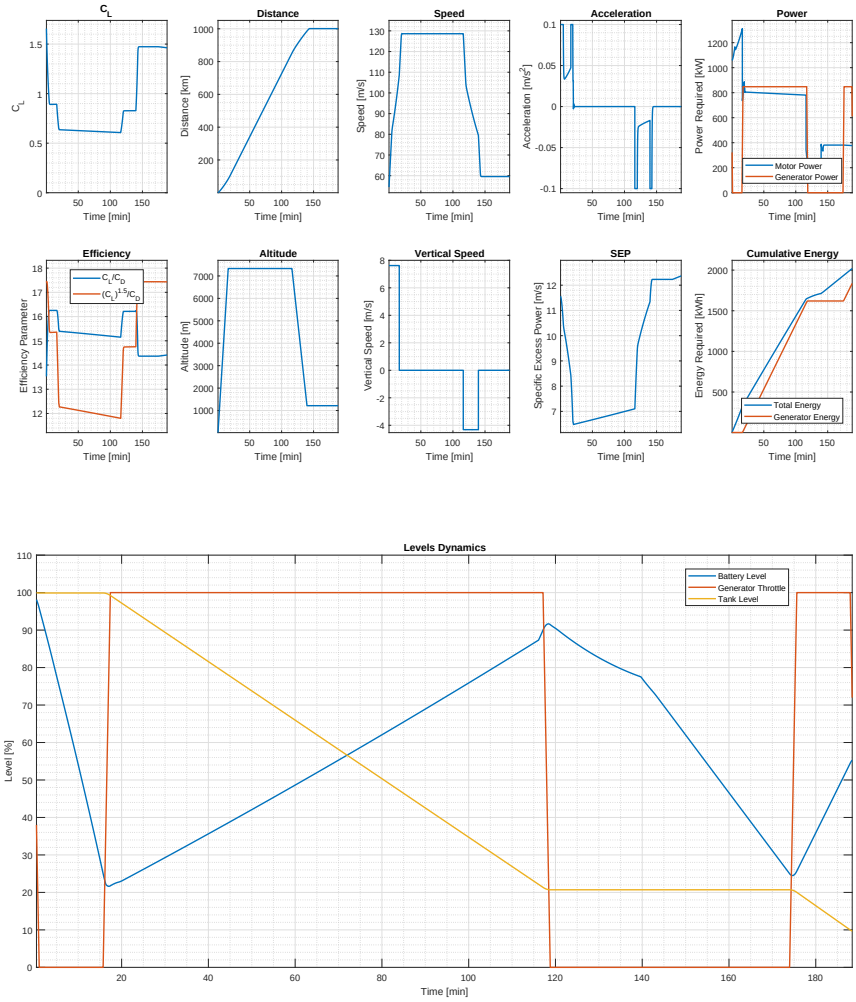

Figure 5.7: Parameters evolution for commuter cyclic charging design example.

Variable	Value	Variable	Value	Unit
Takeoff lift coefficient	2.0	Stall speed	105	kn (TAS)
Landing lift coefficient	2.6	Cruise speed	275	kn (TAS)
Wing aspect ratio	12	Climb/descent speed	160	kn (EAS)
Oswald efficiency (clean)	0.82	Climb rate	1350	ft min^{-1}
Oswald efficiency (takeoff)	0.75	Descent rate	-850	ft min^{-1}
Propeller efficiency	0.85	Takeoff field length	1325	m
Number of engines	4	Cruise altitude	25000	ft
Number of passengers	70	Loiter altitude	5000	ft
Number of pilots	4	Loiter time	45	min
Landing gear ΔC_{D_0}	0.015	Battery specific power	1500	W kg^{-1}
Takeoff flaps ΔC_{D_0}	0.035	Battery specific energy	500	Wh kg^{-1}

Table 5.13: Common input values for large regional hybrid-electric design examples.

	Variable	H-70(S)	H-70(C)	Unit
Mass	Takeoff	29722	28491	kg
	Empty	16093	16093	
	Generator	956	956	
	Battery	3985	2753	
	Fuel	2029	2030	
	Payload	7615	7615	
Aircraft	Wing Loading	4751	4554	N m^{-2}
	Power Loading	70.6	67.7	N kW^{-1}
	Wing Surface	61.4	61.4	m^2
	Wing Span	27.1	27.1	m
Power	Takeoff	4045	4045	kW
	Climb	3766	3766	
	Cruise	2723	2723	
	Descent	728	728	
	Loiter	1646	1646	
	Generator	2867	2867	
Time	Climb	23.1	23.1	min
	Cruise	117.3	117.3	
	Descent	26.3	26.3	
	Loiter	45.0	45.0	
	Total	166.7 (211.7)	166.7 (211.7)	

Table 5.14: Results of large regional design examples.

5.2.4 Large regional

A large regional aircraft is considered, using common parameters used in ATR 72-600 validation, to assess feasibility of the application of a hybrid-electric solution to this aircraft class. A lower range of 1300 km was selected for the 70-seater airliner, with a 16:1 turboshaft generator operating above 8000 ft and a high-performance Li-S battery; as for the commuter case, we compare the two considered charging strategies.

Results are presented in table 5.14: as for the commuter case, the cyclic strategy allows for a reduction of the overall aircraft mass, with a 4% mass saving, this time only due to battery mass reduction; this is once again the result of a better energy management that allows to end the mission with 55% SoC, instead of just 25%. Comparing the above results with the ATR 72-600 we can immediately see that serial hybrid-electric propulsion, as shown in figure 3.2, is still not competitive enough: selected battery setting can be achieved around 2030, and the obtained results show that required block fuel is roughly the same, but with a heavier, and thus more expensive, aircraft.

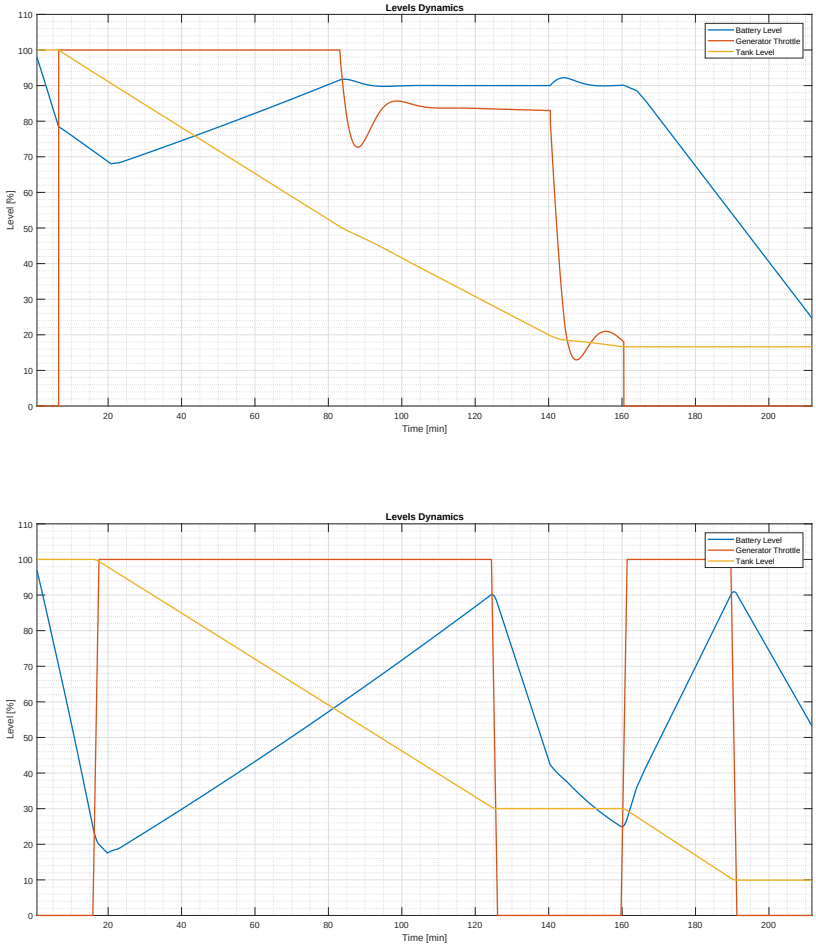

Figure 5.8: Levels evolution comparison for large regional design examples between steady (above) and cyclic (below) charging.

Chapter 6

Parametric Analysis and Sensitivity Studies

The last part of this work is about a parametric analysis on design and simulation input parameters, to assess sensitivity of key results, selected as:

- Takeoff mass;
- Wing surface;
- Battery mass;
- Required motor power;
- Fuel mass;
- Energy degree of hybridization.

where the last two results are assessed only for hybrid-electric aircraft, since trivial values would be found for all-electric cases.

6.1 Procedure Overview

The analysis is carried out by considering that virtually any parameter could be selected for a sensitivity study: thus a general procedure is used. Since *Hyperion* program requires a text input file, the idea is to let the user decide for each parameter the lower and upper bounds and the amount of variables: in this way a set of vectors is obtained and all possible combinations are computed. A temporary input file is written for each possible combination and a standard simulation is launched. Results are then collected and stored in two different `.mat` variables: a *short* version that only stores the set of input data and aforementioned target parameters for each combination, while a *long* version storing all output values, including temporal evolution of variables analyzed in `FMS`. This last *long* solution file, containing a lot of information, is thus very heavy and complex to handle; the second type of solution will be used to produce all the plots in the following sections.

We should keep in mind that, even if an analysis on *every* parameter is possible, it would be particularly difficult to visualize the result: for this reason we will consider

the variation of two parameters at a time. The visualization of results is carried out by considering a 2D and a 3D plot groups for sake of clarity: the 3D version, consisting in carpet plots, is graphically rendered by post-processing the result with a 2D cubic interpolation for a smoother result.

6.2 Case Studies

Three aircraft will be considered for our case studies: the all-electric micro feeder denoted in Section 5.2.2 as *E-8P* and the hybrid-electric micro feeder *H-8PB*, which will be the base airplanes for most of our studies, and then the hybrid electric regional *H-70P(S)*. We will consider steady charging strategy for our studies even if the cyclic one proved to be better, but for coherence reasons: as we could observe, this strategy is not granting a prescribed final state of charge level. We impose a minimum SoC ending level, thus the program is providing a correction only if final value is not *at least* the ζ_{min} that we asked for; with a cyclic strategy, the ending SoC level is usually above the minimum threshold, and thus is beyond our control: in this way it has been observed that a rather irregular pattern is found in carpet plots.

6.2.1 Hybrid-Electric 8-seater

With reference to Section 5.2.2, using aircraft data reported here in table 6.1 for convenience, we analyze the sensitivity on key parameters as range, battery specific power and energy, generator power-to-weight ratio and pressure ratio, rate of climb, climb speed, cruise speed, cruise altitude and final state of charge level.

Variable	Value	Variable	Value	Unit
Takeoff lift coefficient	2.0	Stall speed	60	kn (TAS)
Landing lift coefficient	2.6	Cruise speed	200	kn (TAS)
Wing aspect ratio	12	Climb/descent speed	150	kn (EAS)
Oswald efficiency (clean)	0.82	Climb rate	500	ft min^{-1}
Oswald efficiency (takeoff)	0.75	Descent rate	-500	ft min^{-1}
Propeller efficiency	0.85	Takeoff field length	325	m
Number of engines	2	Cruise altitude	8000	ft
Number of passengers	8	Loiter altitude	1000	ft
Number of pilots	1	Transition altitude	0	ft
Landing gear ΔC_{D_0}	0.015	Loiter time	45	min
Takeoff flaps ΔC_{D_0}	0.030	Battery specific power	1300	W kg^{-1}
Ending fuel level	0.10	Battery specific energy	400	Wh kg^{-1}
Ending battery level	0.25	Range	600	km

Table 6.1: Reference data for hybrid-electric micro feeder sensitivity study.

Range and Battery Specific Energy

Fixing battery specific power at reference 1300 W kg^{-1} value, we analyze sensitivity on range and battery specific energy. We can observe a linear relationship between most parameters and total range, with the exception of energy degree of hybridization, which is limited to less than 30% with the most performing considered battery. Looking at the various plots it is possible to see that fixing the takeoff mass to a certain value we can gain up to 50 km of total range by moving from the 250 Wh kg^{-1} to 500 Wh kg^{-1} battery.

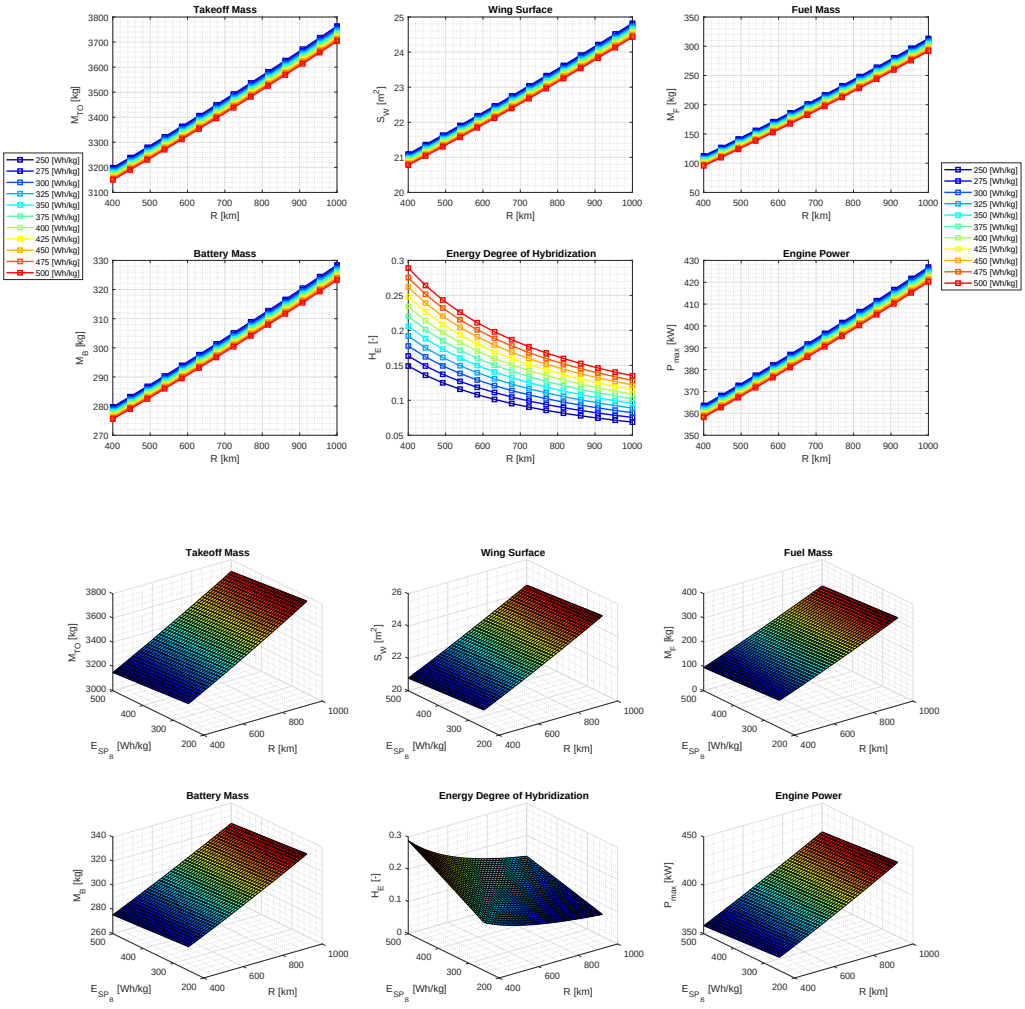

Figure 6.1: Hybrid 8-seater sensitivity on aircraft range and battery specific energy.

Battery Specific Power and Battery Specific Energy

Two different battery data will be compared: in figure 6.2 we will consider current Lithium-Sulfur values, with a specific energy ranging from current 250 Wh kg^{-1} to 2021 trend of 500 Wh kg^{-1}; specific powers are still evolving, thus a 1000 ÷ 2500 W kg^{-1} span has been considered, using the reference range of 600 km. We can observe that battery mass is determined by power requirement for this aircraft, thus not depending on battery specific energy; fuel mass, on the contrary, increases as battery specific energy decreases and as specific power increases, since a lighter battery will contain less energy. An interesting pattern can be observed on fuel mass: for values below 325 Wh kg^{-1} we can see that needed fuel decreases as specific power increases, while the opposite is true for specific energy values above 325 Wh kg^{-1}. This behavior may be explained by

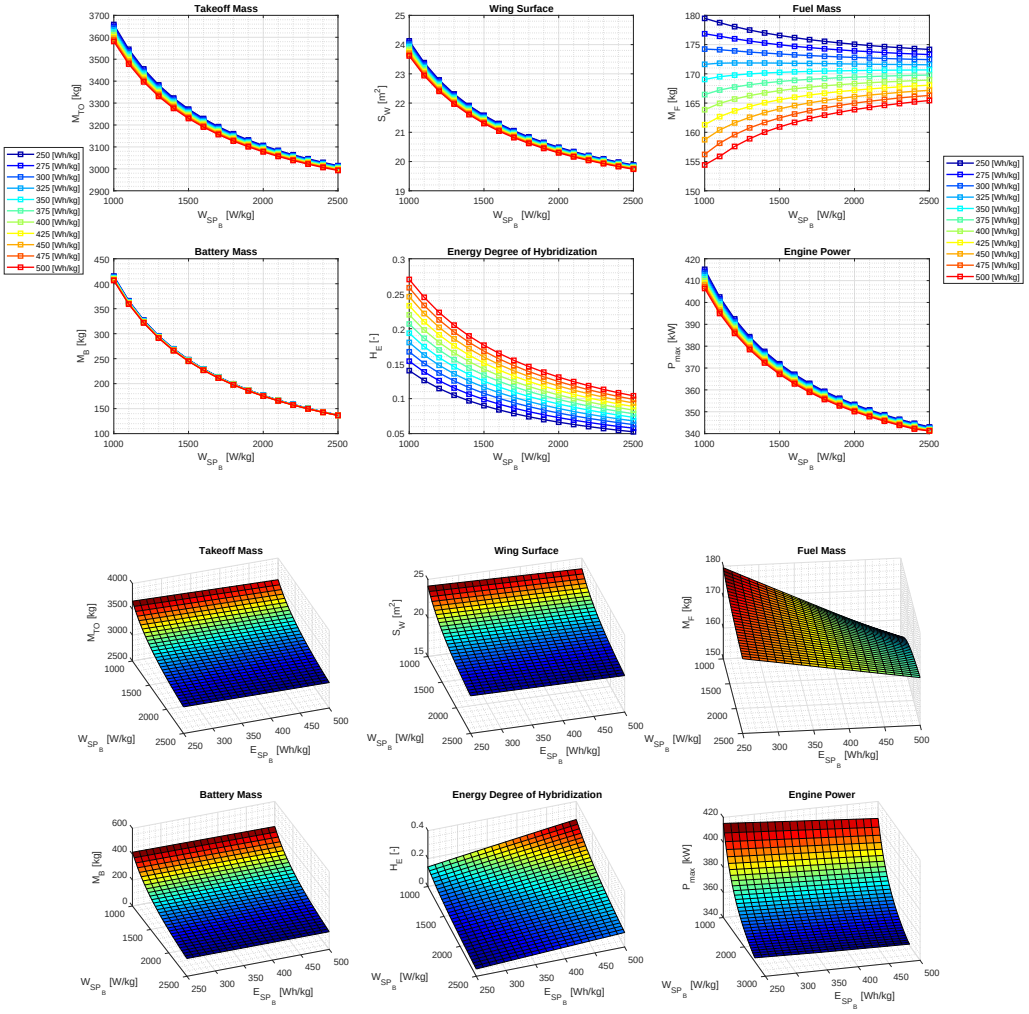

Figure 6.2: Hybrid 8-seater sensitivity on battery specific power and specific energy of close future batteries.

considering that as specific power decreases, battery mass increases: if specific energy is high enough (where in this case the threshold is 325 Wh kg^{-1}) an increase in battery mass results in a steep increase in battery energy, while if it is too low, penalty due to mass increase dominates. This explanation is supported by the degree of hybridization: for low specific energy batteries the slope is rather small, while it increases as specific energy increases.

A second parametric analysis can be carried out by considering a wider range of specific energy values, going from feasible values trend for next few years to very large and optimistic values predicted for next 30 years; this time we focus on sensitivity to specific energy at different specific power values. As observed also in figure 6.2, a high degree of hybridization is obtained in case of battery setting at the lowest specific power, because of larger battery mass and thus higher energy content.

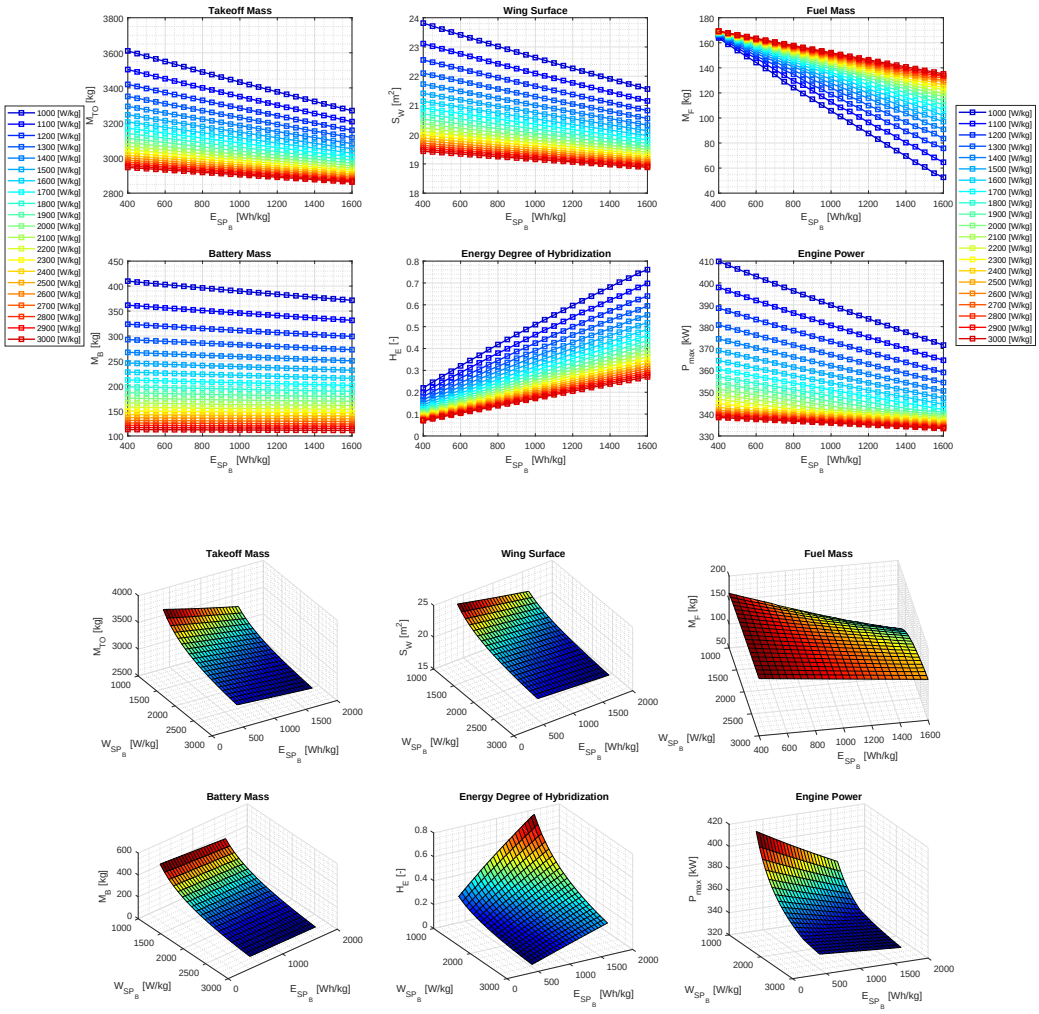

Figure 6.3: Hybrid 8-seater sensitivity on battery specific power and specific energy of long time-span batteries.

Generator Power-to-Weight Ratio and Pressure Ratio

We analyze the sensitivity on generator performance: considering a turboshaft engine, we consider variations of its pressure ratio and power-to-weight ratio. As we may expect, the higher the pressure ratio, the better the overall performance, but little improvement can be obtained with values above 16. An interesting result is given by engine power and battery mass plots: for power-to-weight ratio values below 2500 W kg^{-1} we experience a steeper rise of overall mass; higher power leads to higher battery mass, but low impact on fuel consumption at a fixed pressure ratio means a higher degree of hybridization, even if we see that generator has a fairly low impact on this parameter.

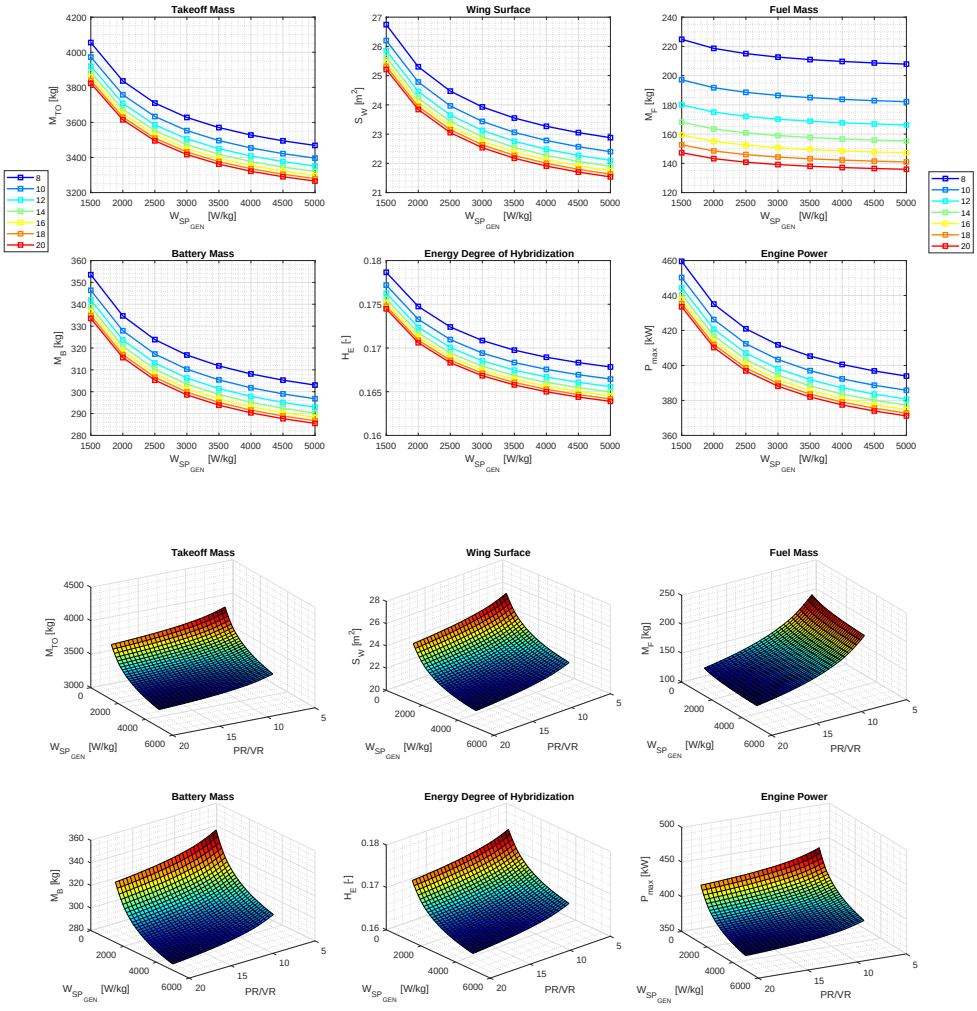

Figure 6.4: Hybrid 8-seater sensitivity on generator power-to-weight ratio and pressure ratio.

Climb Speed and Battery Specific Energy

Another possible analysis involves the impact of climb speed on relevant parameters at different battery specific energy values. As we can observe, the optimal value seems to be 130 kn, since mass is lowest with this setting, although we can see that this parameter has little influence on the overall result.

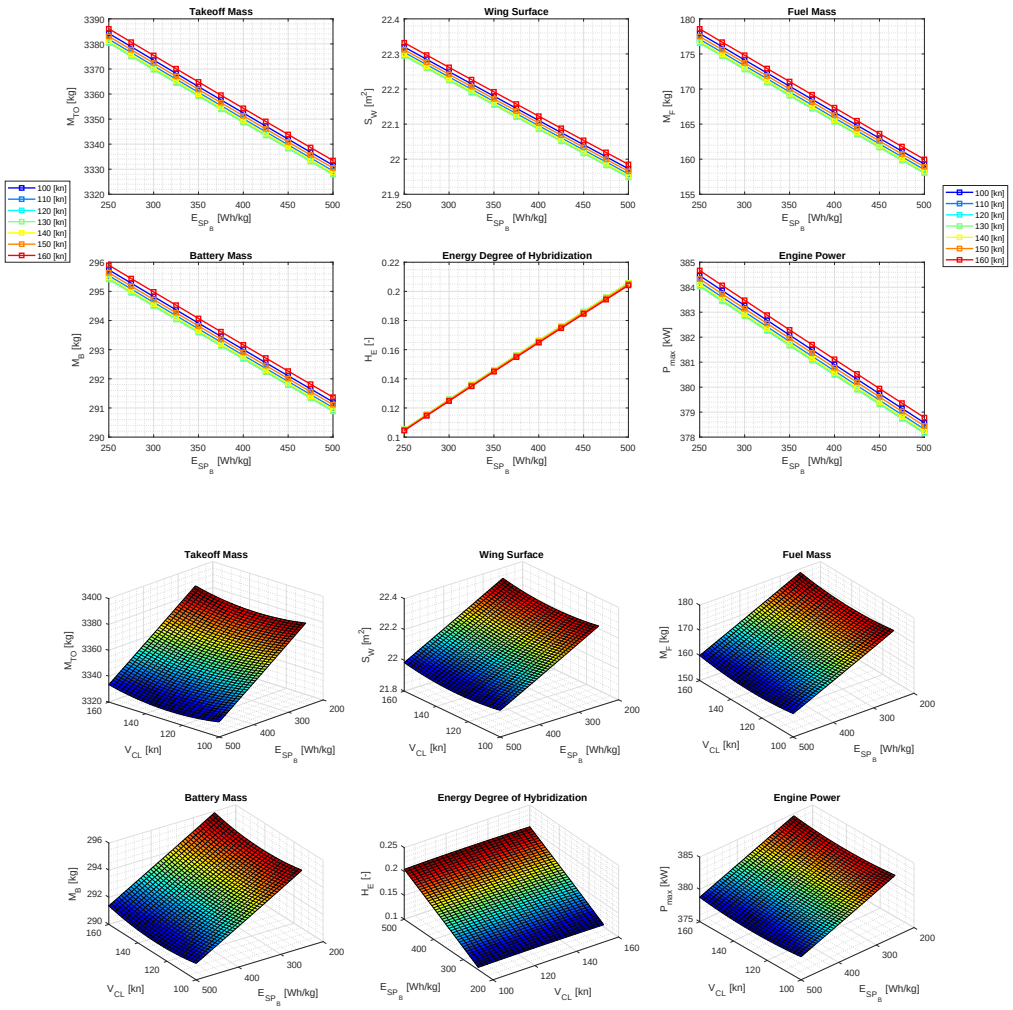

Figure 6.5: Hybrid 8-seater sensitivity on climb speed and battery specific energy.

Rate of Climb and Battery Specific Energy

Concerning climb phase, a more interesting analysis can be carried out by evaluating the impact of vertical speed (climb rate) instead of horizontal one. As predictable, the lower the vertical speed the lower the mass; for values up to 1000 ft min^{-1} we can see a rather flat evolution of key parameters, due to the fact that power constraint is still due to takeoff maneuver, thus mass increase is only related to higher fuel need, as also seen in the degree of hybridization slight reduction. Above 1000 ft min^{-1}, though,

power is determined by climb power: battery mass starts increasing with a steeper slope and thus overall mass and wing surface. An interesting consideration can be made regarding fuel mass: for some specific energy values required fuel increases as rate of climb increases beyond 1000 ft min^{-1}, while for other values it keeps increasing. As said before concerning specific power evolution, this behavior lies in the compromise between mass penalty and energy content: since battery mass increases a lot, if specific energy is at least 325 Wh kg^{-1} its energy content increase is more beneficial than mass penalty, while the opposite is true for specific energy values below 325 Wh kg^{-1}.

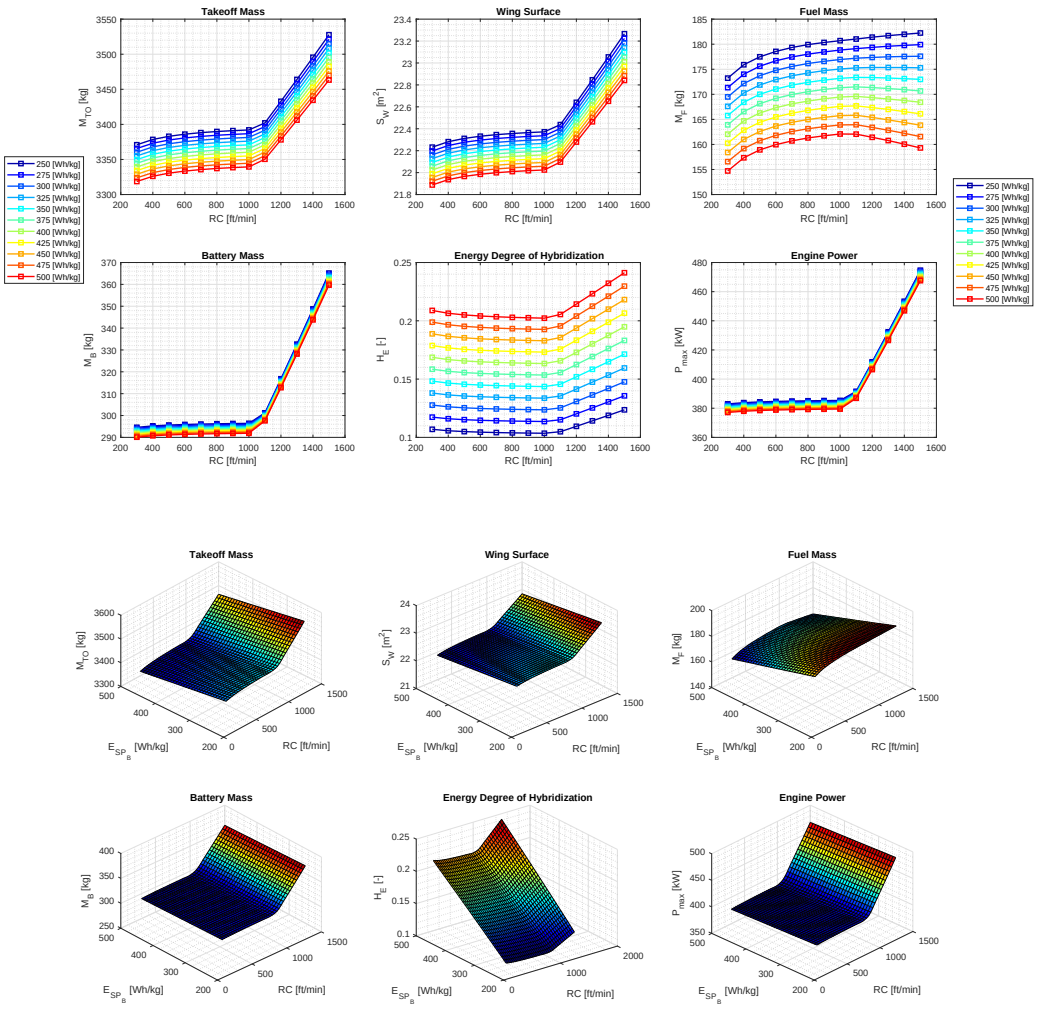

Figure 6.6: Hybrid 8-seater sensitivity on rate of climb and battery specific energy.

Cruise Speed and Battery Specific Energy

We can now study the impact of cruise speed on the overall parameters. As we can observe from all plots, the true airspeed value of 205 kn should not be exceeded, since a steep rise of required power is observed: in this way a large battery mass is needed, increasing overall aircraft weight. The degree of hybridization presents a minimum for a cruise speed of 205 kn: this may be explained by considering that below this value motors power is not determined by cruise condition, but by takeoff, thus battery mass increases with a small slope, simply because of increased fuel mass due larger required energy. In this way, increasing the speed we don't increase power (and thus battery mass) as much as fuel; when cruise speed increases above 205 kn, power is now determined by cruise phase, battery mass starts increasing with a larger slope and thus battery contribution to energy is larger than before: hence, the degree of hybridization starts increasing.

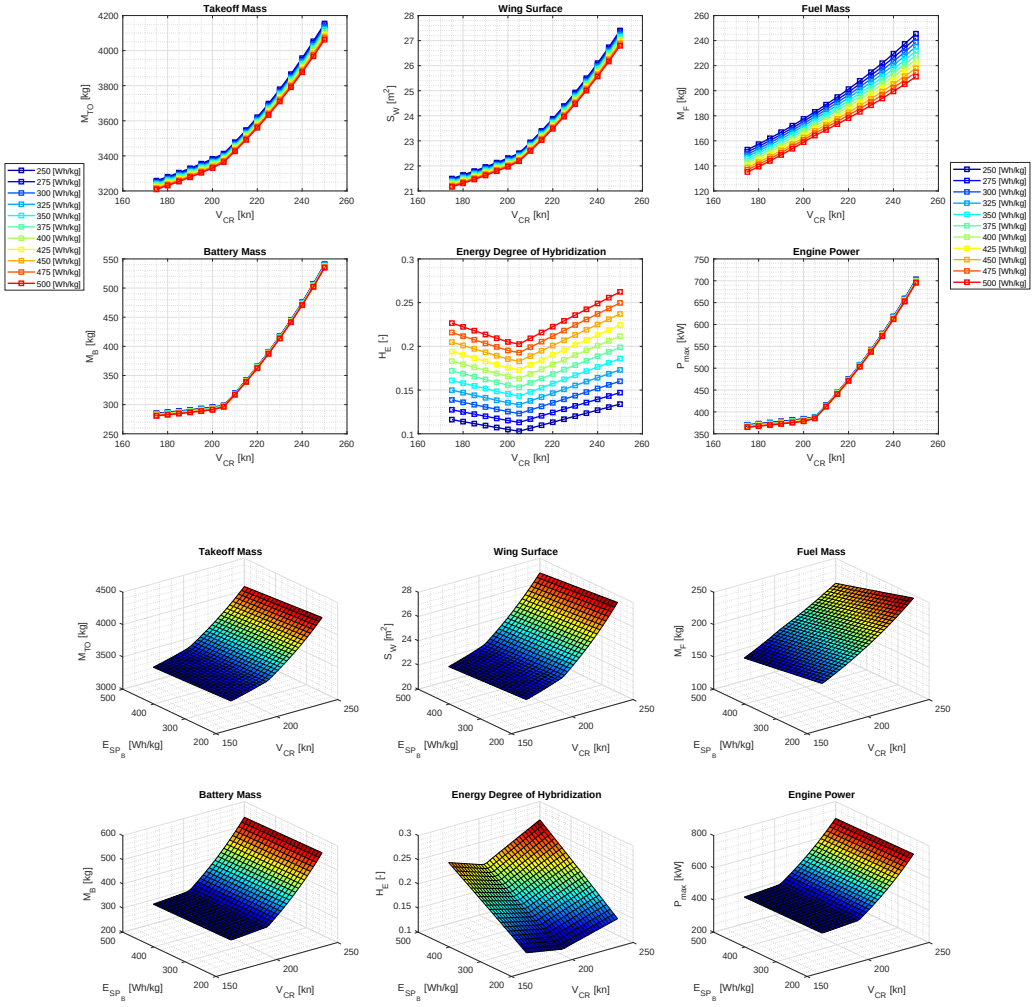

Figure 6.7: Hybrid 8-seater sensitivity on cruise speed and battery specific energy.

Cruise Altitude and Battery Specific Energy

An interesting result is given by cruise altitude effect. Recall the correction on battery and fuel mass described in Section 4.3.2: we assumed that these corrections were small an thus there was no need to re-design the aircraft. As we can observe from battery mass plot that corrections are needed for cruise altitude values above 10000 ft: these corrections are satisfying the 2% requirement, since we can estimate from the battery mass plot a maximum of 25 kg correction over more than 3 ton of aircraft.

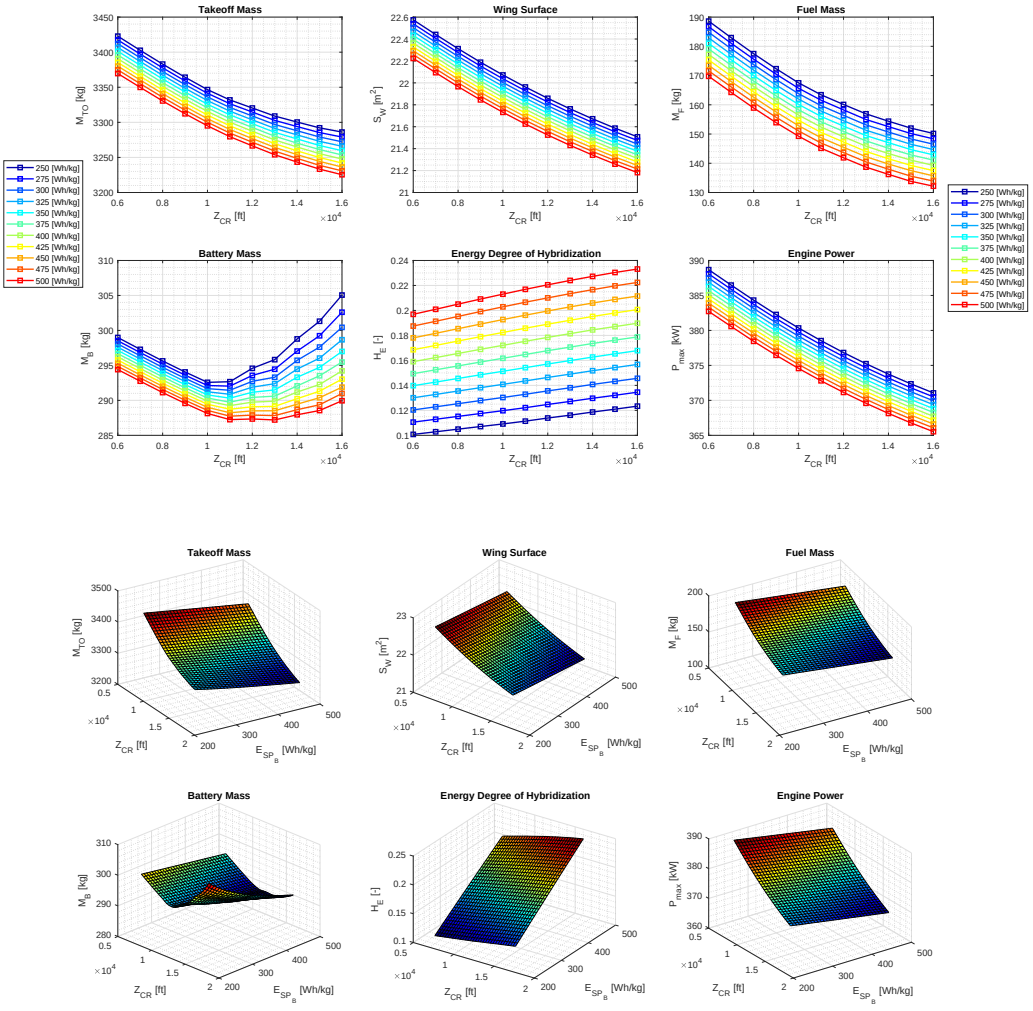

Figure 6.8: Hybrid 8-seater sensitivity on cruise altitude and battery specific energy.

Final State of Charge and Battery Specific Energy

Another interesting result is given by the relation between final state of charge and other parameters at different battery settings; final state of charge basically means how much of stored battery energy is unused, and it is spared for emergency reasons: how large is the impact on overall design? We can see that the higher the specific energy of the battery, the higher the impact of final state of charge level on the solution: with a final 10% SoC the difference between aircraft using 250 and 500 Wh kg^{-1} batteries is about 60 kg, while it is riduced at 20 kg with final SoC of 75%.

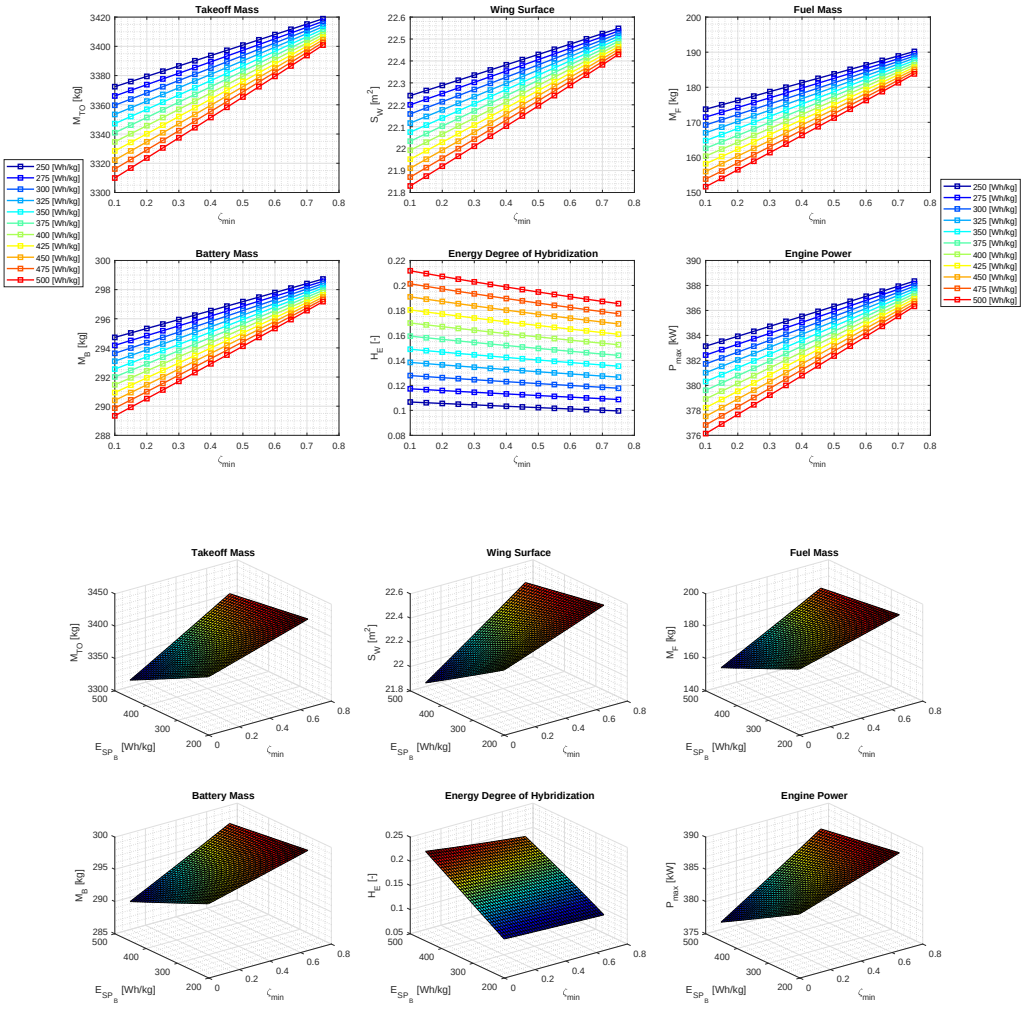

Figure 6.9: Hybrid 8-seater sensitivity on final state of charge and battery specific energy.

Final State of Charge and Battery Specific Power

The last sensitivity analysis is still about final state of charge, but this time is conducted by fixing the specific energy to 400 Wh kg^{-1} and changing values of specific power. What we can observe is that the lower the specific power, the higher the impact of high SoC levels at the end of the mission: for a 1000 W kg^{-1} battery it takes 100 kg to move from 10% to 75% final SoC, while about 25 are needed for a 2500 W kg^{-1} battery. This mass increment is mostly due to fuel mass increment: from the plot it is possible to see the different slope characterizing different batteries; for this special case it is possible to state that below 40% of final desired SoC a (relatively) low-power battery will require less fuel, due to high energy content, while above this value the opposite is true, due to excessive mass penalty.

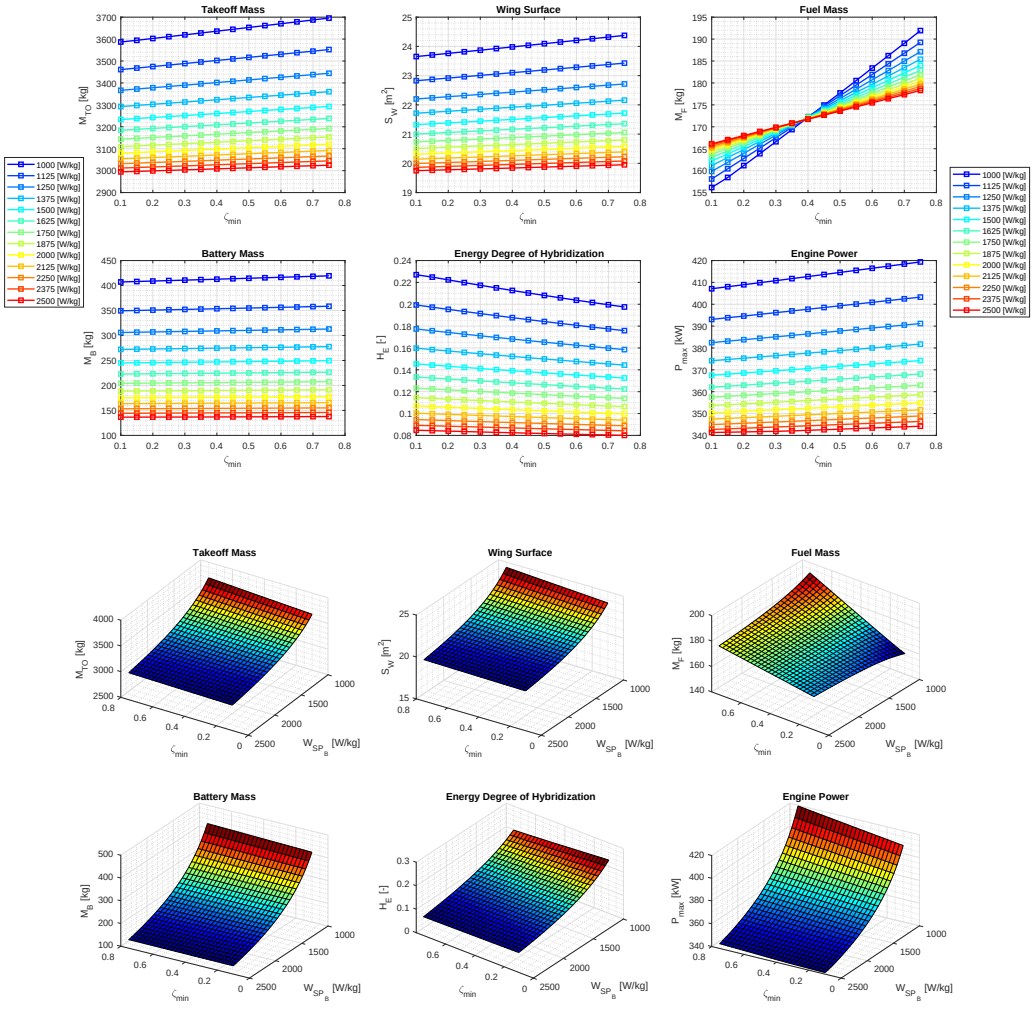

Figure 6.10: Hybrid 8-seater sensitivity on final state of charge and battery specific power.

6.2.2 All-Electric 8-seater

Again with reference to Section 5.2.2, using aircraft data reported in table 5.8, we analyze the sensitivity on range, battery specific power and energy, rate of climb and cruise altitude. This time, since the aircraft is all-electric no degree of hybridization or fuel mass will be presented, since they will be 1 and 0 everywhere respectively.

Battery Specific Power and Battery Specific Energy

The first analysis is carried out by considering the effect of batteries on overall results; as done before, we consider close future batteries first and then long time-span batteries later. In figure 6.11 we can observe that, unlike the hybrid-electric case, batteries are sized only by energy requirements instead of needed power. Moreover, we can observe that a specific energy of at least 425 Wh kg^{-1} is required to keep aircraft mass below reasonable bounds.

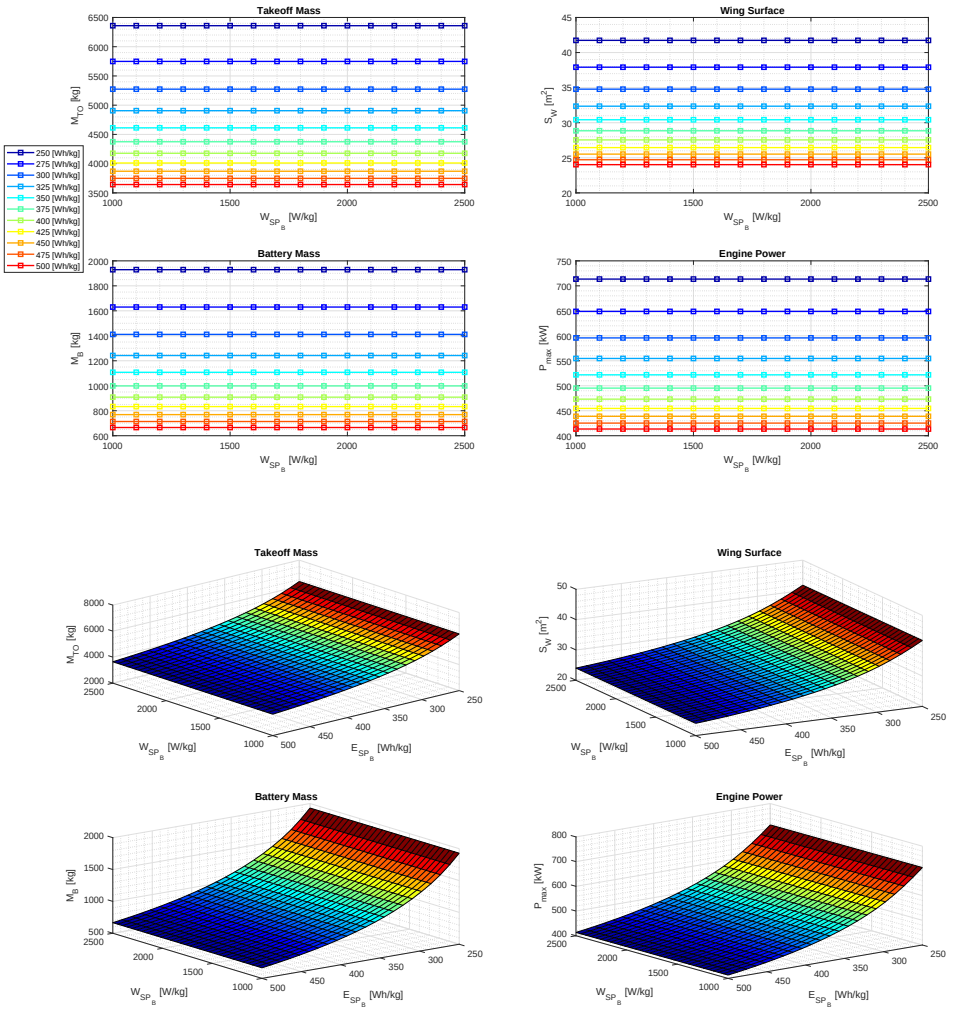

Figure 6.11: Electric 8-seater sensitivity on battery specific power and specific energy of close future batteries.

A more interesting pattern in shown in figure 6.12: if we let specific energy span from near-future values of 400 Wh kg^{-1} to very high value of 1600 Wh kg^{-1}, we observe that there will be a transition energy value at which battery constraint will switch from required energy to needed power. This behavior is observed for specific power values below 2000 W kg^{-1}, starting from 825 Wh kg^{-1} at 1000 W kg^{-1}. Recall that an optimal battery setting for an electric aircraft is such that the same battery mass is obtained by both energy and power requirements: for this reason we can observe for instance that for a 1000 W kg^{-1} battery no mass benefit is obtained for specific energy values beyond 825 Wh kg^{-1}, although of course we would have the chance to extend the overall range.

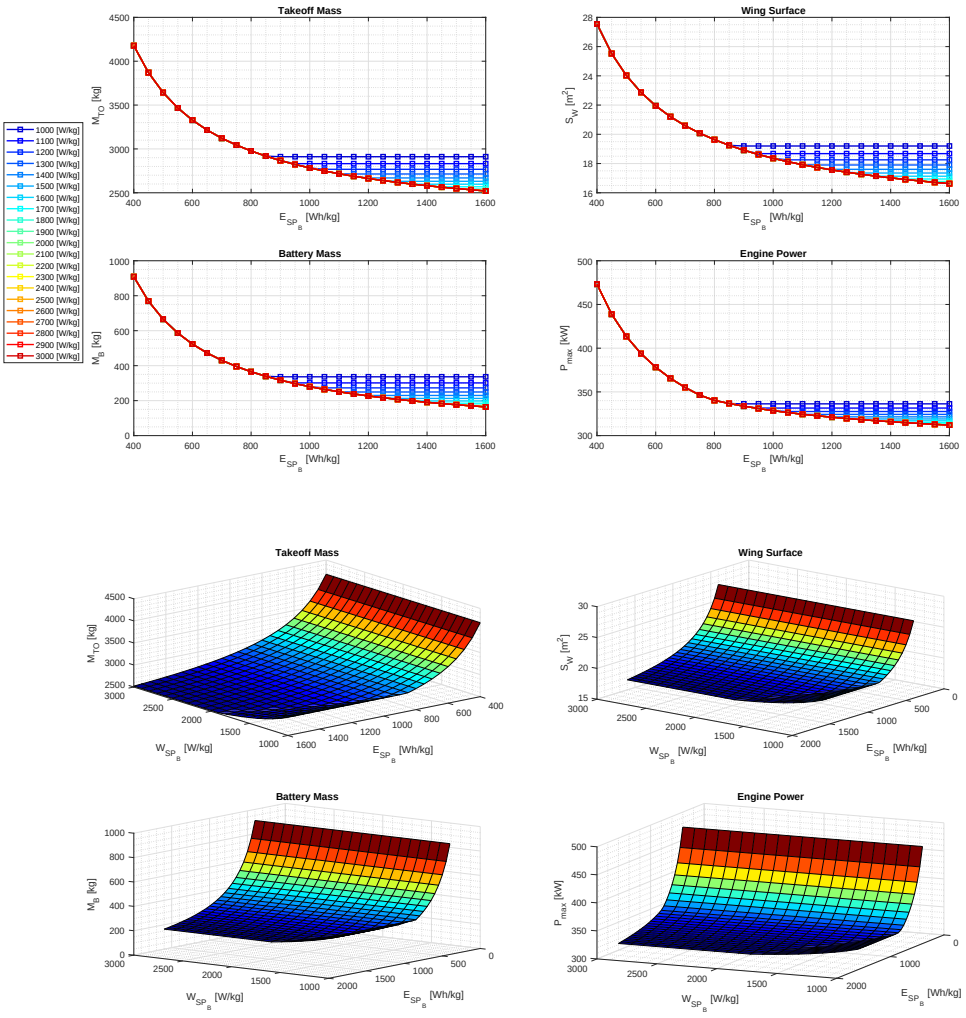

Figure 6.12: Electric 8-seater sensitivity on battery specific power and specific energy of long time-span batteries.

Range and Battery Specific Energy

The relationship between range and specific energy is considered to analyze feasibility of medium-to-long range all-electric aircraft application; from results in figure 6.13 we can discuss some aspects. The first consideration is about present batteries: with today's Lithium-Sulfur batteries characterized by specific energy values around 250÷280 Wh kg^{-1} electric aircraft applications are still not allowed to a medium-range micro feeder. Technology improvement is required for this mission and a value of at least 400 Wh kg^{-1} is needed, in order to avoid huge and not realistic required battery mass.

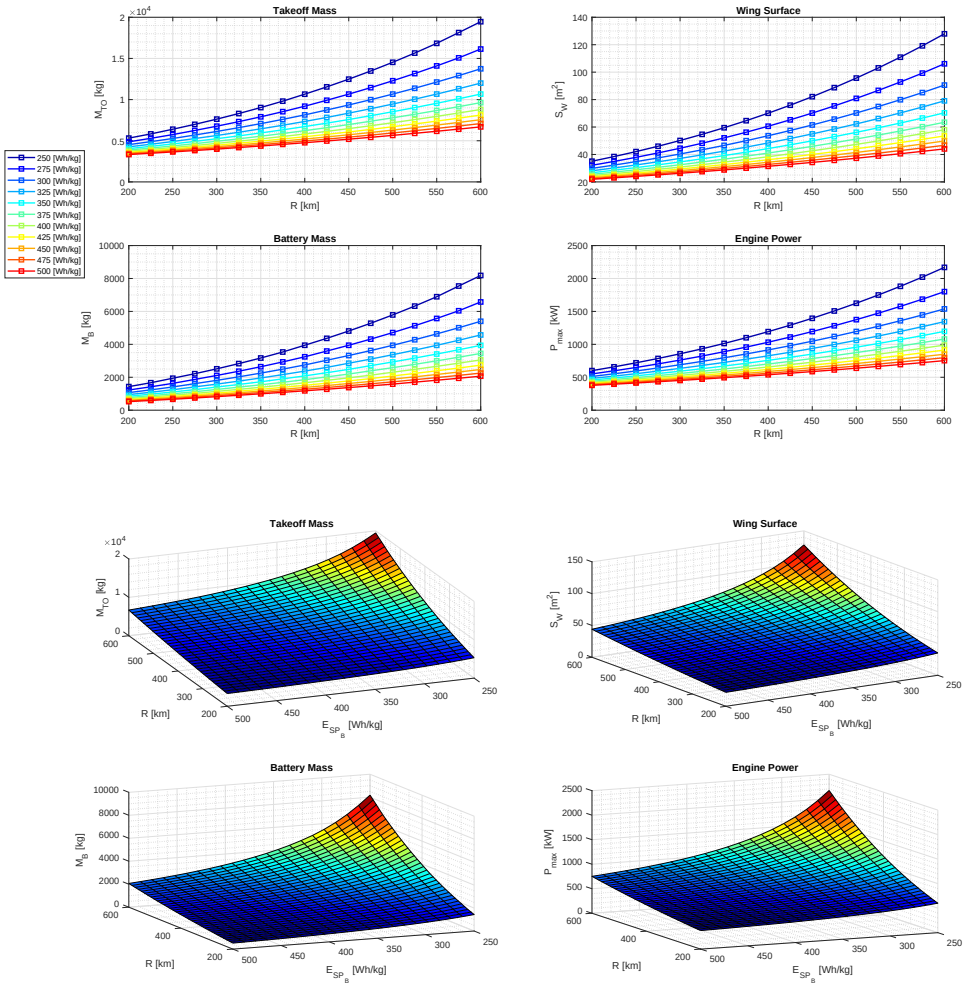

Figure 6.13: Electric 8-seater sensitivity on range and battery specific energy.

Cruise Altitude and Battery Specific Energy

We can analyze the effect of cruise altitude on all-electric aircraft performance. An interesting result is observed: an optimal altitude of about 11000÷12000 ft is found to minimize takeoff mass at a given battery setting. This result must be integrated with an external consideration: we fixed climb rate at 500 ft min^{-1} in such a way to avoid pressurization systems on board, but above 10000 ft external pressure is rather low for a comfortable flight, thus such a system would be needed, thus increasing structural mass to sustain pressure difference.

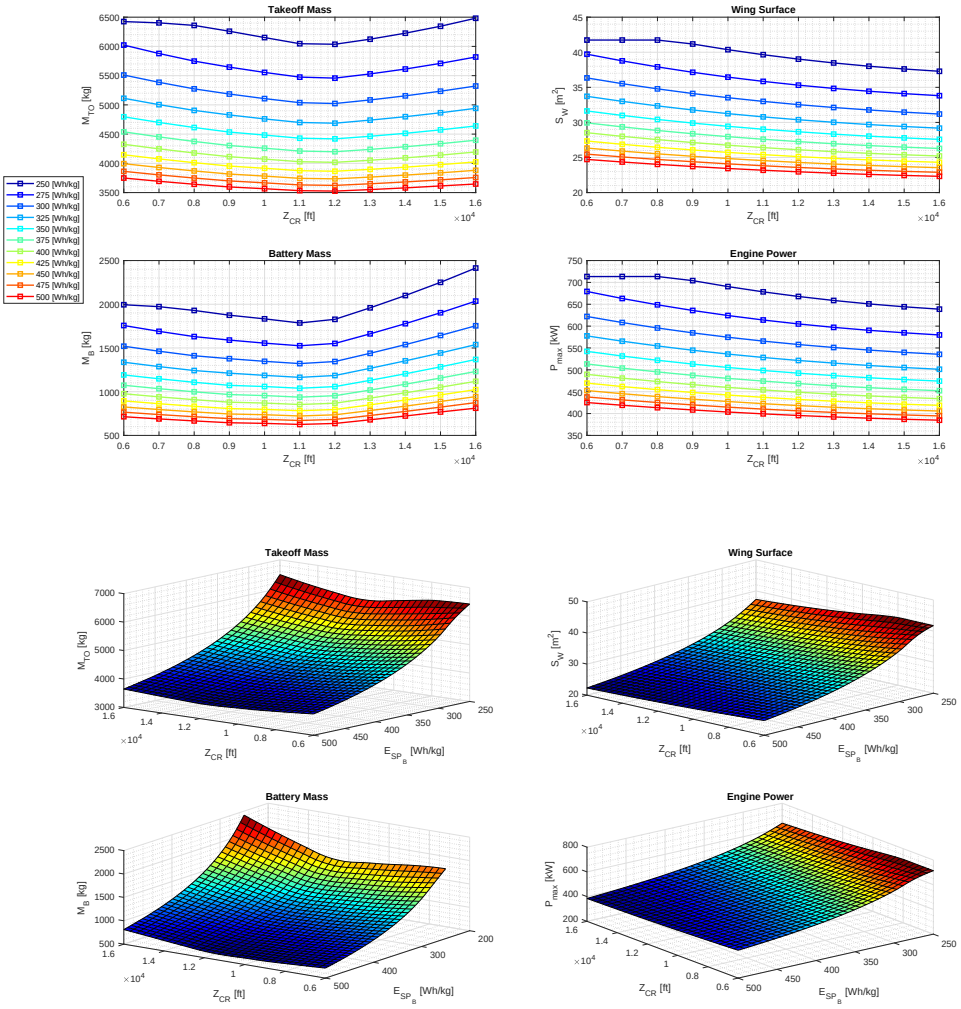

Figure 6.14: Electric 8-seater sensitivity on cruise altitude and battery specific energy.

Rate of Climb and Battery Specific Energy

As for the hybrid-electric case, rate of climb value starts having an impact on needed motor power starting from 1100 ft min^{-1}, but with a key difference: since all-electric airplanes are mostly sized by energy requirement, as we observed in previous parametric analyses, a steeper increase in needed power is not resulting in an increase in battery mass, and thus its impact is rather low. As for cruise altitude, rate of climb is mostly related to pressurization systems: too high pressure gradient, found for vertical speed values above 500 ft min^{-1}, could harm the passengers, thus a pressurization system would be required, further increasing takeoff mass.

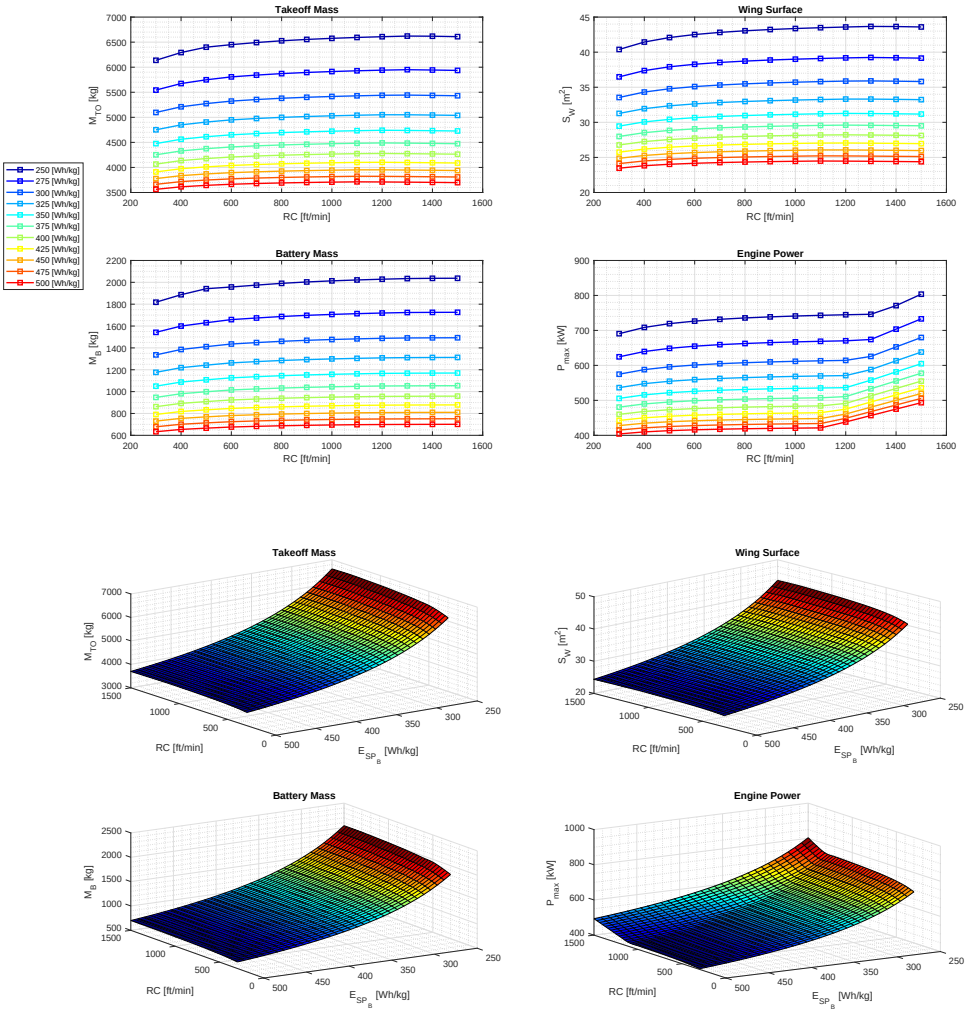

Figure 6.15: Electric 8-seater sensitivity on rate of climb and battery specific energy.

6.2.3 Hybrid Regional Aircraft

The last set of simulation concerns a regional aircraft; the commuter class is not considered due to regulations: while exploring the impact of input parameters we would constantly jump from CS-23 to CS-25, thus the results would not be very meaningful. We consider the regional case instead, considering input values found in table 5.13; we could observe that serial hybrid propulsion is not quite suitable with close future battery technology: what are the minimum values of specific power and energy to result in a feasible aircraft solution?

Battery Specific Power and Battery Specific Energy

Since we already observed that close future battery performance is not sufficient, we move directly to the long time-span case. In figure 6.16 we can observe that, as for the *H-8P* case, since battery mass is determined by power needs, the higher the specific power the lower the takeoff mass.

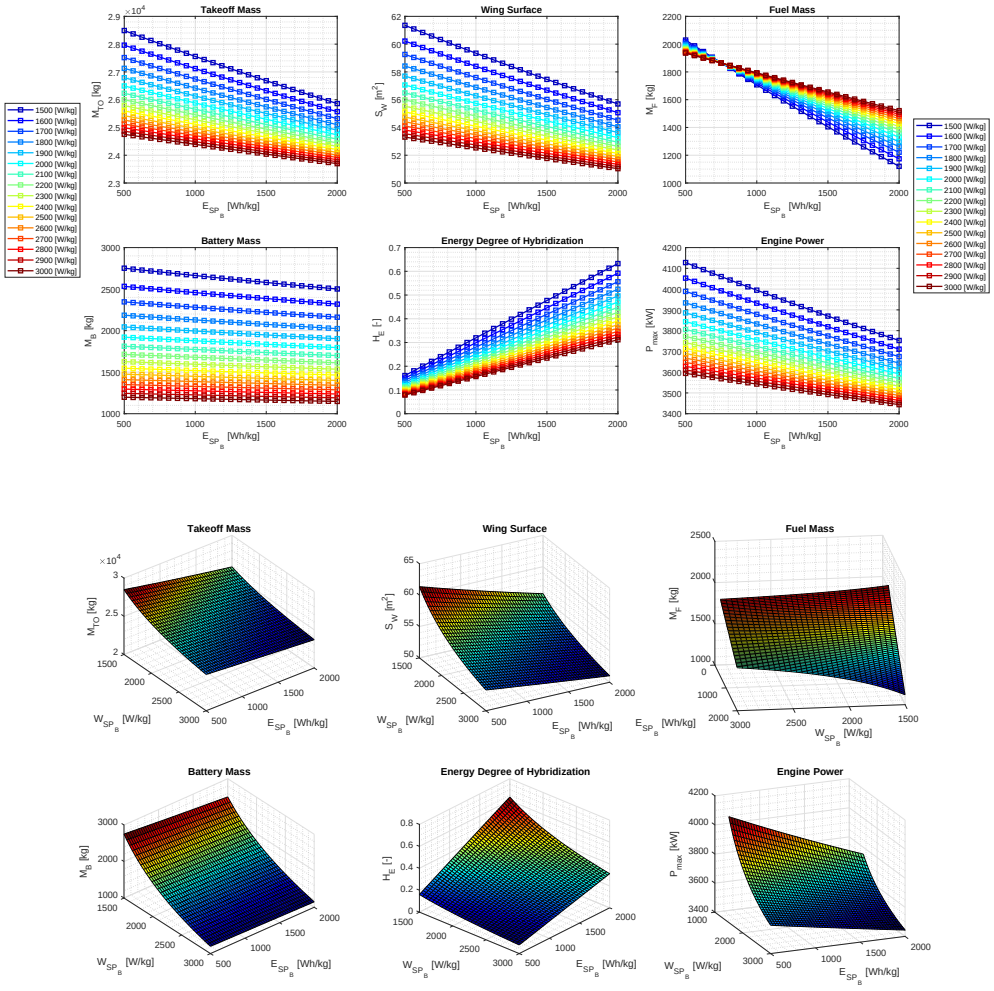

Figure 6.16: Hybrid regional aircraft sensitivity on battery specific power and specific energy.

A value of 2200 W kg^{-1} is desirable, to keep takeoff mass as low as possible, even at low energy battery settings. An interesting result can be observed in fuel mass plot: for specific energy values below 750 Wh kg^{-1} an increase in specific power results in a decrease in required fuel, while the opposite is true above that threshold. This is once again due to balance between battery mass penalty and stored energy: above 750 Wh kg^{-1} an increase in battery mass due to lower specific power results in an energetic surplus that overcomes mass penalty, thus resulting in lower fuel needed.

Range and Battery Specific Energy

A study about sensitivity on range is presented, considering a specific power of 1500 W kg^{-1}. Without surprises we see that the higher the range, the greater the mass: heavier aircraft requires more powerful engines, thus heavier batteries and more fuel to provide the required energy.

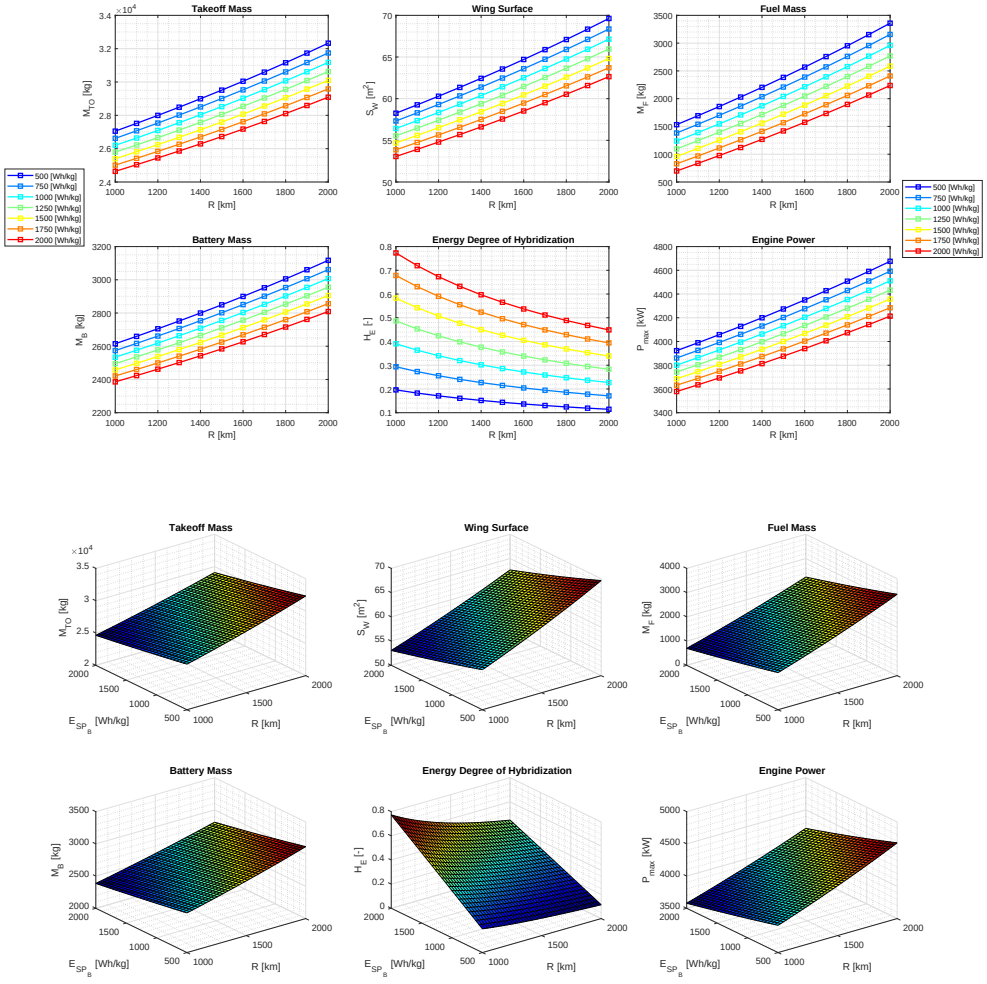

Figure 6.17: Hybrid regional aircraft sensitivity on range and battery specific energy.

An interesting consideration can be made by looking at takeoff mass. Let's consider a 28000 kg aircraft: a 500 Wh kg^{-1} battery allows a 1200 km mission and we observe that an increase in specific energy of 250 Wh kg^{-1} is needed to grant a range increase of 100 km.

Number of Passengers and Battery Specific Energy

An analysis can be made by considering the number of passengers as an unknown: we can observe that battery specific energy becomes more and more relevant as the number of passenger increases. We can see that a hybrid-electric version of ATR 42, with a *MTOW* of 16700 kg, is feasible also with close future Li-S batteries, with a takeoff mass of no more than 18000 kg. As we increase the amount of passengers the serial hybrid electric solution proves not to be feasible anymore, due to large increase in terms of required fuel.

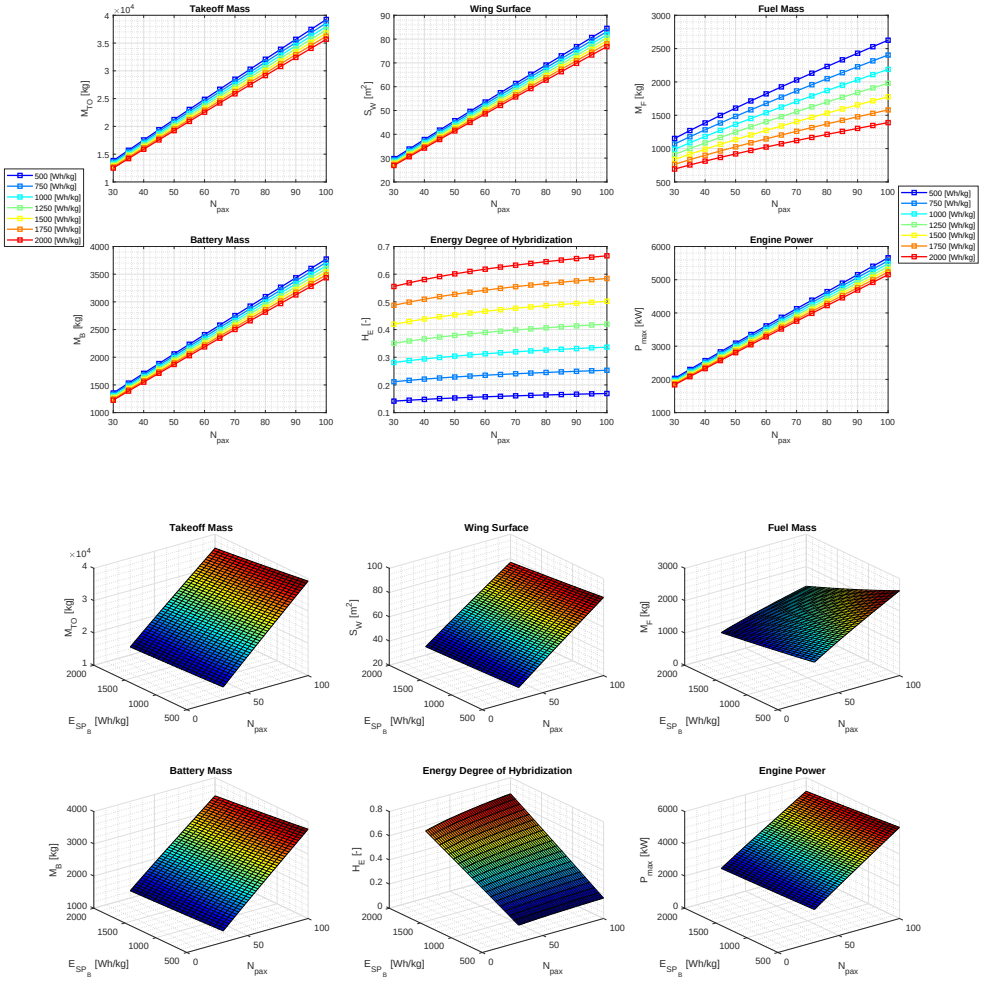

Figure 6.18: Hybrid regional aircraft sensitivity on number of passengers and battery specific energy.

Let's consider as before a fixed aircraft mass: at a value of 25000 kg we can observe that a 500 Wh kg^{-1} battery allows an accommodation of 60 passengers, while only 8 more can be allocated increasing this parameter four times.

Cruise Speed and Battery Specific Energy

A distinction is usually made while considering cruise speed, between so called economy, standard and high-speed cruise: what is the impact on the results? We can see that at 25000 ft a cruise speed of 360 KTAS, corresponding to 0.60 Mach, should not be exceeded since a large increase in battery mass is observed. Although there is no optimal cruise speed value from these plots, we can observe the degree of hybridization: even though we observe rather flat lines, a somewhat good speed range is found between 260 and 300 KTAS.

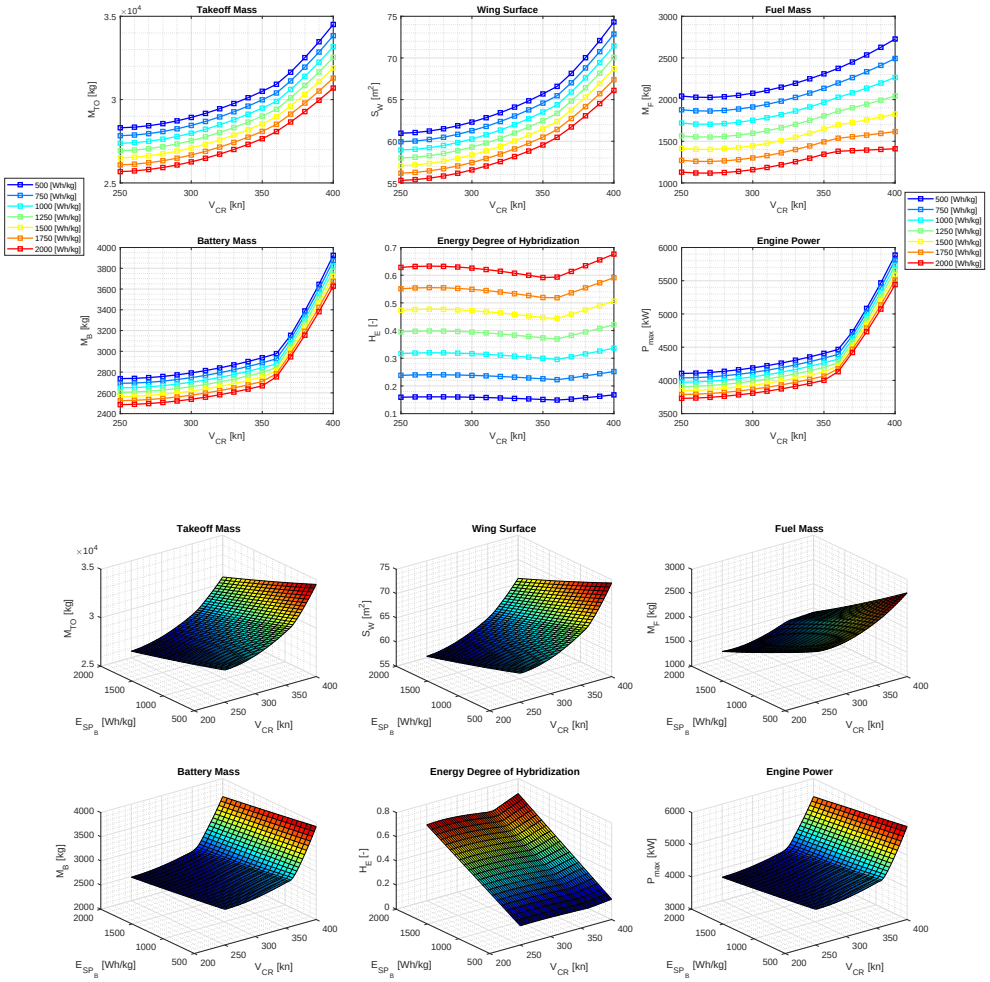

Figure 6.19: Hybrid regional aircraft sensitivity on cruise speed and battery specific energy.

Cruise Speed and Battery Specific Power

We analyzed cruise speed effect by letting the specific energy span from 500 to 2000 Wh kg^{-1} at a reference specific power of 1500 W kg^{-1}; we now evaluate the effect of specific power, considering an energy setting of 1000 Wh kg^{-1}, instead of the reference value of 500 Wh kg^{-1}. Once again, no surprises in terms of decrease in takeoff mass as specific power increases, but an interesting behavior can be observed in fuel mass. With this specific energy we can find a minimum fuel mass at a speed value of 270 KTAS for a 1500 W kg^{-1} battery, while this optimum is found at a slightly lower cruising speed as we increase specific power; this means we found economy cruise speed.

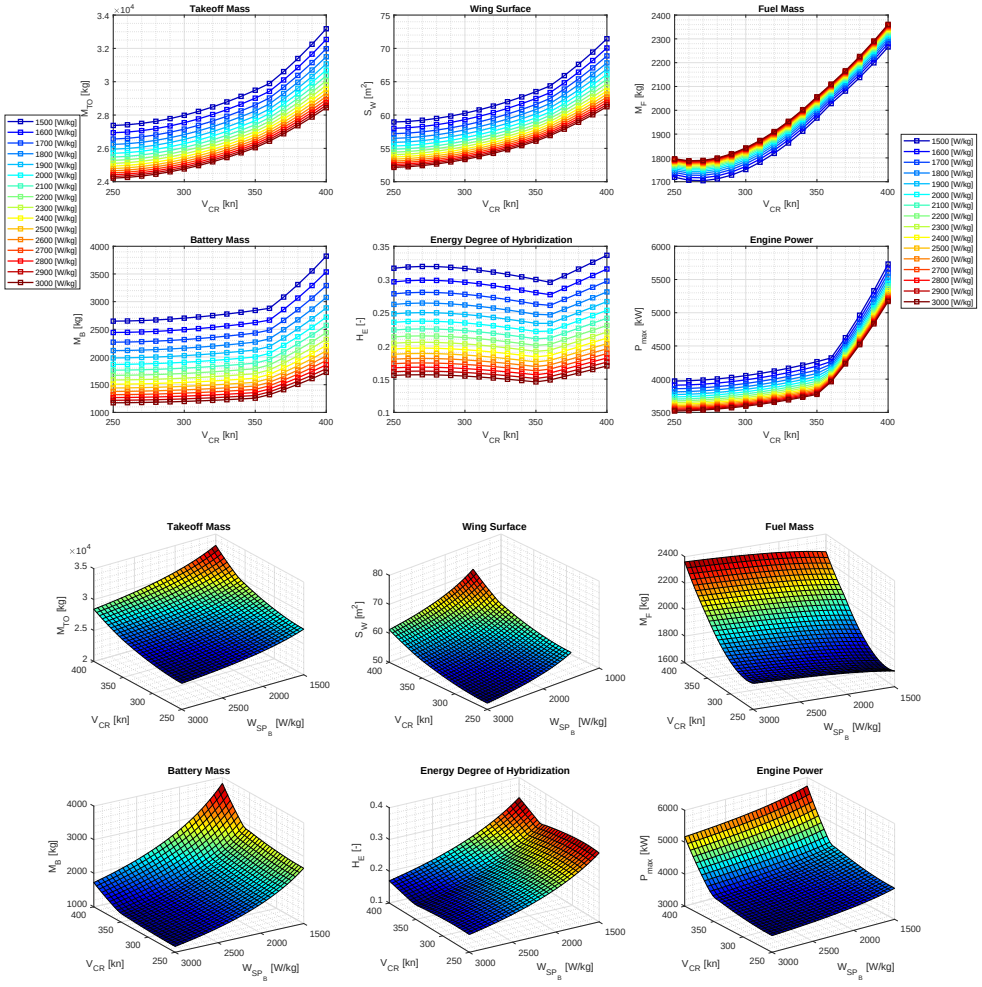

Figure 6.20: Hybrid regional aircraft sensitivity on cruise speed and battery specific power.

Chapter 7

Conclusions and Future Work

In the present work a general method to design and simulate all-electric or serial hybrid-electric aircraft has been presented. A technology survey has been conducted to assess the present available batteries, electric motors, thermal engines and airplanes, and to predict future trends.

A literature study has been carried out to compare different methods and projects developed by different authors: while a general method can be considered for all-electric aircraft, it has been found that the same is not true for hybrid-electric airplanes. For this reason the literature study allowed to distinguish between different architectures, that can be divided in the two main families of serial hybrid and parallel hybrid architectures. Different case studies analyzed in literature have shown that parallel architectures are more case-sensitive, thus serial hybrid propulsion has been considered.

The overall procedure that led to the *Hyperion* program has been described, starting from the assumptions on serial or turboelectric hybrid architecture; a model to simulate both turboshaft and reciprocating engine generators has been presented, as well as the flight mechanics model used for mission simulation. Different strategies have been employed for both flight mission and battery in-flight charging, and an iterative process has been implemented to obtain prescribed final levels for both battery state of charge (SoC) and tank level.

A validation process has been carried out on four aircraft classes: general aviation, micro feeder, commuter and large regional, by considering the limit case of a simulated conventional aircraft; acceptable agreement with real aircraft has been observed for these limit cases.

A set of design examples has been presented. Two airplanes have been presented for each class: an all-electric and a hybrid-electric aircraft for general aviation and micro feeder classes and hybrid-electric for commuter and regional, using two different charging strategies. In particular, cyclic charging strategy has been found to be more convenient in terms of mass reduction, due to better energy management; it has also been observed, though, that it does not allow a good control on final SoC level, thus a conservative decision has been made, by choosing a steady charging strategy for the subsequent analyses.

A wide sensitivity study has been carried out for three main reference aircraft: a hybrid-electric 8-seats micro feeder, an all-electric 8-seats micro feeder and a hybrid-electric regional airplane, with a reference accommodation of 70 passengers. Interesting results have been found; first of all, it has been observed that battery specific energy

is a key parameter in terms of balance between battery mass penalty and stored energy increase: a threshold value below which an increase in battery mass results in an increase of required fuel and above which the opposite is true has been observed. Several parametric studies have shown the impact of climb and cruise horizontal speed and of climb rate: a change of slope on curves due to a change in the most stringent constraint has been observed. Studies have also shown the feasibility bounds of all-electric and serial hybrid-electric aircraft applications: concerning all-electric micro feeder aircraft, a specific energy value of at least 400 Wh kg^{-1} has been found to be required; hybrid-electric airplanes have been found to be more dependent on specific power. Regional aircraft sensitivity studies have shown that serial hybrid propulsion is feasible up to 50 passengers, with competitive results if compared to existing aircraft, while are still not convenient for larger applications.

Future work and studies should rely on flexibility granted by this model:

- A general flight profile could be considered, with different strategies for climb, cruise, descent and loiter phases: a parametric description of these phases could show optimal flight strategy, that may or may not be close to standard constant indicated airspeed climb/descent and then constant altitude and speed cruise phases.
- A more realistic power-train model could be implemented and used to simulate energy and power flow from batteries to electric motors, as well as from the generator.
- A parametric description of charging strategy could be implemented as for the flight profile, to evaluate the optimal strategy, including the description of battery wear due to partial charging cycles.
- A study on emissions could be carried out, by analyzing possible improvement in generators technology, as suggested in Chapter 2, considering possible ways to reduce pollution by passive or active means that would be not possible for conventional applications.

Bibliography

[1] European Commission, *Fligthpath 2050: Europe's Vision for Aviation*, 2011.

[2] H. Kuhn, *Fundamental Prerequsites for Electric Flying*, Deutscher Luft und Raumfahrtkongress, 2012.

[3] D.V. Ragone, *Review of Battery Systems for Electrically Powered Vehicles*, SAE Technical Paper, 1968.

[4] T. Christen, M.W. Carlen, *Theory of Ragone plots*, Journal of Power Sources 91, 2000.

[5] R.A. Huggins, *Advanced Batteries: Materials Science Aspects*, Springer, 2009.

[6] P. Birke, *Electric Battery, Actual and future Battery Technology Trends*, Continental Powertrain Division, May 2010.

[7] A.T. Isikveren, C. Pornet, Y. Fefermann, C. Maury, *Hybrid-Electric Motive Power Systems for Commuter Transport Applications*, 30^{th} Congress of the International Council of the Aeronautical Sciences, September 2016.

[8] F. Ritzert, R. Bowman, D. Steingart, B. Hertzberg, *Structural Batteries for Hybrid Electric Propulsion Systems*, NASA Aeronautics Research Institute and Princeton University, July 2013.

[9] S. Ekstedt, M. Wysocki, L.E. Asp, *Structural batteries made from fibre reinforced composites*, Plastics Rubber and Composites 39, June 2010.

[10] L.E. Asp, S. Leijonmarck, T. Carlson, G. Lindbergh, *Realisation of structural battery composite materials*, 20^{th} International Conference on Composite Materials, Copenhagen, July 2015.

[11] T. Pereira, Z. Guo, *Embedding thin-film Lithium energy cells in structural composites*, Composites Science and Technology, April 2008.

[12] E. Jacques, M.H. Kjell, D. Zenkert, G. Lindbergh, M. Behm, M. Willgert, *Impact of electrochemical cycling on the tensile properties of carbon fibres for structural Lithium-ion composite batteries*, Composites Science and Technology, 2012.

[13] E. Jacques, M.H. Kjell, D. Zenkert, G. Lindbergh, M. Behm, *Impact of mechanical loading on electrochemical performance of carbon fibres* Proc. 18th Int. Conf. on Composite Materials, South Korea, 2011.

[14] E. Jacques, M.H. Kjell, D. Zenkert, G. Lindbergh, M. Behm, *Expansion of carbon fibres induced by Lithium intercalation for structural electrode applications*, Carbon, 59, 2013.

[15] E.D. Wetzel, *Reducing weight: Multifunctional composites integrate power, communications, and structure*, AMPTIAC Q, 8, 2004.

[16] L.E. Asp, A. Bismarck, T. Carlson, G. Lindbergh, S. Leijonmarck, M. Kjell, *A battery half-cell, a battery and their manufacture*, PCT Intl Appl. No. PCT/EP2013/068024, 2013.

[17] N. Imanishi, O. Yamamoto, *Rechargeable Lithium-air batteries: characteristics and prospects*, Materials Today 17, January/February 2014.

[18] P.G. Bruce, S.A. Freunberger, L.J. Hardwick, J. Terascon, *Li-O_2 and Li-S batteries with high energy storage*, Nature Materials 11, December 2011.

[19] Fraunhofer Institute for Systems and Innovation research, *Technology Roadmap Energy Storage for Electric Mobility 2030*, BMBF Innovationsallianz, 2015.

[20] Siemens, *Electric propulsion components with high power densities for aviation*, Transformative Vertical Flight Workshop, March 2015.

[21] T. Shinzato, S. Arakawa, H. Oyama, H. Saka, T. Hayasaki, *Development of High-Temperature Superconducting Motor for Automobiles*, SEI Technical Review 75, October 2012.

[22] G.V. Brown, *Weights and Efficiencies of Electric Components of a Turboelectric Aircraft Propulsion System*, 49th AIAA, Orlando 2011.

[23] A.T. Isikveren, C. Pornet, A. Seitz, K.O. Plötner, *Conceptual Studies of Universally-Electric Systems Architectures Suitable for Transport Aircraft*, Deutscher Luft- und Raumfahrtkongress, Berlin 2012.

[24] A.T. Isikveren, M. Hornung, M. Cole, *Ce-Liner-Case Study for eMobility in Air Transportation*, Aviation Technology, Integration and Operations Conference, August 2013.

[25] A.T. Isikveren, Y. Fefermann, C. Maury, *Long-term Hybrid-Electric propulsion architecture options for transport aircraft*, Conference: Greener Aviation, Brussels 2016.

[26] F. Ali, I. Goulos, V. Pachidis, *Helicopter Mission Analysis for a Regenerative Turboshaft Engine*, 69th Annual Forum of the American Helicopter Society, May 2013

[27] A. Broglia, L. Clozza, M. Russo, C. Spada, L. Vendemini, A.G. Zuanetti, C.E.D. Riboldi, L. Trainelli, *Flynk – The future all-electric commuter concept for metropolitan areas*, XXIV Congresso Nazionale AIDAA, Palermo-Enna, 2017.

[28] A. Bernasconi, L. Capoferri, C.E.D. Riboldi, L. Trainelli, *Hybris - An Innovative Concept for Future General Aviation*, 13th Pegasus-AIAA Student Conference, At Berlin, Germany, April 2017.

[29] G.E. Bona, M. Bucari, A. Castagnoli, L. Trainelli, *Flybrid: Envisaging the Future Hybrid-Powered Regional Aviation*, AIAA/3AF Aircraft Noise and Emissions Reduction Symposium, Atlanta, June 2014.

[30] D.J. Paisley, *Hybrid-Electric Propulsion*, Boeing Commercial Airplanes, 2015.

[31] C.E.D. Riboldi, F. Gualdoni, *An integrated approach to the preliminary weight sizing of small electric aircraft*, Aerospace Science and Technology 58, 2016.

[32] A.T. Isikveren, M. Schmidt, *Future Transport Aircraft Ultra-Low Emissions Technology Options*, GARS Workshop 2014

[33] A.T. Isikveren, C. Pornet, P.C. Vratny, M. Schmidt, *Optimization of Commercial Aircraft Utilizing Battery-based Voltaic-Joule-Brayton Propulsion*, Journal of Aircraft, December 2016.

[34] A.T. Isikveren, A. Sizmann, M. Hornung, *Realising Flightpath 2050: Initial Investigation of Potential Technological Solutions*, SAE 2011 AeroTech Congress and Exhibition, Toulouse, France, 2011.

[35] K.T. Chau, Y.S. Wong, *Overview of power management in hybrid electric vehicles*, Energy Conversion and Management 43, 2002.

[36] Committee on Propulsion and Energy Systems to Reduce Commercial Aviation Carbon Emissions, Aeronautics and Space Engineering Board, Division on Engineering and Physical Sciences, National Academies of Sciences, Engineering, and Medicine. *Commercial Aircraft Propulsion and Energy Systems Research: Reducing Global Carbon Emissions*, National Academies Press, Washington DC, USA, 2016.

[37] C. Friedrich, P.A. Robertson, *Hybrid-Electric Propulsion for Aircraft*, Journal of Aircraft 52, January-February 2015.

[38] J. Roskam, *Airplane Design, Part I*, Roskam Aviation and Engineering Corporation, 1985.

[39] L. Trainelli, *Lezioni di Meccanica del Volo*, 2011.

[40] P. Hill, C. Peterson, *Mechanics and Thermodynamics of Propulsion*, second edition, Pearson Education, 1992.

Sitography

[41] *MAHEPA Project*, https://mahepa.eu, 2017.

[42] Tesla Model S specifications, https://en.wikipedia.org/wiki/Tesla_Model_S.

[43] Oxis Energy, https://oxisenergy.com/products/.

[44] SionPower, http://www.sionpower.com/technology-licerion.php

[45] Aerospace Technology, http://www.aerospace-technology.com/projects/extra-330le-electric-aircraft/.

[46] Fédération Aéronautique Internationale, https://fai.org/records, 25 November 2016.

[47] Alpha Electro pictures http://www.pipistrel.si/plane/alpha-electro/gallery

[48] Alpha Electro specifications http://www.pipistrel.si/plane/alpha-electro/technical-data

[49] E-Fan aircraft http://company.airbus.com/responsibility/airbus-e-fan-the-future-of-electric-aircraft.html

[50] E-Fan specifications https://en.wikipedia.org/wiki/Airbus_E-Fan

[51] Solar Impulse 2 adventure http://aroundtheworld.solarimpulse.com/adventure

[52] Solar Impulse 2 specifications http://www.solarimpulse.com/pdf/hb-sia/hb-sia_en.pdf

[53] Pipistrel HY-4 specifications http://hy4.org/hy4-technology

[54] Panthera Hybrid aircraft overviewhttp://www.pipistrel.si/plane/panthera/overview

[55] Panthera Hybrid aircraft pictures http://www.panthera-aircraft.com/gallery

[56] Panthera Hybrid specifications http://www.panthera-aircraft.com/technical-data

[57] NASA X-57 Maxwell specifications https://en.wikipedia.org/wiki/NASA_X-57_Maxwell

[58] Airbus E-Fan X http://www.airbus.com/newsroom/press-releases/en/2017/11/airbus--rolls-royce--and-siemens-team-up-for-electric-future-par.html

[59] A. De Cesco, *L'aerotaxi del Politecnico di Milano che ha conquistato New York", Corriere della Sera, Novembre 22, 2015* http://www.corriere.it/tecnologia/cyber-cultura/15_novembre_22/aerotaxi-politecnico-milano-che-ha-conquistato-new-york

[60] Hybris aircraft, http://www.aero.polimi.it/education/student-competitions/2016/.

[61] Flybrid aircraft, http://www.aero.polimi.it/education/student-competitions/2013/.